Oka, M., Birn, J., Battaglia, M., Chaston, C. C., Hatch, S. M., Livadiotis, G., Imada, S., Miyoshi, Y., Kuhar, M., Effenberger, F., Eriksson, E., Khotyaintsev, Y. V., Retinò, A. (2018): Electron Power-Law Spectra in Solar and Space Plasmas. - *Space Science Reviews*, *214*.

DOI: http://doi.org/10.1007/s11214-018-0515-4

Space Science Reviews manuscript No.
(will be inserted by the editor)

Electron Power-Law Spectra in Solar and Space Plasmas

M. Oka · J. Birn · M. Battaglia · C. C. Chaston · S. M. Hatch · G. Livadiotis · S. Imada · Y. Miyoshi · M. Kuhar · F. Effenberger · E. Eriksson · Y. V. Khotyaintsev · A. Retinò

Received: date / Accepted: date

Abstract Particles are accelerated to very high, non-thermal energies in solar and space plasma environments. While energy spectra of accelerated electrons often exhibit a power law, it remains unclear how electrons are accelerated to high energies and what processes determine the power-law index δ. Here, we review previous observations of the power-law index δ in a variety of different plasma environments with a particular focus on sub-relativistic electrons. It appears that in regions more closely related to magnetic reconnection (such as the 'above-the-looptop' solar hard X-ray source and the plasma sheet in Earth's magnetotail),

M. Oka · C. C. Chaston
Space Sciences Laboratory, University of California Berkeley
7 Gauss Way, Berkeley, CA 94720
Tel.: +1-510-642-1350
E-mail: moka@ssl.berkeley.edu

J. Birn
Space Science Institute, Boulder, Colorado, USA
Los Alamos National Laboratory, Los Alamos, NewMexico, USA

M. Battaglia · M. Kuhar
Institute of 4D Technologies, School of Engineering, University of Applied Sciences and Arts Northwestern Switzerland, CH-5210 Windisch,Switzerland

S. M. Hatch
Department of Physics and Astronomy, Dartmouth College, Hanover, New Hampshire, USA

G. Livadiotis
Southwest Research Institute, San Antonio, TX-78238, USA

S. Imada · Y. Miyoshi
Institute for Space-Earth Environmental Research, Nagoya University, Furo-cho, Chikusa-ku, Nagoya, 464-8601 Aichi, Japan

F. Effenberger
Helmholtz Centre Potsdam, GFZ German Research Centre for Geosciences, Potsdam, Germany
Bay Area Environmental Research Institute, NASA Research Park, Moffett Field, CA, USA

E. Eriksson and Y. V. Khotyaintsev
Swedish Institute of Space Physics, Uppsala, Sweden

A. Retinò
Laboratoire de Physique des Plasmas, Palaiseau, France

the spectra are typically soft ($\delta \gtrsim 4$). This is in contrast to the typically hard spectra ($\delta \lesssim 4$) that are observed in coincidence with shocks. The difference implies that shocks are more efficient in producing a larger non-thermal fraction of electron energies when compared to magnetic reconnection. A caveat is that during active times in Earth's magnetotail, δ values seem spatially uniform in the plasma sheet, while power-law distributions still exist even in quiet times. The role of magnetotail reconnection in the electron power-law formation could therefore be confounded with these background conditions. Because different regions have been studied with different instrumentations and methodologies, we point out a need for more systematic and coordinated studies of power-law distributions for a better understanding of possible scaling laws in particle acceleration as well as their universality.

Keywords particle acceleration · magnetic reconnection · shocks · solar flares · magnetotail · solar wind

Contents

1 Introduction . . . 3
1.1 Why Electron Power Laws? . . . 3
1.2 Caveats of Comparing Solar and Space Plasmas . . . 4
1.3 Definitions of Power-Law Index . . . 5
1.4 General Theories of Power-Law Formation . . . 9
1.4.1 Fermi's approach . . . 10
1.4.2 Fokker-Planck approach . . . 11
2 Power Laws in Solar Flares . . . 12
2.1 Overview . . . 12
2.2 Full-Sun Spectra . . . 16
2.3 Non-thermal Emission in Footpoints . . . 17
2.4 Non-thermal Emission in the Corona . . . 17
2.4.1 Above-the-looptop events . . . 18
2.4.2 Coronal thick-target events . . . 19
2.4.3 Other notable events . . . 20
2.5 Relation Between Coronal and Footpoint Sources . . . 20
3 Power Laws in Earth's Magnetotail . . . 21
3.1 Overview . . . 21
3.2 Caveats of Comparing Energy Spectra . . . 25
3.3 Plasma Sheet . . . 25
3.3.1 Active vs Quiet Times . . . 25
3.3.2 Reconnection Region . . . 28
3.3.3 Reconnection Downstream and Collapsing Region . . . 30
3.4 Auroral Region . . . 33
3.5 Radiation Belts . . . 35
4 Power Laws in Other Environment . . . 36
4.1 Solar Energetic Particles (SEPs) . . . 36
4.2 Shocks and Sheaths . . . 38
4.3 Quiet-Time Solar Wind . . . 39
5 Summary and Discussion . . . 41
5.1 Solar Flares vs Earth's Magnetotail . . . 41
5.1.1 Regions close to Reconnection Site . . . 41
5.1.2 Regions away from Reconnection Site . . . 43
5.2 Shocks vs Reconnection . . . 43
5.3 Origin of Power-Law Tails in Earth's Magnetotail . . . 44
5.4 Possible Future Studies . . . 45
A Plasma Parameter Regimes . . . 45
B Non-Extensive Statistical Mechanics . . . 46
C Fermi Acceleration . . . 47

1 Introduction

1.1 Why Electron Power Laws?

A solar flare is an explosive energy-release phenomenon on the sun, and non-thermal (power-law) electrons alone appear to carry up to 50% of the released energy (e.g. Lin and Hudson 1971; Lin et al. 2003; Emslie et al. 2012; Aschwanden et al. 2014, and references therein). While it has been established that magnetic reconnection – a plasma process that converts magnetic energy into particle energy – plays an important role during flares, the precise mechanism for producing such energetic electrons is still unclear.

A substorm is an explosive energy-release phenomenon in Earth's magnetotail that also produces non-thermal ions and electrons reaching energies of hundreds of keV[1]. As in solar flares, magnetic reconnection is thought to play a major role in the energy release and conversion. However, ion fluxes have been shown to dominate the energy outflow from tail reconnection sites (e.g. Øieroset et al. 2002; Eastwood et al. 2013) but the relative contributions of thermal and suprathermal ions were not investigated. Also, thermal and non-thermal electrons do not provide a comparable or even dominant contribution to the energy outflow, due to their lower average energy (typically less than 1 keV compared to 5 – 10 keV mean ion energies).[2]

The similarities and differences between the energetic particle properties in solar and terrestrial environments thus were a strong motivation for this paper. A possible key to understanding and describing the suprathermal populations, here specifically of electrons, is the power-law index, which may be used to measure the amount of energization and provide insight into acceleration mechanisms. Thus, by comparing power-law indices in solar flares (Section 2) and Earth's magnetotail (Section 3), we may be able to find similarities and differences of electron acceleration mechanisms, although both the measurement techniques and the plasma parameters are very different in each environment (Section 1.2, Appendix A). From this perspective, it is instructive to compare these power-law indices with those of other regions such as shocks and the solar wind because electrons in these regions are also known to exhibit a non-thermal tail (Section 4). Through detailed comparisons and discussions of power-law spectra in different environments, we aim to search for and discuss a possible scaling law or universality of electron acceleration that may exist, at least, in the sub-relativistic plasmas in the heliosphere (Section 5). It should be noted that particle acceleration occurs everywhere in the universe, not only in solar and terrestrial settings but also in astrophysical settings. Thus, we hope this review of solar and space plasmas will ultimately contribute toward a better understanding of astrophysical plasmas as well.

1.2 Caveats of Comparing Solar and Space Plasmas

The diagnostics and methodologies of high-energy electrons are very different in solar and space environments, i.e. remote-sensing solar X-rays and *in situ* measurements of particles in space. In principle, an electron distribution $f(t,\mathbf{v},\mathbf{r})$ is intrinsically a function of time t, particle velocity $\mathbf{v}$ and position $\mathbf{r}$, where f is the differential density. However, in our observations of solar flares via X-rays, we can obtain photon distributions as a function of energy E and time t only, with limited spatial/time resolutions and no information along the line of sight. Upon interpreting the observed spectrum from a hard X-ray source (such as footpoint, looptop and above-the-looptop sources, as will be described in Section 2), we have to consider it as the mean distribution of the source at a given time,

$$\langle nVf\rangle = \int_V n(\mathbf{r}) f(E,\mathbf{r}) dV, \tag{1}$$

[1] A 'substorm' occurs over the time scale of up to a few hours, mostly due to phenomena in the magnetotail leading to expansion of aurora in the polar ionosphere. Electron acceleration occurs on a time scale of minutes. There is also a 'storm', which is a disturbance of the magnetic field and associated plasmas mostly in the inner magnetosphere. It occurs over a time scale of hours or days and generally includes multiple substorms.

[2] In the absence of a clearly identifiable Maxwellian in the magnetotail, the term 'thermal' here may denote energies comparable to or less than the mean energy, rather than a Maxwellian component (See Section 1.3 for more details). The separation of thermal from non-thermal populations appears more arbitrary than in the solar case, also because of the absence of collisions that would cause the particle populations to relax toward a Maxwellian.

where n and V are the density and volume of the hard X-ray source, respectively. In reality, a hard X-ray source is not necessarily uniform and there could be a variety of different spectral forms at various positions within the source. It is also difficult to estimate the size and shape of the source volume V. In some cases, a stereoscopic observation can be achieved with multiple telescopes, but the error bars of the V estimates are still large with current instruments. In addition, we need to convert a photon spectrum to an electron spectrum for comparison, which involves an assumption on how electrons lose their energy.

On the other hand, *in-situ* measurement in space by a spacecraft provides full 3D distributions of particle velocities $f(\mathbf{v})$ at a given time t and position $\mathbf{r}$, where f is the phase space density. While anisotropies and other kinetic and/or non-thermal features can be inferred from $f(\mathbf{v})$, it is often difficult to distinguish between spatial and temporal variations from the f data alone. For example, when a spacecraft detected an increase of $f(\mathbf{v})$, it could be a passage of a plasmoid filled with a larger number of particles (i.e., spatial variation) or an arrival of particles from a remote structure that released the particles (i.e., temporal variation). A contextual data from different plasma parameters (such as magnetic fields) and/or multi-point measurements (with multiple spacecraft) are used to discuss such spatial/temporal variations.

Because of these differences, we have not focused on the details of, for example, pitch angle distributions. If a magnetotail study reported the power-law index of spectra for both parallel and perpendicular directions with respect to the magnetic field, then we have taken the values from the spectrum that showed the largest flux to represent the power-law index of the features/phenomena. Also, *in situ* measurements often show time variations within particular features/phenomena. In such cases, we focused on an average value and the standard deviation.

1.3 Definitions of Power-Law Index

While there are different definitions of the power-law index, we will use δ as measured in electron differential flux throughout this paper. In this section, we summarize some commonly used definitions so that we can more easily compare power-law indices reported in the literature. Table 1 provides a conversion table.

In an isotropic, three-dimensional (3D) form, the **phase space density** of the power-law distribution can be written as

$$f(p) \propto p^{-s} \tag{2}$$

where p is the particle momentum and s is the power-law index. Of course, for many cases of solar and space plasma, the particle distributions are not necessarily isotropic, and the data obtained by *in-situ* measurements is often analyzed in 3D velocity space $f(\mathbf{v})$ where $\mathbf{v}$ is the particle velocity. The phase space density is also used for analyzing energy spectra (especially in magnetospheric studies), as a function of particle energy E, i.e. $f(E)$, after taking an average over all or a part of the pitch-angles. In this form the power-law index becomes

$$f(E) \propto E^{-\Gamma}, \tag{3}$$

where $\Gamma = s/2$ for sub-relativistic particles ($E = p^2/2m$) and $\Gamma = s$ for ultra-relativistic particles (i.e., $E = pc$).

The **differential density** ($\mathrm{cm}^{-3}\ \mathrm{keV}^{-1}$) is defined as $N(E)dE = 4\pi p^2 f(p)dp$ and the power law can be written as

$$N(E) \propto E^{-\delta'}, \tag{4}$$

Table 1 A conversion table for various power-law indices in the sub-relativistic regime (See text for values in the ultra-relativistic regime). From left to right are phase space density ($f(p), f(E)$), differential density $N(E)$, differential flux (or flux density) $\mathscr{F}(E)$, the kappa distribution $f_\kappa(v)$, thin- and thick-target X-ray emission $I_{thin}(\varepsilon)$ and $I_{thick}(\varepsilon)$. Note $\delta = \kappa$ and $\Gamma = \gamma_{thin}$. $f(E)$ is listed in addition to $f(p)$ because it has been used in magnetospheric observations.

$f(p)$ $\propto p^{-s}$	$f(E)$ $\propto E^{-\Gamma}$	$N(E)$ $\propto E^{-\delta'}$	$\mathscr{F}(E)$ $\propto E^{-\delta}$	$f_\kappa(v)$ $\propto v^{-2(\kappa+1)}$	$I_{thin}(\varepsilon)$ $\propto \varepsilon^{-\gamma_{thin}}$	$I_{thick}(\varepsilon)$ $\propto \varepsilon^{-\gamma_{thick}}$
s	$\frac{s}{2}$	$\frac{s-1}{2}$	$\frac{s-2}{2}$	$\frac{s-2}{2}$	$\frac{s}{2}$	$\frac{s-4}{2}$
2Γ	Γ	$\Gamma-\frac{1}{2}$	$\Gamma-1$	$\Gamma-1$	Γ	$\Gamma-2$
$2\delta'+1$	$\delta'+\frac{1}{2}$	δ'	$\delta'-\frac{1}{2}$	$\delta'-\frac{1}{2}$	$\delta'+\frac{1}{2}$	$\delta'-\frac{3}{2}$
$2(\delta+1)$	$\delta+1$	$\delta+\frac{1}{2}$	δ	δ	$\delta+1$	$\delta-1$
$2(\kappa+1)$	$\kappa+1$	$\kappa+\frac{1}{2}$	κ	κ	$\kappa+1$	$\kappa-1$
$2\gamma_{thin}$	γ_{thin}	$\gamma_{thin}-\frac{1}{2}$	$\gamma_{thin}-1$	$\gamma_{thin}-1$	γ_{thin}	$\gamma_{thin}-2$
$2\gamma_{thick}+4$	$\gamma_{thick}+2$	$\gamma_{thick}+\frac{3}{2}$	$\gamma_{thick}+1$	$\gamma_{thick}+1$	$\gamma_{thick}+2$	γ_{thick}

where $\delta' \equiv (s-1)/2$ for sub-relativistic particles and $\delta' \equiv s-2$ for ultra-relativistic particles. Many studies of particle simulations use this form, because an energy spectrum can be directly obtained from a histogram of energies of particles in the simulation box.

The **differential flux** or flux density ($\mathrm{cm^{-2}s^{-1}keV^{-1}}$) is defined as $\mathscr{F}(E)dE = vN(E)dE$ and the power law can be written as

$$\mathscr{F}(E) \propto E^{-\delta} \tag{5}$$

where $\delta = (s-2)/2$ for sub-relativistic particles. For ultra-relativistic particles, $v \sim c$ so that $\mathscr{F} \sim cN$ and δ remains the same as in the differential density case, $\delta = s-2$.

To diagnose accelerated electrons in the solar corona, hard X-ray (HXR) observations of electron bremsstrahlung emission are used (e.g. Brown 1971; Tandberg-Hanssen and Emslie 1988; Holman et al. 2011) as summarized below. A caveat is that the initial distribution $\mathscr{F}(E_0)$ may evolve into a different distribution $\mathscr{F}(E)$ by energy loss processes (primarily Coulomb collisions) within the duration of the X-ray measurement. These distributions are often described as 'injected' and 'instantaneous' distributions in solar flare studies, respectively. Two extreme models can be considered for the evolution.

In the *thin-target* model, non-thermal electrons do not lose much energy and preserve their distribution so that $\mathscr{F}(E) = \mathscr{F}(E_0)$. The **differential photon flux** (or flux density) $I(\varepsilon)$ (photons $\mathrm{cm^{-2}s^{-1}keV^{-1}}$) can be derived by

$$I(\varepsilon) = \frac{S\Delta N}{4\pi R^2} \int_\varepsilon^\infty \mathscr{F}(E_0)\, \sigma_B(\varepsilon, E_0) dE_0, \tag{6}$$

where S is the flare area, σ_B is the Bremsstrahlung cross section (differential in photon energy ε, $\mathrm{cm^2\ keV^{-1}}$), R is the distance between the observer and the X-ray source, $\Delta N = \int_{\mathrm{source}} n_p(s) ds$ is the column density of the source observed, and $n_p(s)$ is the ambient proton density as a function of the distance along the injected electron path (e.g. Tandberg-Hanssen and Emslie 1988). It has been shown that, for a single power-law electron population $\mathscr{F}(E_0) \propto E_0^{-\delta}$, $I(\varepsilon)$ is also a power-law of the form

$$I(\varepsilon) \propto \varepsilon^{-\gamma_{thin}}, \tag{7}$$

where $\gamma_{thin} = \delta + 1$.

In this conversion, the nonrelativistic Bethe-Heitler (NRBH) bremsstrahlung cross section is used for σ_B. Thus, there would be an error in this conversion if there were significant flux at and above (near-)relativistic energies. Some studies report electron power-law index δ obtained by numerical computations with the relativistic Bethe-Heitler cross-section incorporated into the RHESSI spectral analysis software (OSPEX) (Holman et al. 2011), removing our need to convert from γ to δ. However, some other studies report photon power-law index γ only. Furthermore, in addition to the assumption in the cross-section, there are other important sources of errors and uncertainties in spectral analysis (See Section 3 of Holman et al. (2011)). It is beyond the scope of this paper to correctly and accurately derive the electron power-law index δ for all published values of γ. Thus, for the sake of comparison with the δ values in space obtained via *in-situ* measurements, we simply keep using this conversion as needed (i.e., Eq. (7)), while focusing on the values obtained in the sub-relativistic energy range (typically $\lesssim 100$ keV).

In the *thick-target* model, non-thermal electrons lose all of their non-thermal energies and thermalize. By considering the energy loss (from E_0 to E), the photon spectrum can be described as

$$I(\varepsilon) = \frac{S}{4\pi R^2}\frac{1}{C}\int_{E_0=\varepsilon}^{\infty} \mathscr{F}(E_0)\int_{\varepsilon}^{E_0} E\,\sigma_B(\varepsilon,E)dE dE_0, \tag{8}$$

where $C \equiv 2\pi e^4 \ln\Lambda$ and Λ is the Coulomb logarithm. Comparing this expression with Equation (6), we can define the effective column density $\Delta N_{\rm eff}$ as

$$\Delta N_{\rm eff} \equiv \frac{1}{C\sigma_B(\varepsilon,E_0)}\int_{\varepsilon}^{E_0} E\,\sigma_B(\varepsilon,E)dE. \tag{9}$$

This model considers the case where all non-thermal electrons thermalize due to Coulomb collisions, and the X-ray emission does not explicitly depend on the source density. However, the effective column density $N_{\rm eff}$ arises from a consideration of the evolution from E_0 to E. This thick-target model is valid if the actual (observed) column density is sufficiently large, i.e., $\Delta N \gtrsim \Delta N_{\rm eff}$. Otherwise ($\Delta N \ll \Delta N_{\rm eff}$), the model should not be applied. It has been shown that, for a single power-law electron population $\mathscr{F}(E_0) \propto E_0^{-\delta}$, $I(\varepsilon)$ is also a power law of the form

$$I(\varepsilon) \propto \varepsilon^{-\gamma_{thick}}, \tag{10}$$

where $\gamma_{thick} = \delta - 1$. (Again, the nonrelativistic Bethe-Heitler (NRBH) bremsstrahlung cross section is used for σ_B.) Because higher energy electrons lose energy and emit more photons than in the case of thin-target model, the resultant thick-target photon spectrum becomes harder, i.e., $\gamma_{thick} < \gamma_{thin}$.

While a single power-law is already useful when characterizing particle energy spectra with a clear distinction between thermal and non-thermal components (Figure 1(b,c)), the kappa distribution is also useful when there is no clear spectral break between the lower and higher energy components (Figure 1(d)). The isotropic, three-dimensional (3D) form of the **kappa distribution** $f_\kappa(v)$ (s^3 cm^{-6}) is written as

$$f_\kappa(v) = \frac{N_\kappa}{(\pi\kappa\theta^2)^{3/2}}\frac{\Gamma(\kappa+1)}{\Gamma(\kappa-1/2)}\left(1+\frac{v^2}{\kappa\theta^2}\right)^{-(\kappa+1)}, \tag{11}$$

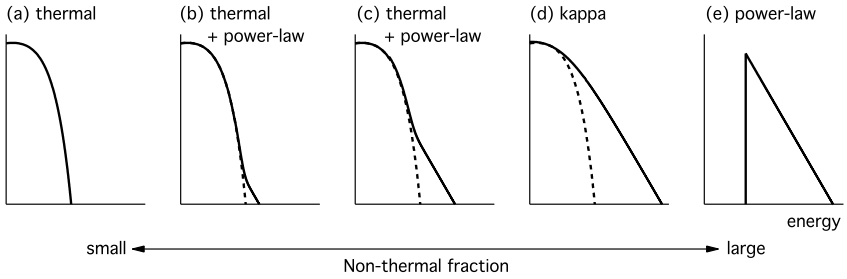

Fig. 1 Schematic illustrations of basic non-thermal distributions, adapted from Oka et al. (2015). The horizontal and vertical axes (both logarithmic) represent particle energy and differential density, respectively. The core distribution and the power-law slope are fixed while the intensity of the power-law component is varied. To quantify non-thermal fraction of particle densities/energies, a lower-energy cutoff E_c of the power-law tail is required. For the kappa distribution, E_c is no longer needed and a formula for estimating the non-thermal fraction is proposed in Oka et al. (2015).

where v is the particle speed, κ is the power-law index, Γ is the Gamma function, N_κ is the number density, and θ is the most probable particle speed at which the differential flux becomes maximum[3].

Note that the thermal speed (of a particle with mass m) depends only on the temperature T of the system, $v_{th} = \sqrt{2k_BT/m}$, and it actually represents the temperature in speed units (k_B is the Boltzmann constant). The auxiliary quantity $\theta \equiv v_{th} \cdot \sqrt{(\kappa - 3/2)/\kappa}$ is used in 3-D kappa distributions, as it coincides with the most probable speed. Nevertheless, care is needed because (i) the coincidence of θ with the most probable speed holds only for the 3-D case, and (ii) the temperature and not the most probable speed constitutes a fundamental thermodynamic parameter, as it is determined from the equipartition theorem and the thermodynamic definition of temperature; therefore, the speed θ depends on κ, and should not be used for demonstrating the kappa distributions for various kappa indices, while the temperature, v_{th} or T, is independent of κ, and is preferred when considering variations of κ (see Livadiotis (2015a) and Chapter 1 of Livadiotis (2017) for further details; see also Lazar et al. (2016) for different perspectives of the definition of the temperature).

The kappa distribution is suitable for characterizing an observed energy spectrum with no clear distinction at the interface between the thermal core and the power-law tail (Figure 1(d)). For such a distribution, a fit with the combined 'thermal+power-law distribution would lead to systematically higher temperatures and lower densities due to an artificial, lower-energy cutoff of the power-law (Oka et al. 2015). A combined 'thermal+power-law' model is suitable if there was a clear spectral transition, from soft (steep) to hard (flat), at the interface between the two component (Figure 1(b,c)). It should also be noted that the kappa distribution maximizes the entropy of nonextensive statistical mechanics, providing an important context for our studies of power laws (Appendix B).

In space, a particle velocity distribution can often have a non-thermal tail extending from a flattop core distribution (e.g. Feldman et al. 1982, 1983a; Thomsen et al. 1983; Chateau

[3] This kappa distribution is equivalent to the modified kappa distribution formulated by Leubner (2004) and used by, for example, Bian et al. (2014). The transformation can be expressed as $\kappa^* = \kappa + 1$ and $\theta^* = \theta\sqrt{\kappa/\kappa+1}$ where κ^* and θ^* are the spectral index and the most probable speed of the modified kappa distribution, respectively (Livadiotis and McComas 2009).

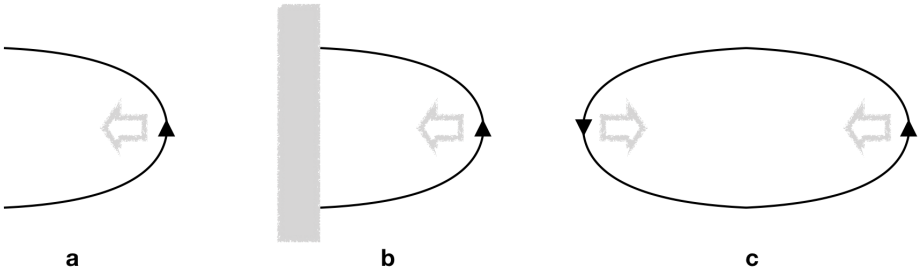

Fig. 2 Schematic illustrations of a magnetic field line favorable for Fermi Type B acceleration: (a) a curved magnetic field line as in the original illustration by Fermi (1949), (b) a line-tied version, and (c) a magnetic island version. In the line-tied version, particles can be trapped due to mirror reflection at the footpoints. An energization 'kick' can occur at the curved tip of the field line and/or the mirror points. See Appendix C for more details.

and Meyer-Vernet 1989). Such a **flattop distribution** is sometime expressed empirically as

$$f_L(v) = \frac{N_L \kappa \sin(\pi/2\kappa)}{\pi^2 v_{\perp L}^2 v_{||L}} \left[1 + \left(\frac{v_\perp}{v_{\perp L}} \right)^{2\kappa} + \left(\frac{v_{||}}{v_{||L}} \right)^{2\kappa} \right]^{-\frac{\kappa+1}{\kappa}}, \tag{12}$$

where N_L is the density, κ is the spectral index and v_L is the location and sharpness of the spectral break (or 'shoulder'). In the higher energy limit ($v \gg v_L$), the distribution approaches a power-law $f \propto v^{-2(\kappa+1)}$ as is the case with the kappa distribution (e.g. Vasyliunas 1968). In the lower energy limit ($v \ll v_L$), the distribution becomes flat at $f = N_L \kappa \sin(\pi/2\kappa)/(\pi^2 v_{\perp L}^2 v_{||L})$. Also, Štverák et al. (2009) proposed a similar but slightly different form of the flattop distribution.

The flattop distribution has been observed in a kinetic-scale region where a potential drop develops. Examples include the shock transition layer (e.g. Feldman et al. 1982, 1983a; Thomsen et al. 1983) and the vicinity of magnetic reconnection diffusion region (e.g. Asano et al. 2008; Chen et al. 2009; Egedal et al. 2010; Wang et al. 2010; Teh et al. 2012; Nagai et al. 2013; Oka et al. 2016). We note that there have been some physical explanations to the flattop core component (e.g. Dum 1978; Karlický et al. 2012; Fujimoto 2014; Egedal et al. 2015). For the entire spectral shape including both the flattop and non-thermal tail features, there has been a discussion from the non-Euclidean-normed statistical mechanics (Eq.(66) of Livadiotis 2016).

1.4 General Theories of Power-Law Formation

Where does a power law come from? There is a wide variety of theories of particle energization in both solar and space physics contexts, and readers are referred to comprehensive reviews for the details of those theories (e.g. Miller et al. 1997; Aschwanden 2005; Zharkova et al. 2011; Birn et al. 2012; Petrosian 2012). When it comes to the formation of power laws, however, many of those theories resort to stochasticity (i.e., random motion of particles). Fermi's approach (Section 1.4.1) is the classical way to treat stochastic acceleration. A Fokker-Planck approach is a convenient way to study stochastic acceleration in detail, and it even leads to the kappa distribution as a solution under certain conditions (Section 1.4.2).

1.4.1 Fermi's approach

In a stochastic process, particles bounce back and forth between scattering agents (such as plasma waves and turbulence). A net energy gain is achieved when the frequency of head-on collision with scattering agents is larger than the frequency of head-tail collision. If there is a probabilistic escape process in the system, then a power-law energy spectrum can be formed and the power-law index depends on the timescale of the particle energization process as well as the timescale of the probabilistic escape process. In the original theory by Fermi (1949) who pioneered the stochastic process in the context of the origin of galactic cosmic rays, the resultant energy spectrum is derived as

$$N(E) \propto E^{-\left(1+\frac{\tau_{\rm acc}}{\tau_{\rm esc}}\right)} \tag{13}$$

where E is the particle energy, $\tau_{\rm acc}$ is the acceleration time scale, and $\tau_{\rm esc}$ is the escape time scale (The quantity $\tau_{\rm acc}/\tau_{\rm esc}$ is assumed to be energy independent). See Appendix C for the derivation and variations of the theory, i.e., the first and second-order Fermi acceleration for relativistic and non-relativistic conditions. It should be noted that, even if the acceleration region was sufficiently large or there was no escape process such that $\tau_{\rm esc} \to \infty$, we can still expect a power law.

Usually, waves and turbulence are invoked in many applications of the stochastic acceleration process. The importance of turbulence in a stochastic process is more fully described in Petrosian (2012). The widely-known application of the stochastic process with waves and turbulence is the diffusive shock acceleration (DSA) (e.g. Blandford and Eichler 1987). In DSA, particles experience stochastic first-order Fermi acceleration by moving back and forth across the shock front. They can be confined at and around the shock front by waves and turbulence.

However, we emphasize that stochasticity is not always required for particle energization, although it appears necessary for a power-law formation. For example, during shortening of a magnetic flux tube (as schematically illustrated in Figure 2b), all particles moving along the flux tube (with small pitch angles) may experience multiple Fermi acceleration (via, for example, mirror reflection and 'slingshot' effect (See Appendeix C)) but not necessarily escape or scattering (if waves/turbulence were absent). Here we simply define **Fermi acceleration** as an energization 'kick' by a moving structure (such as a curved magnetic field line, waves, turbulence). Fermi acceleration usually works statistically through multiple kicks. A **stochastic acceleration** is statistical Fermi acceleration combined with stochasticity with the form of, for example, probabilistic escape process. In the Fokker-Planck approach (also described in the following subsection), an escape process may not be included explicitly, but the stochasticity is represented by diffusion. It can lead to a power-law energy spectrum when a power-law form of turbulence spectrum is assumed. Sometimes, the two terms (i.e., Fermi acceleration and stochastic acceleration) are used interchangeably, probably because the original work by Fermi (1949) considered stochastic process to derive a power law. However, it is customary to distinguish the two terms (especially in the mangetospheric community) and we also follow the same definitions throughout this paper.

Another example that illustrates the difference between Fermi and stochastic acceleration is the particle energization process in magnetic islands (or fluxropes in 3D). Particles trapped within an island flanked by active X-lines at both ends (as illustrated in Figure 2c) are energized through Fermi Type B acceleration (Kliem 1994). The process is named 'contracting island mechanism' and can be expanded to a stochastic acceleration process in a system with many islands (Drake et al. 2006). The system with many islands may act like turbulence

and produce high-energy particles, especially in a three-dimensional system (e.g. Dahlin et al. 2015). A prediction of the power-law index, however, requires a phenomenological escape or diffusion process. In some cases, a sufficiently large escape time scale ($\tau_{\rm esc} \to \infty$) is considered so as to produce the hardest power law (and the smallest power-law index) (e.g. Drake et al. 2010; Guo et al. 2014) (See Eq. 13). It is also to be noted that, if the distribution of the island sizes followed a power law, i.e., fractal distribution, then the resultant particle energy spectrum may become a power law even if each island did not produce a power law (Nishizuka and Shibata 2013). Such an idea may be connected to the nonextensive statistical mechanics as it was introduced to describe multifractals (Appendix B).

1.4.2 Fokker-Planck approach

A stochastic process can be more conveniently described by a Fokker-Planck approach, and it has been used in various problems of particle acceleration. In collisionless plasmas, pitch angle scattering (by waves and turbulence) and associated diffusion are considered for the effective collisional term. This leads to the particle transport equation, which has been used to explain power-law spectra at shocks (e.g. Blandford and Eichler 1987). In such a treatment, particle distributions are typically a function of time t, velocity $\mathbf{v}$ and space $\mathbf{x}$, where $\mathbf{x}$ is needed to describe the shock structure.

However, a Fokker-Planck approach shows that turbulence alone (without a shock) can still lead to a non-thermal power-law tail, although the turbulence spectrum must be in a power-law form (e.g. Miller et al. 1996; Yoon et al. 2006; Zhdankin et al. 2017). Furthermore, the Fokker-Planck equation can also yield the kappa distribution as an analytical solution, as shown by e.g., Hasegawa et al. (1985) and Ma and Summers (1998). These authors included collisional friction in addition to diffusion by a specific type of waves such as high-intensity radiation field (Hasegawa et al. 1985) and whistler waves (Ma and Summers 1998).

Interestingly, Bian et al. (2014) followed the same derivation but made it clearer that the power-law index κ^* is the ratio between the acceleration time scale and collisional friction/deceleration time scale. (As noted in the footnote in Section 1.3, their definition of kappa (κ^*) is slightly different from the conventional definition of kappa (κ) and $\kappa^* = \kappa + 1$.) Their argument implies that any type of waves/turbulence can lead to a power-law as long as the diffusion coefficient D has the form of $D \propto 1/v$. Their result, i.e., $\kappa^* = \tau_{\rm acc}/2\tau_{\rm c}$ where $\tau_{\rm acc}$ and $\tau_{\rm c}$ are the acceleration and collisional friction time scales, respectively, reminds us of the power-law index given by Fermi (Eq. (13)). A caveat is that this formula and the observed values of κ (as reviewed in this paper) implies the collision time to be only an order of magnitude smaller than the acceleration time scale. In contrast, the collision time-scale can be many orders of magnitude larger in Earth's magnetotail and in solar flares where a thin-target model of the hard X-ray emission can be assumed. And yet, the electron kappa distribution has been directly observed in Earth's magnetotail (Section 3) and it may also exist in a thin-target hard X-ray source of flares (Section 2.4.1).

Nevertheless, the possible involvement of Coulomb collisions in the generation of kappa distributions is not surprising if we consider the energy dependence of the collision frequency. The cross-section for the Coulomb collisions among particles varies with particle energy E as E^{-2} and the collision frequency scales as $E^{-3/2}$ (See textbooks by, for example, Benz (1993) and Kulsrud (2005)). Thus, it takes longer for higher-energy particles to equilibrate (e.g. Dudík et al. 2017). Such an effect can be considered in an environment with density gradient (such as the solar atmosphere) to explain the origin of the non-thermal tail without resorting to wave-particle interactions (e.g. Scudder and Olbert 1979). (A detailed review of

non-thermal particles in a collisionally dominated non-equilibrium plasma can be found in Dudík et al. (2017).)

On the other hand, many of the theories of power-law formation by waves and turbulence (as reviewed above) consider the test-particle limit in which there is no feedback to particles from the waves and turbulence, although recent particle simulations of relativistic plasmas produce power laws (e.g. Guo et al. 2014; Zhdankin et al. 2017). In this regard, Yoon et al. (2006) considered the self-consistent acceleration of electrons to suprathermal energies by weak turbulence processes which involve the Langmuir/ion-sound turbulence and the beam-plasma interaction. In their theory, the spontaneously emitted thermal fluctuations act like the collisional drag in the Fokker-Plank equation. Further developments of the theory can be found in their recent work (e.g. Yoon et al. 2012; Yoon 2014; Yoon et al. 2016). Because they argue that the kappa distribution represents what they call 'turbulent equilibrium' between electrons and enhanced Langmuir turbulence, their theory may have a connection to the nonextensive statistical mechanics in which the kappa distribution is illustrated as the state of maximum entropy of non-equilibrium plasmas as we discuss in Appendix B.

2 Power Laws in Solar Flares

There are many reviews of solar flares and associated particle acceleration (e.g. Miller et al. 1997; Aschwanden 2005; Krucker et al. 2008c; Lin 2011; Kontar et al. 2011; Fletcher et al. 2011; Zharkova et al. 2011; Holman et al. 2011; Petrosian 2012; Benz 2017; Dudík et al. 2017). Here we focus on the power-law index measured in the sub-relativistic energy range (typically < 100 keV), as summarized in Figure 3.

2.1 Overview

Solar flares are the most energetic phenomena in our solar system. They release energy, previously stored in the magnetic field, of the order $10^{32} - 10^{33}$ erg in only seconds to minutes, converting it to accelerated particles and heating all the layers of the solar atmosphere.

The standard solar flare scenario envisages energy release via reconnection near or above the top of magnetic loops that are rooted to the solar surface. As a result, electrons, protons, and ions are accelerated up to relativistic speeds. The accelerated particles are then either ejected into interplanetary space along open field lines (and may be observed *in-situ* as solar energetic particles (SEPs)) or get trapped in closed magnetic loops where they propagated downward toward the dense chromosphere and photosphere. In the latter case, the accelerated particles deposit their energy into the chromosphere. This results in heating and expansion of chromospheric plasma upwards into the magnetic loop (termed chromospheric evaporation). Figure 4 illustrates this model. See also Holman (2016) and references therein for the standard flare model.

The signatures of accelerated electrons and heated plasma are readily observed in X-rays at energies of a few keV up to a few hundred keV. They are bremsstrahlung emission caused by electrons suffering Coulomb collisions with the ambient plasma (e.g. Holman et al. 2011, and references therein). Their intensity depends on the plasma temperature, amount of heated plasma (emission measure), ambient density, and electron number, but not on the magnetic field strength[4] (Eqs. (6) and (8) in Section 1.3). If a photon energy spectrum exhibits a

[4] In addition to X-rays, radio emissions can also be used to diagnose energetic electrons during flares (e.g. White et al. 2011; Nita et al. 2015). The radio emission can depend on the magnetic field strength.

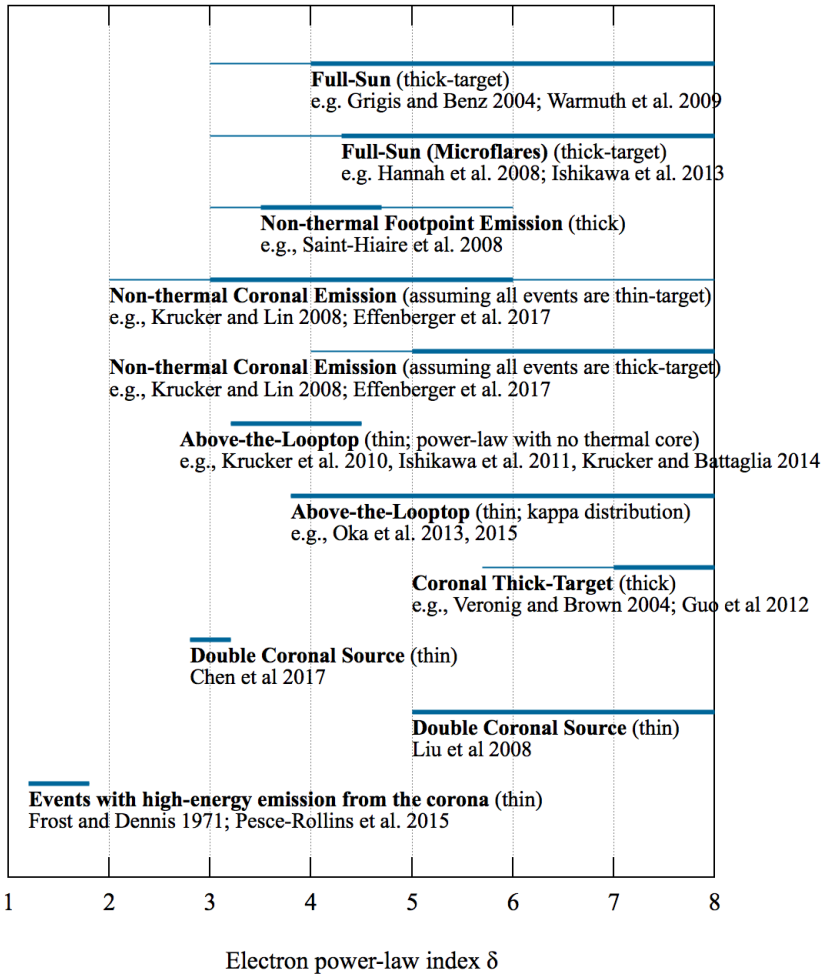

Fig. 3 An overview of electron power-law index δ reported by different studies of solar hard X-ray measurements in the < 100 keV energy range. Various assumptions and/or different degrees of uncertainties could be involved in the conversion from the photon power-law index γ to the electron power-law index δ (See Sections 1.3 and 2.1). The assumption of thin- or thick-target emission model is indicated in the parenthesis for each category. For statistical studies, typical values are shown by thick lines. For non-statistical studies, only the thick lines are used to display reported values. See texts in this section for more details and caveats of each category.

power-law distribution (with the power-law index γ), then the spectrum of the electrons that emitted the X-rays must also have a power-law component (with the power-law index δ). In converting γ to δ, a caveat is that one has to make an assumption on the density of the *target* (the ambient plasma) with which X-ray-emitting electrons collide. For large column densities, such as in the dense chromosphere, in which the electrons lose their energy completely in collisions, the thick target model for bremsstrahlung emission is applicable (e.g. Brown 1971; Kontar et al. 2011). For smaller column densities, the electron spectrum will not be affected significantly and a thin target approximation is used. Whether a target acts as thin or thick

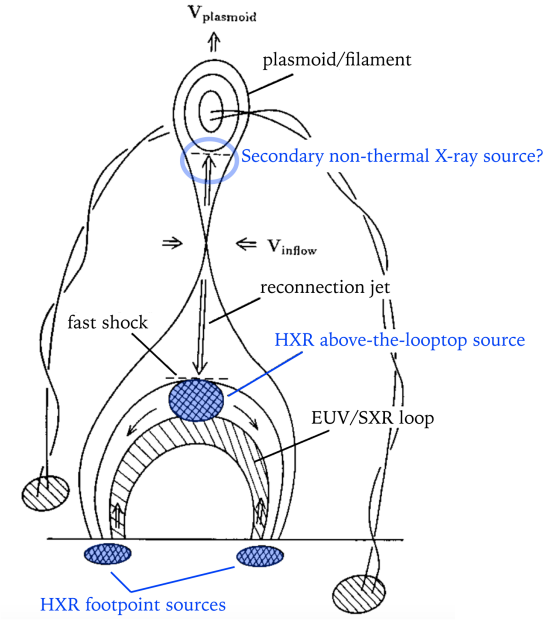

Fig. 4 Cartoon of the standard solar flare scenario, as adapted from Shibata et al. (1995). This cartoon is based on the discovery of the Masuda flare in which the coronal hard X-ray (HXR) source was located 'above' the EUV/SXR loop (See also Section 2.4.1 and Figure 6). A power-law spectrum has been observed in the blue-shaded regions at the footpoints and the above-the-looptop region. In many cases, however, the flare size is smaller than that of the Masuda flare, and the coronal HXR source appears cospatial with the lower-energy X-ray source and closer to the apex of the EUV/SXR loop.

depends on the energy of the accelerated electron and the ambient density. Hence, in many cases, an 'intermediate thin-thick target' model (e.g. Wheatland and Melrose 1995; Battaglia and Benz 2007) may be needed to describe the full spectrum. See Section 1.3 for more details of the conversion between γ and δ and the target-assumptions.

While hard X-ray (HXR) imaging capability was already available by the 1980s (e.g. Van Beek et al. 1980), the observationally easiest and most often applied analysis of flare spectra is the fitting of 'full-Sun,' i.e. spatially integrated, spectra. Figure 5 shows an example of a full-Sun X-ray spectrum with no spatial information, as obtained by Reuven Ramaty High Energy Solar Spectroscopic Imager (RHESSI, Lin et al. 2002)[5]. There is clearly a spectral break at around 18 keV in this case. (Typically, the break energy is in the 10 – 20 keV range.) Thus, when characterizing and fitting spectral data, thermal and non-thermal power-law distributions are used for the lower and higher energy components, respectively. For the lower energy range (typically $<$ 10 keV or 'soft X-rays (SXRs)'), this iso-thermal (single Maxwellian) model usually fits the data well, although flaring plasma is known to be multi-thermal (However, RHESSI's temperature sensitivity range (upward of $\sim$ 8 MK) does not allow for constraining cooler temperatures). For the higher energy range (typically $>$ 20 keV or 'hard X-rays (HXRs)'), the power-law model also fits the data well, although

[5] RHESSI observes the full Sun through 9 rotating collimators, allowing to make images of flaring sources and infer spectra from individual sources (e.g. Battaglia and Benz 2006; Krucker and Battaglia 2014). However, in Figure 5, the data is spatially-integrated to produce the full-sun spectrum. Similar spectral forms have been already obtained by earlier works (e.g. Lin et al. 1981)

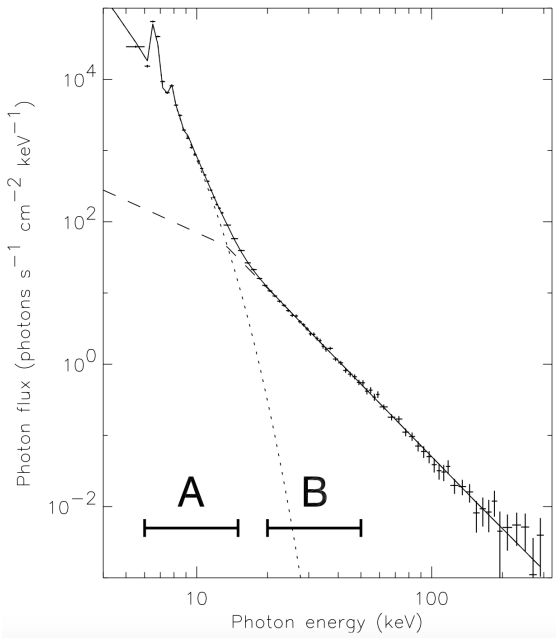

Fig. 5 A typical 'full-sun' (spatially integrated) X-ray spectrum during flares, adapted from Figure 1 of Grigis and Benz (2004). Reproduced with permission ©ESO. The dotted line is a thermal distribution model, representing the lower-energy component. The dashed line is a power-law model with a lower-energy cutoff at $E_{\rm cutoff}$ = 13.4 keV, representing the higher-energy component. Note the extension of the power-law below the cutoff energy. This part of the spectrum is unobservable due to the intense low-energy component. However, under the assumption that the electron spectrum has a sharp cut-off at $E_{\rm cutoff}$, the resulting photon spectrum would have the shape of the dashed line, as every electron of a given energy (say 10 keV), can emit many photons below this energy. The narrow peaks in the lower energy range are the Fe ($\sim$6.7 keV) and Fe - Ni ($\sim$8 keV) excitation line complexes.

it requires a somewhat unphysical, lower-cutoff energy $E_{\rm cutoff}$. There is a wide variety of discussions on $E_{\rm cutoff}$ as reviewed by Holman et al. (2011) (See also Holman (2016) for more details on the terminology).

X-ray imaging revealed that the higher-energy, non-thermal component comes primarily from the chromosphere at the footpoints of the flaring loop, while the lower-energy, thermal component comes from the corona at and around the top of the flaring loop, as illustrated in Figures 4 and 6. The higher-energy non-thermal emissions can also come from the corona at and around the looptop region, although the intensity is much lower than that of the footpoint emissions. In rare cases, such faint and non-thermal emissions are originating from somewhat 'above' the mostly thermal looptop region (e.g. Masuda et al. 1994, See also Figures 4 and 6). The separation distance between the thermal 'looptop' region and non-thermal 'above-the-looptop' region can be roughly 10 - 20 Mm (e.g. Krucker et al. 2010; Oka et al. 2015). This does not necessarily mean that thermal component does not exist in the 'above-the-looptop' region. Due to observational constraints (in particular, the limited dynamic range) and the presence of the very bright emission from the looptop region, it has been difficult to measure the thermal component that exists locally in the above-the-looptop region. (With the similar reason, the thermal components from the footpoint sources are difficult to observe.)

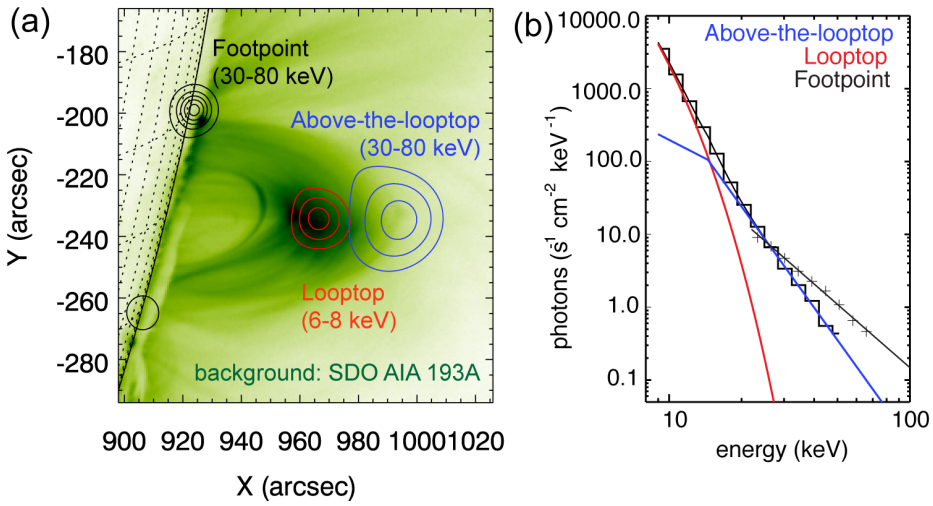

Fig. 6 Imaging spectroscopy from the solar limb flare SOL2012-07-19T05:58. Left: X-ray images as measured by RHESSI (contours) superposed on an extreme ultra-violet (EUV) image as measured by SDO/AIA. Right: Photon energy spectra from the chromospheric footpoint sources (crosses) and the combined coronal sources (histogram). The crosses are fitted with a power-law (black) and the histogram is fitted with a combined thermal (red; representing the looptop source) and non-thermal (blue; representing the above-the-looptop source) spectra. Both the right and left panels are adapted from Fig. 1 of Krucker and Battaglia (2014) but the color scheme is altered so that the same color indicates the same source in both panels. The left panel is actually a reproduction by Oka et al. (2015).

Below, we focus only on the non-thermal, power-law component observed in full-sun spectra, chromospheric footpoint sources, and in the corona.

2.2 Full-Sun Spectra

Full-sun spectra allow for investigating the time-evolution of single events and for statistical studies of larger sets of flares of different sizes (e.g. Holman et al. 2003; Grigis and Benz 2004; Emslie 2004; Warmuth et al. 2009). It has been shown that, in many flares, the time-evolution of the non-thermal tail follows the so-called soft-hard-soft pattern (e.g. Grigis and Benz 2004), i.e. the photon spectrum starts out rather soft, becomes harder (flatter) as the X-ray flux increases, and becomes softer (steeper) again as the emission decreases. This pattern has even been observed for individual peaks of the same flare (Grigis and Benz 2005). One interpretation of this is that the acceleration mechanism itself undergoes a change in efficiency as the flare progresses (e.g. Grigis and Benz 2006; Bykov and Fleishman 2009). Full-sun spectra have also been used in various studies of correlations between flare parameters, such as temperature, emission measure, X-ray flux and power-law index of flares of different sizes (as measured by GOES class). A typical finding is that larger flares tend to be hotter and have more non-thermal flux (e.g. Ryan et al. 2012; Warmuth and Mann 2016). However, Battaglia et al. (2005) showed that there seems to be no correlation between the photon power-law index γ and the GOES class, i.e. even some smaller flares exhibit rather hard spectra. In fact, there have been statistical studies of power-law spectra in microflares (e.g. Christe et al. 2008; Hannah et al. 2008). Using Suzaku data, Ishikawa et al. (2013) showed that the power-law spectrum can reach up to at least 100 keV even in smaller events.

In the compilation of the reported numbers of the power-law index δ in Figure 3, we assumed the thick-target model for full-sun spectra. This is because, in many cases, non-thermal X-ray emission originates primarily from the footpoint sources located in the dense chromosphere, which acts as a thick-target on all electrons.

2.3 Non-thermal Emission in Footpoints

As outlined above, hard X-ray (HXR) sources at the footpoints of magnetic loops are non-thermal, thick target emission of accelerated electrons as they are stopped in the dense chromosphere (e.g. Hoyng et al. 1981a,b; Sakao 1994; Sakao et al. 1996; Aschwanden et al. 1999; Krucker and Lin 2002; Emslie et al. 2003; Saint-Hilaire et al. 2008; Yang et al. 2012). Due to the high chromospheric density they are typically bright and thus easy to observe, often up to energies of more than 100 keV. Most flares show two footpoints (e.g. Saint-Hilaire et al. 2008), although events with three or more footpoints have been reported (e.g. Emslie et al. 2003). Because of their brightness, HXR footpoints have invaluable diagnostic potential for the locations and amount of energy deposition into the chromosphere the acceleration mechanism and even chromospheric properties such as density (e.g. Kontar et al. 2008; Battaglia and Kontar 2011; Chen and Petrosian 2013).

According to a statistical analysis by Saint-Hilaire et al. (2008), the typical photon power-law index γ is 2.5 - 4.5. These authors also reported that, in double-footpoint structures, the power-law index differences $\Delta\gamma$ is not large, ranging mostly between 0 and 0.6. Such an asymmetry can be attributed to (a) different magnetic field intensities and associated mirror effect (e.g. Sakao 1994; Sakao et al. 1996; Aschwanden et al. 1999; Saint-Hilaire et al. 2008; Liu et al. 2009) or (b) different column densities and associated acceleration and/or transport effect along the loops (e.g. Emslie et al. 2003; Liu et al. 2009). Recently, Daou and Alexander (2016) used 1D Fokker-Planck simulations to investigate the relationship between the footpoint X-ray emission and the magnetic field ratio. They reported that the asymmetry A of the X-ray intensity I, where $A \equiv (I_1 - I_2)/(I_1 + I_2)$ (See also Alexander and Metcalf 2002; Liu et al. 2009), reaches its saturation value close to unity when the footpoint magnetic field ratio reaches $\sim$4. As the bremsstrahlung emission itself does not depend on the magnetic field intensity, these studies indicate that the X-ray emitting electrons behave differently in the two end of the loop.

2.4 Non-thermal Emission in the Corona

As outlined above, non-thermal X-ray emission from the corona is significantly fainter when compared to that from the footpoint sources. Thus, characterizing the spectral properties of non-thermal coronal emission remains challenging as described below.

If the standard flare configuration was viewed from the top by an earth-orbiting satellite, it would be difficult to distinguish between emission originating from the chromosphere and emission from the corona, due to projection effects. Hence, a large number of studies has focused on flares that occurred typically a few degrees or more behind the solar limb (e.g. Tomczak 2001; Krucker and Lin 2008; Tomczak 2009; Effenberger et al. 2017). In such 'occulted' events, footpoint sources are masked by the solar disk, and high-energy emissions in the corona can be observed without being limited by the dynamic range of the instrument. Krucker and Lin (2008) studied 55 occulted events in the RHESSI database and found higher-energy emissions that could be fitted with a power law in 50 events, establishing

the presence of non-thermal plasmas in the corona. They also reported that the centroid positions of such non-thermal sources are close to the location of thermal emission observed at lower energies to within ∼2 Mm, consistent with an earlier finding by Yohkoh (Tomczak 2001). More recently, Effenberger et al. (2017) added 61 occulted flares and, from the total of 116 occulted flares, confirmed the results by Krucker and Lin (2008).

Typical electron power-law indices δ in these events range from 3 to 6 (compare Figure 3). These were inferred under the thin-target assumption, as the density in these sources can be expected to be sufficiently low for the target to act as thin. However, without a rigorous determination of the density and the column depths, one cannot exclude the possibility that, at least some of these events act as a thick target on most electron energies.

In addition to these frequently observed emissions, there is a number of special types of events, as described in the following subsections.

2.4.1 Above-the-looptop events

A special case of coronal hard X-ray (HXR) source is sometimes observed above the top of the EUV loop. Such above-the-looptop (ALT) sources are also called 'Masuda-type' sources, after the author who first reported them (Masuda et al. 1994). Only a few cases of above-the-looptop sources have been reported by RHESSI (e.g. Krucker et al. 2010; Ishikawa et al. 2011; Oka et al. 2015; Liu et al. 2013; Liu 2013). Unlike the aforementioned, typical cases in which the non-thermal source height H (from the solar surface) ranges between roughly 4 - 20 Mm, the above-the-looptop source is found in large flares with H roughly 20 - 60 Mm. The separation distance d between the ALT source and the thermal X-ray source around the looptop (LT) region is also large, 10 - 20 Mm, in contrast to the values in the typical cases, i.e., $|d| < 2$ Mm (Krucker and Lin 2008; Effenberger et al. 2017).

The X-ray spectrum from the above-the-looptop source exhibits a non-thermal power-law component. It was argued that a standard scenario, with hard X-rays produced by a beam comprising the tail of a dominant thermal core plasma, does not work (Krucker et al. 2010). Instead, it was proposed that all electrons in the ALT source are 'bulk-energized' to form a power law with no thermal particles left (Krucker et al. 2010; Krucker and Battaglia 2014; Ishikawa et al. 2011) and that precipitating electrons are emptying out of the ALT source to produce the footpoint emissions (Ishikawa et al. 2011).

What leads to such a 'bulk-energization' of electrons remains unclear to date. Radio emission from the above-the-looptop region can exhibit spectral features similar to solar Type II radio bursts (which are associated with propagating shocks in the outer corona), suggesting that there could be a fast-mode shock in the above-the-looptop source as a consequence of collision between the downward reconnection outflow and the pre-existing flaring loop (e.g. Aurass et al. 2002; Aurass and Mann 2004; Mann et al. 2009). A recent study provided more direct evidence of dynamically evolving (instead of stationary) fast-mode shock (Chen et al. 2015). On the other hand, another study of microwave emissions indicated the hardest power law at and around the reconnection point, suggesting that the reconnection region (instead of the above-the-looptop region) is the key location of electron acceleration (Narukage et al. 2014).

The spectral analysis of the above-the-looptop (ALT) source is challenging because of the limited dynamic range (and hence limited energy coverage, say, $\lesssim$80 keV). The lower-energy end of the ALT spectrum is masked by the intense emission from the adjacent (mostly thermal) source at the looptop (LT) and, in fact, it is difficult to completely separate the spectra from LT and ALT regions. Thus, the combined spectrum from both LT and ALT regions is fitted with a combined, thermal and power-law model where the thermal and

power-law components represent the LT and ALT sources, respectively (e.g. Krucker et al. 2010). Such a model implicitly assumes (and can lead to a conclusion) that there is no thermal electron in the ALT region (e.g. Krucker and Battaglia 2014). The possibility of a presence of a cold thermal core within the ALT region is rejected by a constraint derived separately from imaging analysis. An alternative (and yet simple) approach is to assume a hot thermal core in the ALT region while maximizing the intensity of the power-law component (Oka et al. 2013, 2015). Such a model can be represented by the kappa distribution as illustrated in Fig. 1 and used in other flare studies (e.g. Kašparová and Karlický 2009; Hannah et al. 2010; Battaglia et al. 2015). We emphasize that the kappa distribution model is still consistent with the idea of 'bulk energization' in a sense that all electrons in the ALT region have experienced energization. It should also be noted that a super-hot component has been identified in full-sun spectra in 'on-disk' events in addition to the brightest thermal component originating from the loop (e.g. Caspi and Lin 2010; Longcope et al. 2010; Caspi et al. 2014). Such a super-hot plasma may be related to the hot thermal core component in the ALT source as inferred by the kappa distribution model.

Regarding the power-law index, the introduction of the hot thermal core (and hence the extension of the thermal component toward the higher energy range) in the ALT region leads to a slightly softer power-law tail, although the boundary between thermal and non-thermal components is not explicitly visible in the case of the kappa distribution. For example, in the limb flare of SOL2012-07-19T05:58, Krucker and Battaglia (2014) used a single power-law with no thermal core to represent the ALT source and obtained $\delta \sim 3.6$ while Oka et al. (2015) used the kappa distribution and obtained $\delta \sim 4.1$. Of course, in principle, both models should return the same power-law index if the power-law tail extended toward much higher energies ($\gg$ 80 keV) and if the dynamic range of the measurement was large enough to cover such higher energy ranges. After all, the spectral form of the ALT source is not well constrained leading to the somewhat different values of the estimates of the power-law index.

2.4.2 Coronal thick-target events

While many solar flares display the typical morphology with two footpoints, there are cases for which footpoint sources are absent (even though they occur 'on-disk' where footpoint sources would not be masked) and flare emission at all energies originates from the corona (e.g. Veronig and Brown 2004; Sui et al. 2004). It has been described that the flaring loop was dense enough to become collisionally thick at observed energies and that all electrons deposit most of their energy before reaching the footpoints. Thus, such cases are referred to as coronal thick-target events and have been studied by different approaches (e.g. Xu et al. 2008; Guo et al. 2012b,a; Lee et al. 2013; Fleishman et al. 2016). Based on analysis and modeling of the source properties (such as the source size and number density distributions), it was argued that the coronal thick-target sources can be interpreted as sites of electron acceleration (e.g. Xu et al. 2008; Fleishman et al. 2016).

As for the energy spectra, the power-law slope is steep with the photon power-law index $\gamma > 6$ (e.g. Veronig and Brown 2004; Krucker et al. 2008c). Guo et al. (2012b) presented 22 cases of spectral analyses obtained from 11 flare events. It was reported that the lowest value of the electron power-law index δ (with the assumption of thick-target emission) is 5.7 but the typical value is in the range 7 - 9. They pointed out that, while the steepness could be a property of the electron acceleration process, it is also consistent with the absence of footpoint emission that the higher-energy electrons would produce in less-dense cases.

2.4.3 Other notable events

Magnetic reconnection generates bi-directional jets. In the standard flare model (Fig. 4), the 'above-the-looptop' source is found at or near the location where the downward jet would be obstructed by the flaring loop. However, in rare cases, a secondary, non-thermal emission can be found on the opposite (i.e., non-obstructed) side of the presumed location of magnetic reconnection (See the open circle in Figure 4) (e.g. Sui and Holman 2003; Sui et al. 2004; Liu et al. 2008, 2013; Chen et al. 2017). The dependence of source height on energy (temperature) was positive and negative in the primary (lower) and secondary (upper) source, respectively, suggesting a presence of highest temperature electrons in between the two sources. Sui and Holman (2003) interpreted this finding as evidence for a large-scale current sheet. Because of the dependence of source height on energy, the lower source can be viewed as the above-the-looptop (ALT) source. Furthermore, in the events reported by Sui and Holman (2003) and Sui et al. (2004), the lower source was actually considered thick-target, as described by Veronig and Brown (2004) and reviewed in the previous subsection.

Liu et al. (2008) reported a case in which both sources are non-thermal and the photon power-law index γ was 6 - 9. While the dependence of source height on energy was similar to that of Sui and Holman (2003), they argued that the inner emissions (i.e., those closer to the center of the primary (lower) and secondary (upper) source) showed a harder power-law spectrum than the outer emissions. Chen et al. (2017) argued, in another case study, that the upper source could be where side lobes (two different arcades) are rapidly approaching toward each other as a result of breakout eruption. The photon index was relatively small $\sim$4.

While coronal emission is generally faint and can be detected typically up to $\sim$ 100 keV, some cases show coronal emissions that extend up to γ-ray ranges. For example, Krucker et al. (2008a) reported very hard spectra with the photon power-law index γ between 1.5 and 2 in the 200 – 800 keV range. These events are not shown in Figure 3 because of the very different energy range.

Frost and Dennis (1971) also reported a high-energy coronal emission up to at least 250 keV in a behind-the-limb event. While the power-law spectrum was soft in the $\gtrsim$ 100 keV range, it was very hard in the $\lesssim$ 100 keV range with the photon power-law index $\gamma \sim 2.3$. With the thin-target emission model, the electron power-law index is $\delta \sim$1.3. This event was associated with Type II radio bursts and solar energetic particles (SEPs, see Section 4.1), indicating that a coronal mass ejection (CME) occurred and a CME-driven shock had formed in the solar corona.

While the precise origin of such a hard power law from the corona remains unclear, similar behind-the-limb events with CME/SEP signatures were reported (Pesce-Rollins et al. 2015). The main focus of this new study was a detection of $>$100 MeV gamma-rays for $\sim$ 30 min by the *Fermi* satellite, but it also showed a relatively hard power-law in the X-ray range ($\lesssim$ 100 keV). The authors reported that the photon power-law index γ was $\sim$3.8. This corresponds to the electron power-law index δ of $\sim$ 2.8 with the thin-target emission model. Possible connections between the $>$ 100 MeV gamma-rays, hard X-ray flare, and CME/SEPs are still debated (e.g. Ackermann et al. 2017).

2.5 Relation Between Coronal and Footpoint Sources

If the loop size is sufficiently large, the non-thermal coronal source can be well separated from the footpoint sources even in 'on-disk' events. In such a case, imaging spectroscopy (i.e., using multiple image to construct an energy spectrum for individual sources) allows us

to compare spectral relation between the two sources. In the simplest flare scenario, where the corona acts as a thin target on the same accelerate electron beam that, after propagation and neglecting transport, results in the observed thick target footpoint emission, the inferred spectral indices δ have to agree. In terms of the photon power-law index γ, it must be somewhere between the two extreme assumptions, i.e., $\gamma_{thin} = \delta + 1$ and $\gamma_{thick} = \delta - 1$. Thus, the difference between γ_c in the coronal source and γ_f in the footpoint sources must be no larger than 2.

However, Battaglia and Benz (2006) reported that, in 2 events out of 5, $\gamma_c - \gamma_f$ was larger than 2, indicating there was additional process that would make the footpoint spectra harder. They proposed transport effects due to return current, causing lower-energy electrons to preferentially lose their energies. On the other hand, Simões and Kontar (2013) reported 4 events that showed the electron power-law index δ_f in the footpoint sources significantly softer than that of the non-thermal coronal source δ_c. They suggested a presence of mechanisms that would keep a fraction of non-thermal electrons trapped inside the coronal loop. It is also to be noted that Krucker et al. (2008a) reported 3 cases of coronal γ-ray emission. While the energy range was much higher (200 - 800 keV), the photon power-law index γ (between 1.5 and 2) was substantially smaller than that of footpoint sources (between 3 and 4). Thus, they suggested that flare-accelerated high-energy ($\sim$MeV) electrons stay long enough in the corona to lose their energy by collisions producing γ-ray emission, while lower energetic electrons precipitate more rapidly to the footpoints. Regarding the theoretical interpretation of data, Chen and Petrosian (2013) examined two different flare events to discuss the energy dependences of basic characteristics in the framework of a stochastic acceleration mechanism.

3 Power Laws in Earth's Magnetotail

A comprehensive review of particle acceleration mechanisms in Earth's magnetotail and auroral region can be found in Birn et al. (2012). Here we focus on the power-law index measured in the magneotail in the typical energy range of less than a few hundreds of keV.

3.1 Overview

It has been reported that Earth's magnetotail extends more than 1000 R_E (or 6000 Mm) from Earth (e.g. Ness et al. 1967; Scarf 1987). Some studies reported possible detections of the magnetotail at farther locations such as 3000 R_E (Intriligator et al. 1979) and 15,000 R_E (or 0.63 AU) (Ashford et al. 1998) from Earth. Based on previous observations at various distances from Earth, it is now generally considered that, while a reconnection X-line forms sporadically at near-Earth, typically 20 – 30 R_E from Earth, there also exists a quasi-stationary X-line at the typical distance of 100 – 200 R_E.

Figure 7 shows a schematic illustration of an evolution of the magnetotail, involving both 'near-Earth neutral line' (NENL) and 'distant neutral line' (DNL). This illustration, based on observations in 1970s, indicates a formation and tailward (i.e., anti-sunward) motion of a plasmoid in the distant magnetotail. Previous missions such as *International Sun-Earth Explorer-3* (ISEE3, later renamed as *International Cometary Explorer*), *Geotail*, *Wind* and *ARTEMIS* explored the distant tail. These missions contributed to our understanding of the basic structure and convective motions of the distant magnetotail including slow shocks and plasmoids (e.g. Nishida et al. 1998, and references therein). Energetic electrons are

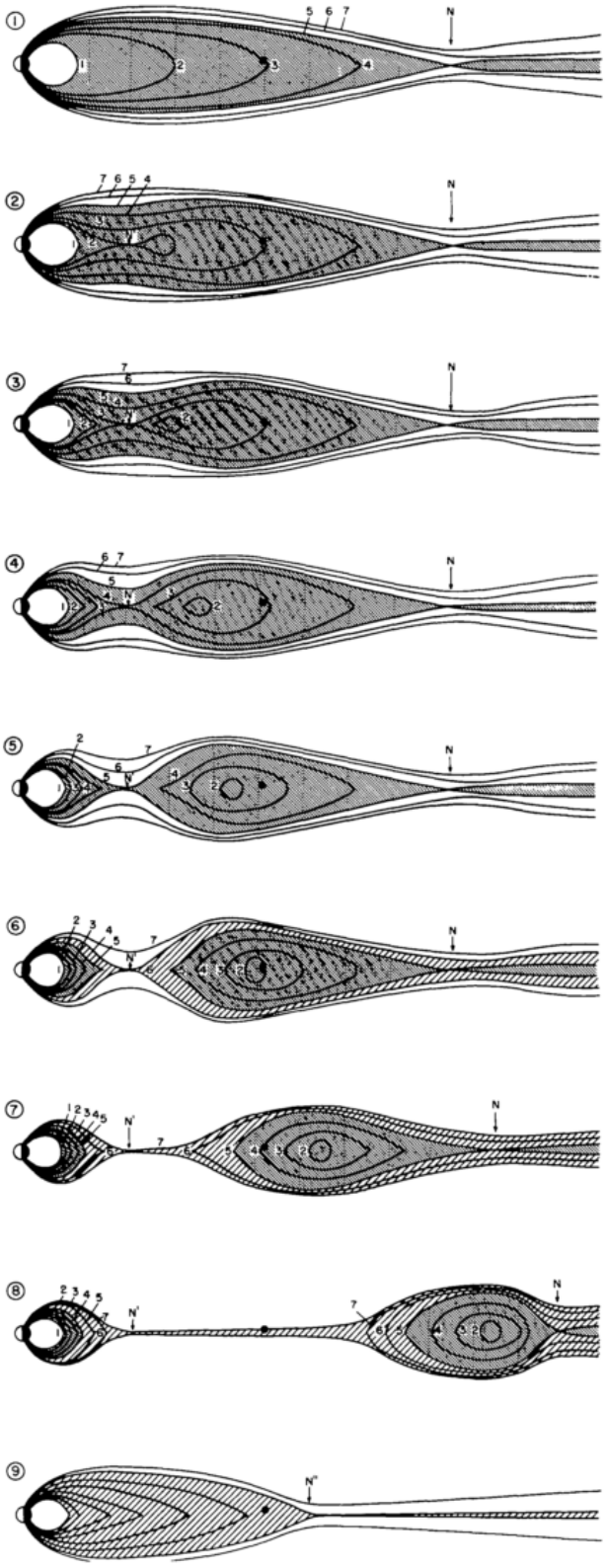

Fig. 7 Schematic illustration of an evolution of Earth's magnetotail, illustrating how and where magetic reconnection can take place, adaptes from Hones (1977). Each line represents a magnetic field line and the numbers (1 - 7) follow the same field lines. The near-Earth reconnection site (as illustrated in panels 3 - 8) is typically located at 20 - 30 R_E away from Earth, where R_E is Earth's radii ∼6378 km. The distant reconnection site (as illustrated in all panels) are typically located at 100 - 200 R_E away from Earth.

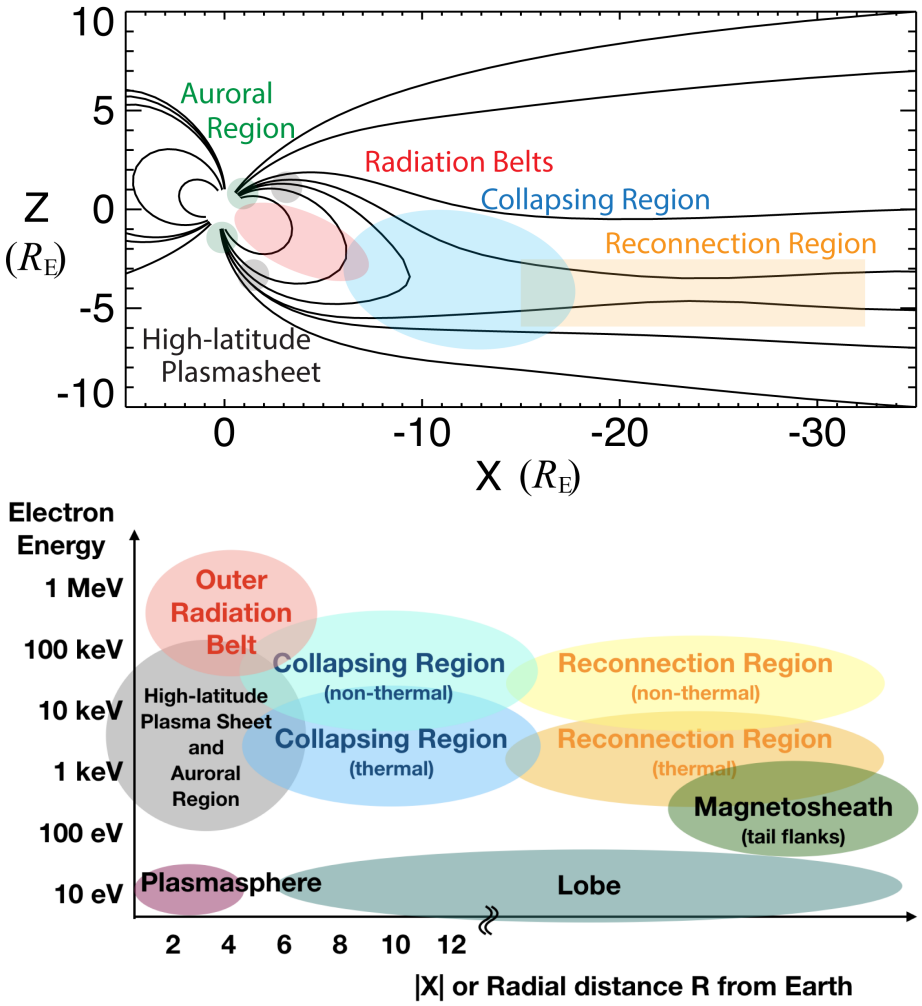

Fig. 8 Schematic illustrations of the regions referred to in this paper. *Upper panel*: The regions with respect to a semi-empirical model of the magnetic field lines (solid lines) (Tsyganenko 1995). The date of the model, i.e., 2009 February 7, is chosen arbitrarily for illustrative purpose. The Geocentric Solar Ecliptic (GSE) coordinate is used with the unit of Earth's radii R_E, ~6378 km. The GSE coordinate system is defined by X toward the sun, Z perpendicular to the plane of Earth's orbit around the Sun (positive North), and Y completing the right-hand system (approximately toward dusk). *Lower panel*: Key regions in the magnetotail and the typical electron energy ranges in those regions.

also observed in the distant tail as a detectable signature of the Hall effect of magnetic reconnection (e.g. Fujimoto et al. 1997; Manapat et al. 2006).

Figure 8 shows a typical structure of Earth's magnetotail more focused on the near-Earth region. Some of the regions discussed in this paper are schematically highlighted with colors. The **plasma sheet** is centered around the (magnetic equatorial) plane at which B_x reverses its sign and contains a relatively hot and dense plasma. It starts to be bifurcated in the collapsing region and extends along the inner magnetospheric field lines. When a polar-orbit spacecraft crosses such a bifurcated plasma sheet at high latitude (for example,

at the locations highlighted by the gray-shaded regions), it is referred to as 'high-latitude plasma sheet'. The typical parameters of the plasma sheet at the location of $X \sim 8 - 11$ R_E can be found in Table 3 of Appendix A.

In the plasma sheet, a spacecraft can detect additional features that indicate a passage of the **reconnection region**. During magnetic reconnection, magnetic field lines of opposite directions 'break' and 'reconnect' in the diffusion region. Within the ion diffusion region (or more precisely the Hall region), a quadrupolar structure of the magnetic field in the out-of-plane direction (i.e., Y direction) can be identified. A passage of the X-line can be identified by a correlated reversal of ion bulk flow V_x and magnetic field north-south component B_z. Such features are found typically between X = -15 and -30 R_E (but may occur even farther out). Reconnection in this location occurs sporadically and is closely related to magnetotail activity including the so-called 'substorms'.

On the earthward side of the near-tail reconnection site, magnetic field lines quickly collapse toward Earth's intrinsic dipole (**collapsing region**). This is typically associated with magnetic field dipolarization, manifested primarily by an increase of the north-south component of the magnetic field (B_z). Reconnection also results in fast plasma flows, which may be grouped into a ∼10-min sequence of multiple ∼1-min bursts ('Bursty Bulk Flows' (BBFs), Angelopoulos et al. (1992)). Such events need not be associated with substorms, but are generally correlated with activity.

Considering dipolarizations, one has to distinguish transient events, which are characterized by a short, temporary increase in B_z, from more permanent increases, which are generally observed closer to Earth (Nakamura et al. 2009). The transient events propagate earthward in association with earthward flows. Their earthward propagation can often also be demonstrated by multiple, radially spaced, satellites, specifically THEMIS (e.g. Runov et al. 2009). In contrast, the permanent dipolarizations typically do not show fast flows (e.g. Nakamura et al. 2002). While they are sometimes considered separate events, a more likely explanation, strongly supported also by MHD simulations (e.g. Birn et al. 2011), is that they result from the braking and diversion of the fast flows (e.g. Shiokawa et al. 1997; Nakamura et al. 2013). This causes an accumulation and pileup of the intensified B_z field, which then may lead to bouncing (Panov et al. 2010; Birn et al. 2011; Nakamura et al. 2013) and an expansion outward, both azimuthally (Nagai 1982; Miyashita et al. 2009, e.g.) and radially (e.g. Jacquey et al. 1991; Hesse and Birn 1991; Miyashita et al. 2009).

The region, or time interval, of a transient dipolarization is sometimes denoted Dipolarizing Flux Bundle (DFB) (Liu et al. 2013) or Flux Pileup Region (FPR) (Khotyaintsev et al. 2011). It should be noted, however, that this region is not the piled-up flux of the surrounding medium but rather the low-density material of an underpopulated flux tube (e.g. Pontius and Wolf 1990; Birn et al. 2004; Forsyth et al. 2008; Runov et al. 2011a), generated by reconnection.

The leading edge of an earthward DFB (or jet front) typically exhibits a distinct and localized structure of increasing B_z, the thickness of which is of the order of the ion inertia length d_i (e.g. Nakamura et al. 2002; Runov et al. 2009; Sergeev et al. 2009). Thus, the leading edge of the DFB has been termed 'dipolarization front'.

The electric field associated with dipolarization can penetrate even to within geosynchronous orbit. Otherwise one would not see dispersionless injection at the geosynchronous orbit (e.g. Gabrielse et al. 2014). This can make a large difference in allowing the energetic particles to get onto closed drift paths in the inner magnetosphere (from which they are excluded if the dipolarization stops farther out) and thereby increase the ring current population.

In the following sub-sections, we first describe some caveats that arise from the fact that there is a variety of different methodologies, datasets, and instrumentations. Then, we describe previous studies of power-law energy spectra focused on the plasma sheet without any identification of specific features (Section 3.3.1), the reconnection region (Section 3.3.2), the collapsing region (Section 3.3.3), radiation belts (Section 3.5), and the auroral region (Section 3.4). We note that the classifications of previous studies into the reconnection and collapsing region is only for convenience. In Section 3.3.2, we primarily focus on studies of specific features in the Hall region and/or the diffusion region. In Section 3.3.3, we primarily focus on studies of the reconnection downstream region including reconnection fast flows. These studies do not focus on the kinetic features of the Hall region or the diffusion region, but may be presenting some data that were obtained close to (or even within) the reconnection Hall region.

3.2 Caveats of Comparing Energy Spectra

There is a wide variety of different instrumentations, dataset, and methodologies used in observational studies of the magnetotail, as demonstrated in Table 2. For example, different energy ranges and different spectral models are used to derive a power-law index, leading to various concerns. When a study derives a power-law index from a very narrow energy range (say, 40 – 100 keV) using a power-law, there is a concern that the data could be fitted with a Maxwellian with a very high temperature. When a study derives a power-law index from a wide energy range (say, 0.04 – 400 keV) using a kappa distribution, there is a concern how well the spectrum was fitted, because an observed spectrum usually show complexity originating from, for example, a cold thermal component in the lower energy range and a higher-energy (cosmic-ray-like) background. Only some (and not all) studies use a combination of different spectral models.

Instrumentations can be different in different studies. Typically, up to a few tens of keV are covered by electrostatic analyzers. The higher energy ranges are covered by solid state detectors. These data are analyzed separately in some studies, while these data are combined to make one spectrum for fitting in other studies.

Also, methodologies can be different. Some studies take a few samples of measurements at the highest time resolution (say, 3s) for fitting and so their results may not represent average properties. Some other studies performs a superposed epoch analysis, smoothing out the fine structures in the spectrum.

Ideally, a coordinated and systematic study should be carried out with the same instrumentation and methodology, but it is beyond the scope of this paper. By reviewing previous reports of power laws, we hope to obtain some hint for a better understanding of particle acceleration and for possible future studies. The reported values of the power-law index in the magnetotail are summarized in two separate figures, Figures 9 and 10. Some technical details of selected studies are compiled in Table 2.

3.3 Plasma Sheet

3.3.1 Active vs Quiet Times

Pioneering observations revealed the presence of energetic electrons up to several MeV in the magnetotail (e.g. Frank 1965; Anderson 1965; Montgomery et al. 1965; Bame et al.

Table 2 Technical details of selected studies of electron power-law energy spectrum, demonstrating the variety of different methodologies, datasets, and instrumentations. This is not an exhausive list of all the studies mentioned in the text.

Reference	R (R_E)[a]	Rgn.[b]	Energy range, keV[c]	Mdl.[d]	PL Index [e]	Proj.[f]	Type[g]
PLASMA SHEET							
Wu et al. (2015)[h]	11 – 22	PS	2 – 30	PL	3.5 – 5	THM	TV
Imada et al. (2011)	17 – 96	RX	0.07 – (>38)	κ	3 – 4.5	GTL	St
Bame et al. (1967)[i]	16 – 21	PS	0.4 – (>45)	PL	3.7 – 4.5	Vela	Cs.
Oka et al. (2015)[j]	30	RX	0.03 – 28	FT	4 – 5	THM	Cs
Wu et al. (2015)[k]	17 – 21	RX	30 – 200	PL	3.3 – 5.2	THM	TV
Imada et al. (2007)[l]	16	RX	40 – 110	PL	4 – 5.7	CL	Cs
Nakamura et al. (2013)	13 – 15	DF	40 – 200	PL	3.5 – 4.6	CL	Cs
Zhou et al. (2016)	unclear	RX	40 – 244	PL	1 – 6	CL	
Åsnes et al. (2008)[m]	> 15.5	PS	40 – 400	PL	0 – 10	CL	TV
Gabrielse et al. (2014)[n]	6 – 30	Inj	41 – 140	PL	3.4 – 4.1	THM	SE
Runov et al. (2015)[o]	6 – 25	DFB	0.1 – 200	κ	3.4 – 5.5	THM	SE
Øieroset et al. (2002)	60	RX	0.02 – 300	PL	3.8 – 4.7	Wind	Cs
S & A (2015)[p]	7 – 30	PS	0.05 – 500	κ	1.7 – 5.5	THM	St
Christon et al. (1991)	12 – 23	PS	0.03 – 1000	κ	3 – 16	ISEE1	St
AURORAL REGION							
Kletzing (2003)[q]	5 – 6	HL	0.01 – 4	κ	2 – 10	Polar	St
O & J (1998)[r]	0.3	Arr	ϕ – 100	κ	2 – 9	Freja	St
M & A (2014)[s]	800 km	Arr	0.03 – 30	κ	3 - ∞	DMSP	St
Kaeppler et al. (2014)[t]	130 km	Arr	ϕ – 20	κ	2 – 11	SR	Cs

[a] Location of observation indicated by the radial distance R from Earth's center

[b] The region or phenomena observed. The following acronyms are used: PS (plasma sheet without specific features of reconnection and collapsing), RX (reconnection), DF (dipolarization front), Inj (injection event), DFB (dipolarizing flux bundles), HL (high-latitude plasma sheet) and Arr (below/above auroral region).

[c] The energy range (in keV) used to fit the data, as shown in the text or figures in each reference. The ranges do not necessarily represent the coverage by the instruments. ϕ is the potential in the auroral acceleration region and is typically 1 – 10 keV.

[d] Spectral models used to measure the power-law indices. PL, κ, and FT denote power-law, kappa, and flattop distributions, respectively. Note also that $\delta = \kappa$.

[e] Power-law index δ. We show the largest range of values, taken from each study, and it does not necessarily indicate the typical values.

[f] Project (or spacecraft mission). The following acronyms and abbreviations are used: GTL (Geotail), CL (Cluster), THM (THEMIS) and SR (sounding rocket).

[g] Type of methodology. The following abbreviations are used: Cs (specific values from up to a few cases), St (values obtained by a statistical study of many events), TV (time variations of certain time periods), and SE (averaged values from superposed epoch analyses).

[h] Their Event 2; Event 1 had the energy range of 8 – 30 keV.

[i] The electrostatic analyzer covered the lower energy range up to $\sim$ 20 keV. An additional data point was added from the integrated flux in the >45 keV range. We converted their power-law index based on integrated flux (2.7 – 3.5) to that of differential flux, δ. Montgomery et al. (1965) also used integrated flux measured by the Vela satellite and obtained similar power-law indices.

[j] Although unpublished, they performed additional analysis using data from the solid state detector and found κ = 4 – 5 at and around the EDR in the 30 – 300 keV range.

[k] Their main event on 2008 Feb. 26

[l] See also Chen et al. (2009); Huang et al. (2012b)

[m] See also Burin des Roziers et al. (2009b)

[n] Their κ values were defined in differential energy flux. The values are thus converted to our δ here.

[o] Their κ values appear to be defined in differential energy flux and are converted to our δ here.

[p] Stepanova and Antonova (2015)

[q] They used the pitch angle range of 0 – 30° because they interpret that these are the electrons which map to the auroral acceleration region.

[r] Olsson and Janhunen (1998); While they had data points above 20 eV, they used data points with energies above the potential ϕ.

[s] McIntosh and Anderson (2014)

[t] See also Ogasawara et al. (2017)

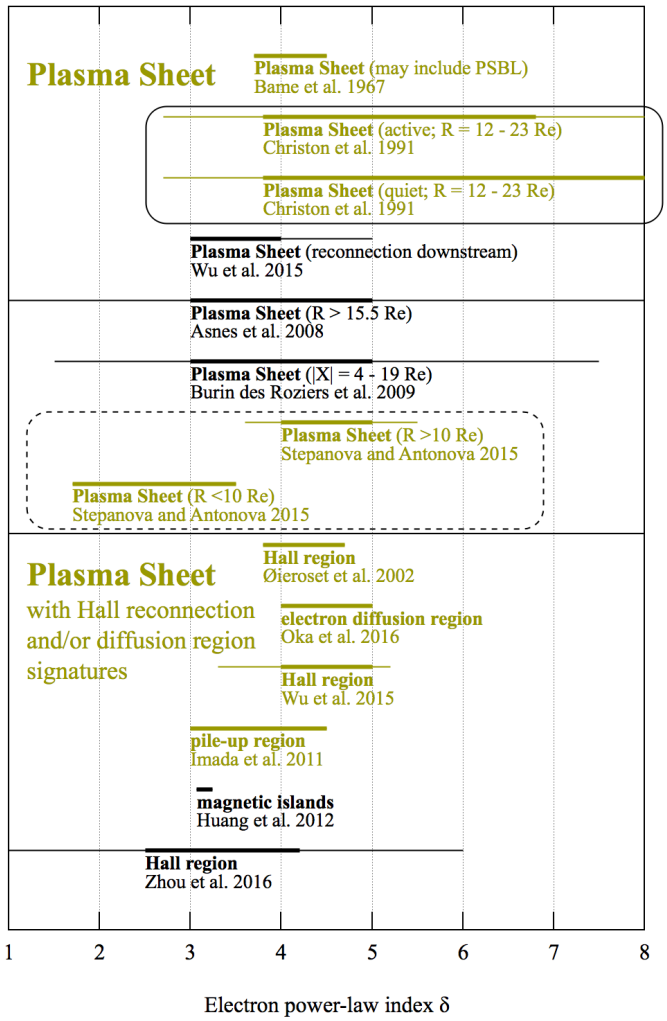

Fig. 9 An overview of electron power-law index δ reported by different studies of electron energy spectra in Earth's plasma sheet (See also Fig. 10). For statistical studies, typical values are shown by thick lines. For non-statistical studies, only thick lines are used to display reported values. Studies (spectral analysis) over an energy range larger than two-orders of magnitudes are shown in ocher color. The other items with narrower energy ranges are shown in black. Note that different studies may be using not only different energy ranges but also different methodologies and instrumentations. The round-corner rectangles highlight the studies that compare power-law indices in different conditions but with the same methodology and instrumentation.

1966, 1967). It was reported that the energetic electrons appear as bursts or 'isolated patches' in the magnetotail plasma sheet (e.g. Frank 1965; Anderson 1965) and that they form a power-law energy spectrum (Montgomery et al. 1965; Bame et al. 1966, 1967). In some cases, the power-law index in the magnetotail plasma sheet between X = -15 R_E and -20 R_E were reported to be δ = 3.7 – 4.5 (Bame et al. 1967), where X is in the geocentric solar magnetospheric (GSM) coordinate and $|X|$ is roughly the radial distance from Earth's center along the sun-Earth line. Not only energetic electrons but also energetic ions were reported

in later years (e.g. Fan et al. 1975; Hones et al. 1976; Sarris et al. 1976a,b; Baker et al. 1979). In particular, Baker et al. (1979) reported that protons form a power-law energy spectrum and that the power-law index δ was 5.1 – 6.5 at geosynchronous orbit.

Anderson (1965) already suggested that the energetic electron fluxes are sensitive to geomagnetic activity as inferred by the K_p index[6]. Later, a more direct association between energetic electrons and reconnection-related features such as magnetic neutral line and plasmoids (or 'fireballs') was identified (Terasawa and Nishida 1976; Baker and Stone 1976), indicating that magnetic reconnection plays an important role in producing energetic electrons (see also a review by, for example, Hones (1979)). Similar associations were also discussed for energetic ions (e.g. Möbius et al. 1983).

A puzzle is that energetic particles exist in the magnetotail even during geomagnetically quiet periods (e.g. Anderson 1965). A systematic analysis using International Sun-Earth Space Explorer (ISEE) data was carried out by Christon et al. (1988, 1989, 1991). Christon et al. (1989) reported that, during quiet times AE $<$ 100, electron energy spectra exhibit a kappa distribution (i.e., a thermal component extending smoothly to a power-law component in the higher energy range). During active times (AE $>$ 100), the spectra become more complex and cannot be represented, in general, by a single functional form although the power-law tail persists. The spectra often show different forms of roll-off and/or excess fluxes in lower energy ranges when compared to a simple Maxwellian or Kappa distribution (Christon et al. 1991). More recently, Åsnes et al. (2008) reported that the power-law index is independent of geomagnetic activity (K_p), while there is a significant local time dependence, with harder spectra observed at dawn compared to the dusk side. Also, Burin des Roziers et al. (2009a) studied the energetic electron fluxes ($>$ 40 keV) instead of the power-law index. They reported that the energetic electron fluxes inside the plasma sheet can still undergo rapid variations when the solar wind is calm and geomagnetic activity is low.

It should be noted that the spatial variation of the power-law index also remains unclear. Wu et al. (2015) reported that the electron power-law index did not fluctuate very much ($\delta \sim$ 3.5 – 5; converted from their values in differential energy flux) when magnetic reconnection and associated phenomena were observed by multiple probes of the Time History of Events and Macroscale Interactions during Substorms (THEMIS) mission (Angelopoulos 2008), distributed over large distances in the magnetotail (in the X-direction). Stepanova and Antonova (2015) studied 5 cases of multi-probe THEMIS observations of the magnetotail. They found that the power-law index δ is $\sim$4 or larger (softer) at X $\lesssim$ -10 R_E but the power-law becomes harder at the inner locations (-5 $<$ X $<$ -10 R_E).

3.3.2 Reconnection Region

During an encounter with the plasma sheet, a spacecraft often detects signatures of the reconnection diffusion region at the ion-scale (or more precisely the Hall region). Some of the studies of such reconnection signatures argue that certain features such as magnetic island and magnetic field pile-up, embedded in the Hall region, could be important for electron acceleration.

[6] The activity level of Earth's magnetosphere has been inferred from different indices derived from different sets of magnetic field measurements on the ground. There are many geomagnetic observatories (stations) across the globe. Some of the widely used geomagnetic indices are the *AE* (Auroral Electrojet) index, K_p index and *Dst* index, which are derived from geomagnetic measurements in the high-latitudes, mid-latitudes, and low-altitudes, respectively. The *AE* index better represents substorms and associated auroral activities. The *Dst* index better represents storm activities.

Øieroset et al. (2002) reported the first observation of energetic particles inside the diffusion region (the Hall region), in a fortuitous encounter by the Wind spacecraft in Earth's distant magnetotail (see also Egedal et al. (2005) for interpretations) . The diffusion region was identified based on (i) an uninterrupted transition of flow reversal without leaving the reconnection layer, (ii) quadrupolar Hall magnetic field signatures, (iii) an electron beam with direction consistent with being the Hall current carrier. They demonstrated that the fluxes become more intense and the power law becomes harder with decreasing distance from the diffusion region center. Also, they fitted the lower and higher part of the observed energy spectrum by a Maxwellian and power-law distributions, respectively. From their analysis, the power-law index (δ) inside the diffusion region was 3.8 – 4.7.

An encounter with the electron diffusion region (EDR) is more challenging as its size is much smaller than the diffusion region at the ion scale (the Hall region). Nevertheless, before the Magnetospheric MultiScale (MMS) mission achieved electron-scale measurements (e.g. Burch et al. 2016), there were observational reports of EDR detection based on (1) decoupling of ion and electron bulk flow velocities (Nagai et al. 2011, 2013), (2) a higher-order scalar measure derived from particle data (Scudder et al. 2012; Zenitani et al. 2012; Tang et al. 2013) and (3) non-gyrotropic distribution of electron velocities (Oka et al. 2016). Oka et al. (2016) reported more than an order of magnitude energization across the EDR, from immediate upstream to immediate downstream. In their analysis, the power-law indices (δ) at the EDR and its immediate downstream region were 4.0 – 5.0.

Based on full-particle simulations and Geotail (Nishida 1994) observations, Hoshino et al. (2001) proposed that electrons are first accelerated at the X-line where electrons can be demagnetized and then further accelerated through gradient B and curvature drift at the 'piled-up' magnetic field lines in the immediate downstream region. This idea spurred interpretations of data with a similar scenario (Imada et al. 2005, 2007; Asano et al. 2008; Wu et al. 2015). While a statistical picture of the locations of energetic electrons relative to the X-line was developed by Imada et al. (2005), Imada et al. (2007) presented a detailed case study using four-spacecraft mission Cluster. They found that the energy spectrum of energetic electrons becomes harder downstream, in the reconnection outflow region where magnetic field intensity increases. In their analysis, the power-law indices (δ) at the magnetic pile-up region were 4.0 – 5.7. Furthermore, Imada et al. (2011) statistically studied the relationship between energetic electrons and reconnection characteristics, using 10 reconnection events observed by Geotail. They argued that the electrons are 'efficiently' accelerated in a thin current sheet during fast reconnection events, and the power-law indices (δ) in and around the reconnection region were 3.0 – 4.5. A caveat is that they used an integrated flux in the $\gtrsim$38 keV range, combined with an *a priori* assumption that electrons exhibit the kappa distribution.

A similar energization process by gradient and curvature drift has been considered in the collapsing region (Section 3.3.3). A notable aspect of the work Hoshino et al. (2001) is their consideration of a chaotic process that occurs when the particle gyro-radius become comparable to the curvature of the magnetic field.

Fluxropes have also received considerable attention in various contexts of electron acceleration (see a review by, for example, Birn et al. 2012). Many of these studies consider electron acceleration in magnetic islands, i.e., a 2D picture of fluxropes. However, the extent to which such 2D pictures can explain observations remains unclear. A recent study of the dayside magnetopause reported the detection of a magnetic fluxrope flanked by two active X-lines, producing colliding plasma jets near the center of the flux rope (Øieroset et al. 2011). While the authors report detection of non-thermal electrons within the flux rope core, they also described departures from the 2D pictures of electron acceleration. Recent theoretical

and simulation studies demonstrated an importance of 3D effects in electron acceleration (e.g. Dahlin et al. 2015) and it remains as an interesting topic of research.

In the magnetotail, energetic electrons have been observed within small-scale fluxropes with spatial scales of a few times the ion inertia length d_i (e.g. Chen et al. 2007, 2009; Retinò et al. 2008; Wang et al. 2010; Huang et al. 2012a). Chen et al. (2007) showed that energetic electron fluxes peak at sites of compressed density within fluxropes. Based on a further analysis, it was reported that the energetic electrons exhibited a power-law energy spectrum inside the fluxropes and that the power-law index Γ ranged from 6 to 7.3 (or δ from 5 to 6.3) (Chen et al. 2009). Retinò et al. (2008) also found an enhanced flux of energetic electrons within a small-scale fluxrope during a crossing of reconnecting current sheet. They argued that, while the hardest spectrum was observed for field-aligned electrons at magnetic separatrices, the highest flux was observed within the small-scale fluxrope for perpendicular electrons. After these observational studies, results from 2D PIC simulations have been reported in the context of electron acceleration by the secondary magnetic islands (e.g. Oka et al. 2010; Wang et al. 2017).

3.3.3 Reconnection Downstream and Collapsing Region

During magnetospheric disturbances, enhancements of energetic electrons are observed at and around the geosynchronous orbit (i.e., the geocentric distance of $6.6R_E$) (e.g. Lezniak and Winckler 1970; Swanson 1978; Erickson et al. 1979; Birn et al. 1997). How energetic electrons can be 'injected' into the inner magnetosphere and contribute toward the radiation-belt formation has long been a subject of debate (e.g. Birn et al. 2012; Lui et al. 2012; Lui 2013, and references therein). Energetic electrons are also observed during an inward motion of dipolarization fronts (jet fronts) and the associated features such as plasma flows and magnetic fluxes (e.g. Deng et al. 2010; Asano et al. 2010; Fu et al. 2011, 2013; Runov et al. 2011b, 2015; Nakamura et al. 2013; Duan et al. 2014; Gabrielse et al. 2014, 2016; Turner et al. 2016; Liu et al. 2016). Example energy spectra from the collapsing region are shown in Fig. 11. A general argument is that electrons are accelerated while bouncing along the collapsing magnetic field lines (e.g. Birn et al. 2012). Based on analyses of pitch angle distributions, Fu et al. (2011) argued that Fermi acceleration dominates inside a decaying flux pileup region (FPR), while betatron acceleration dominates inside a growing FPR. Here, Fermi acceleration refers to Fermi's Type B interaction with an evolving magnetic field line (or the 'slingshot' effect; see Appendix C) and is not necessarily a stochastic acceleration. Recently, more detailed picture of the behaviors of energetic electrons have been developed through statistical analyses (e.g. Duan et al. 2014; Gabrielse et al. 2014; Runov et al. 2015).

As for power laws, Nakamura et al. (2013) reported $\delta = 4 - 6$ in a plasma sheet with multiple dipolarization fronts (jet fronts). In a statistical study focused on dispersionless injection, it was reported that the average electron power-law index of superposed spectra in the background population ($\delta = 3.4 - 3.9$; converted from their values in differential energy flux) was already very similar to that of the injected electrons ($\delta = 3.4 - 4.1$; converted from their values in differential energy flux) (e.g. Gabrielse et al. 2014). Runov et al. (2015) investigated particle energy spectra by taking an average of many cases of dipolarizing flux bundle (DFB) events in both background populations (i.e., before arrival of dipolarization fronts, also known as jet fronts) and intruding populations (i.e., inside the DFBs or bulk flow plasmas). Then they divided the magnetotail into four regions, i.e., $r < 9.5R_E$, $9.5 < r < 12R_E$, $12 < r < 15.5R_E$ and $15.5 < r < 25R_E$ where r is the geocentric radial distance, and measured the power-law index of the average spectra. They found that the power-law index δ is $\sim$5 in

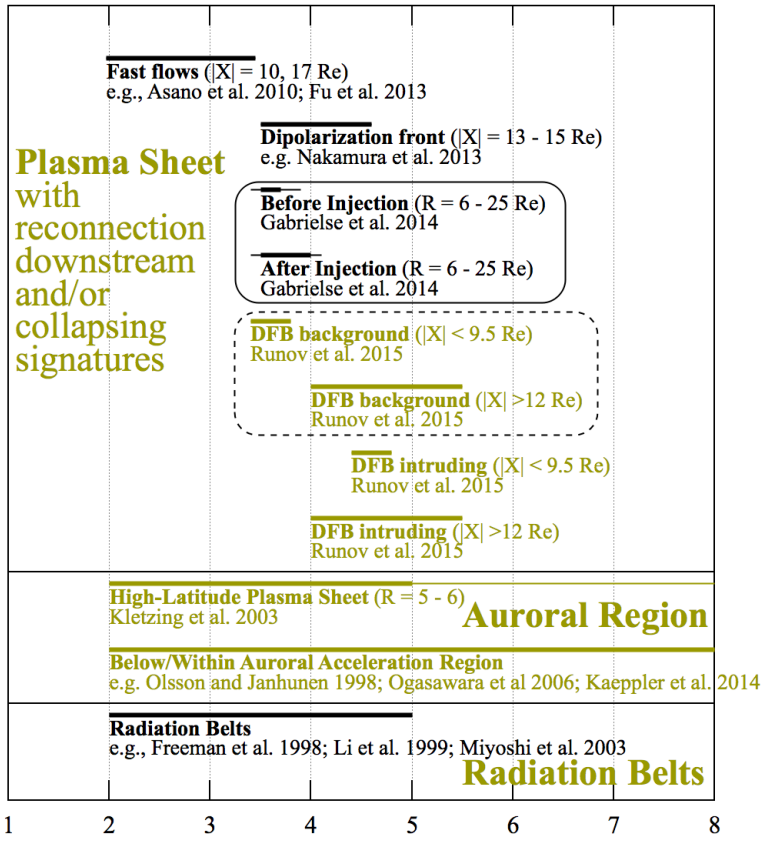

Fig. 10 An overview of electron power-law index δ reported by different studies of electron energy spectra in Earth's plasma sheet and auroral region (See also Fig. 9). The category 'collapsing region' is for studies of specific features in the reconnection region downstream. For statistical studies, typical values are shown by thick lines. For non-statistical studies, only thick lines are used to display reported values. Studies (spectral analysis) over an energy range larger than two-orders of magnitudes are shown in ocher color. The other items with narrower energy ranges are shown in black. Note that different studies may be using not only different energy ranges but also different methodologies and instrumentations. The round-corner rectangles highlight the studies that compare power-law indices in different conditions but with the same methodology and instrumentation. The κ values in Gabrielse et al. (2014) and Runov et al. (2015) were defined in differential energy flux and are converted to the δ values as in differential particle flux in this figure.

the outermost region and the spectra become harder with the decreasing radial distance (Fig. 10).

For ions, Gabrielse et al. (2014) and Runov et al. (2015) found much softer spectra with $\delta \sim 7 - 8$ and $5 - 6$, respectively, in the magnetotail. In the inner magnetosphere and around geosynchronous orbit, flux increases are often limited in energy range and/or do not exhibit a clear power-law (Baker et al. 1981; Birn et al. 1997, 2012).

The observations of energetic particles in the collapsing region have been complemented by a large number of theoretical studies, primarily on the basis of test particle simulations

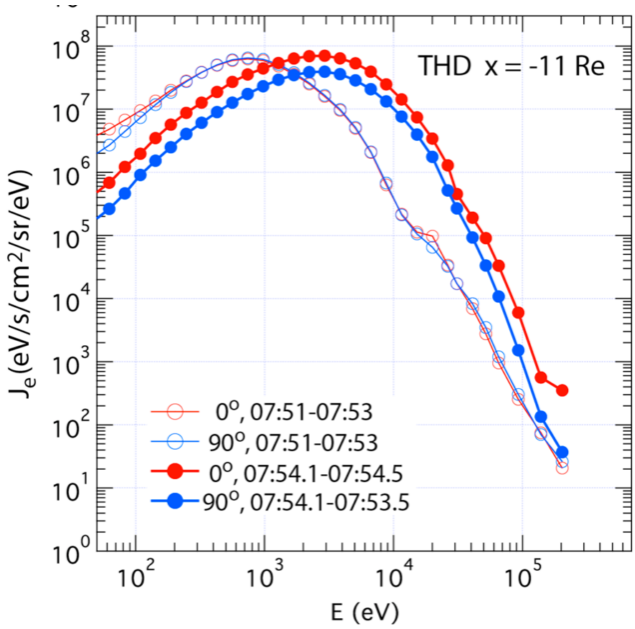

Fig. 11 Electron energy spectrum before (open circles) and after (filled circles) a jet arrival in the collapsing region, adapted from Birn et al. (2014). This observation was made by THEMIS-D (P3) on 2009 February 27. The spectrum is taken by the Electro-Static Analyzer (ESA) and Solid State Telescope (SST) below and above $\sim$ 28 keV, respectively. In general, the pre-existing plasma is cold and dense whereas intruding plasma is hot and tenuous.

in assumed field configurations (e.g., Li et al., 1998; Zaharia et al., 2000; Gabrielse et al., 2012, 2016) or using the dynamic fields of MHD simulations of magnetotail dynamics and reconnection (e.g., Birn et al., 1994, 1997b, 1998, 2004, 2013; Ashour-Abdalla et al., 2011; Pan et al., 2014a,b). The combination, and sometimes direct comparison, of observations and simulations have provided a consistent picture of the particle energization in the near-Earth magnetotail outside the immediate vicinity of the reconnection site (for a summary, see, also, Birn et al., 2012). The most important element is the motional ($v \times B$) electric field associated with earthward flow bursts.

Charged particles can enter the acceleration region of dipolarizing flux bundles (DFBs) (i.e., the region of intensified motional electric field associated with collapsing) in two ways, either from low latitudes via cross-tail drift or from higher latitudes when the field line on which the particle resides becomes reconnected and the particle trapped in the section earthward of the reconnection site (Birn et al., 2015).

Unlike ions, electrons are more adiabatic, except for the vicinity of the X-line, and exhibit either many gyrations (at pitch angles near 90^o) or many bounces (at low pitch angles) between mirror points closer to Earth. The energy gain thus occurs in multiple steps, either by betatron or by first-order Fermi Type B acceleration (Northrop, 1963). At the highest energies (hundreds of keV), however, they also drift across the acceleration region in a simple fashion. This limits the maximum energy gain by the integrated cross-tail voltage difference, associated with the electric field of the DFB, similarly for ions and electrons. Taking the speed of a DFB at 1000 km/s, a magnetic field magnitude of 20 nT, and a typical width

of, ∼20,000 km, this yields a maximum energy gain of 400 keV, close to typical values of injections observed at geosynchronous distance.

A caveat is that some of previous simulations assumed that particles already exhibit a power-law energy spectrum at the boundary of the simulation box. While this is a reasonable assumption based on the fact that power-law tails can exist even during quiet times (See Section 3.3.1), it remains unclear when or in what conditions a power-law forms. It also remains unclear if or how the power-law spectra can be modulated by the energization process in the collapsing region.

3.4 Auroral Region

The electron distributions described above comprise the source population for auroral primaries (Paschmann et al. 2003). These electrons, which stimulate auroral emission, are driven from the magnetospheric source along converging geomagnetic field lines toward the ionosphere with a flux sufficient to satisfy the current or voltage requirements of the magnetospheric generator (Lysak 1990). Consequently, the recognition that the hot tenuous source electron distributions have extended power-law-like supra-thermal tails, often characterized as kappa distributions, is a potentially important development in advancing understanding of auroral arc formation (Pierrard 1996; Dors and Kletzing 1999; Janhunen and Olsson 1998). In the following we briefly review pertinent observations and theoretical results, and in the light of these contributions indicate where further advances could be made.

The recognition of enhanced supra-thermal tails as a prevailing feature of the source distribution for auroral primaries was implicit from the analysis of ISEE particle measurements reported by Christon et al. (1988, 1989, 1991). These authors demonstrated that the observed electron spectra over an energy extending from ∼100 eV to hundreds of keV is well described as a kappa distribution with index κ (= δ) = 4 – 6. At energies above the average energy (E_0) of the electron distribution these fits indicate supra-thermal tails having power-law form with κ = 5 – 7 (i.e. for $E \gg E_0, f \sim E^{-(\kappa+1)}$). Observed distributions such as these in the plasma sheet were explicitly connected to the auroral acceleration process (Kletzing 2003). An example electron spectrum as reported by these authors from the Polar spacecraft in the high latitude nightside plasma sheet is shown in Figure 12a (Kletzing 2003, Figure 6). This plot demonstrates a marked deviation from Maxwellian form well described by a kappa distribution with $\kappa \sim 3.9$ providing a power-law spectrum above 1 keV varying as $E^{-4.9}$. These measurements in the auroral source regions have demonstrated that a Maxwellian is a perhaps a poor starting point for building a kinetic model for the auroral acceleration process.

The realization that auroral primaries have distinct power-law-like supra-thermal tails has also become apparent from measurements performed at altitudes below the auroral acceleration region. Olsson and Janhunen (1998) used observations from the Freja spacecraft to demonstrate that a kappa distribution generally provided a better fit to the observed distribution irrespective of activity level with κ = 4 – 7 for field-aligned primaries. McIntosh and Anderson (2014) performed a statistical study of DMSP spacecraft observations to show that ∼30% of measured precipitating electron spectra require a kappa description. Ogasawara et al. (2006, 2017) reported E-region observations from two separate rocket campaigns over 90 – 140 km and over 90 – 336 km respectively showing κ = 4 – 9 and κ = 3 – 30 through discrete auroral arcs. Similarly, Kaeppler et al. (2014) from the ACES sounding rocket reported κ indices increasing from 2 to 11 as the rocket travelled from the equatorward to poleward side of an auroral arc.

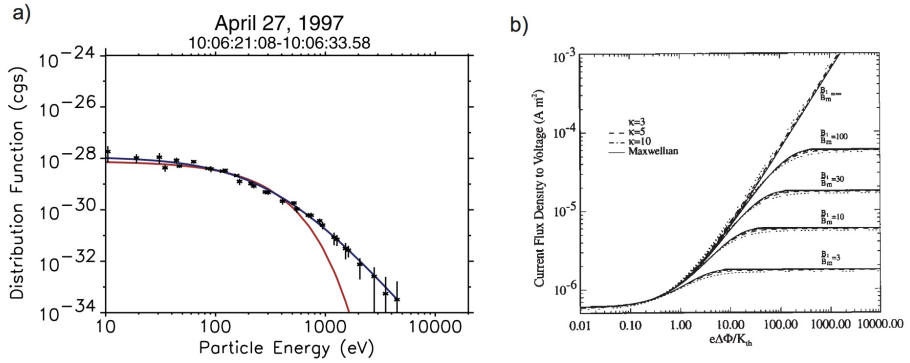

Fig. 12 Electron supra-thermal tails in auroral arcs. (a) Example of Maxwellian (red curve) and kappa (blue curve) distribution fits to electron spectra in an auroral source region observed from the Polar spacecraft in the high latitude plasma sheet. The kappa fit is within the 99% confidence interval, but the Maxwellian is not. The fit finds = 3.9 $\pm$ 0.6 or $f \propto E^{-4.9}$ for $E > 1$ keV (adapted from Figure 6 of Kletzing (2003)). (b) Current density J versus dimensionless acceleration potential ϕ normalized by electron temperature ($K_{\rm th}$) for a generalized kappa current-voltage relationship. Line-styles show a variety of κ indices for different magnetic field ratios between the source region (B_M) and the ionosphere (B_I). The Maxwellian result is shown by the black line. Density is 1 cm^{-3} and $K_{\rm th}$ = 500 eV (adapted from Figure 2 of Dors and Kletzing (1999)).

These observations have been supported by the development of theoretical models which include the contribution of the supra-thermal tail in a time independent relationship between the field-aligned current (J) and accelerating potential (ϕ) for quasi-static auroral arcs (Pierrard 1996; Dors and Kletzing 1999; Janhunen and Olsson 1998). In general these models are extensions of those derived earlier for Maxwellians (Knight 1973; Lemaire and Scherer 1974; Lundin and Sandahl 1978; Fridman and Lemaire 1980) which seek to determine the effective field-line conductivity (K) through the auroral acceleration region from a consideration of the source electron distribution and the converging geometry of the geomagnetic field. Over much of the observed energy range of auroral primaries ($\sim$100 eV - 10s keV) these models predict a simple Ohmic-like 'current-voltage' relationship where K is independent of J and ϕ expressed as

$$J = K\phi \tag{14}$$

Both J and ϕ can be measured by spacecraft to derive the observed value of K (e.g. Lyons et al. 1979; Sakanoi et al. 1995; Elphic et al. 1998). Intuitively, the energy dependence of the electron spectrum enters the evaluation of K because the energy gain required to shift electrons into the loss cone, where they can contribute to the net current, increases with energy. Consequently, K may be expected to be reduced as the spectrum becomes harder. On the other hand more energetic electrons can carry a larger current for a lower density. These competing influences result in a non-obvious variation of K with changes in spectral index (or κ), density, and temperature. Comparisons between results expected for a Maxwellian versus a kappa distribution indicate that the linear relationship suggested by Eq. 14 remains valid up to larger values of ϕ for a kappa distribution before saturating. This allows greater energy deposition. It has also been shown that for the same density and temperature of the plasma sheet source the expected total energization or potential drop along the geomagnetic field to the ionosphere increases by $>$5% for Dors and Kletzing (1999). This rather modest change is apparent in Figure 12b where the current-voltage relation is presented for a range of κ values. However, by combining the current voltage-relation with current continuity

through the ionosphere Dors and Kletzing (1999) demonstrated that kappa distributions with $\kappa = 5$ provide up to double the precipitating energy flux and drive precipitation over a broader region than the equivalent Maxwellian. Olsson and Janhunen (1998) performed an observational test of the effect of a supra-thermal tail by using Freja spacecraft observations in a generalized kappa model derived for MHD simulations (Janhunen and Olsson 1998). Using this approach they derived K based on Maxwellian and kappa fits to the observed electron distribution. Less than 20% variation between functional forms was found, however some measurements suggested a variation of up to 40%.

While these models have shown how the presence of a supra-thermal tail alters the relationship between the field-aligned current and the acceleration potential they are limited by the omission of electron populations occupying classically forbidden regions of phase space in the acceleration region. Observations through the acceleration region show distributions where significant fractions of the total density reside in trapped orbits inaccessible to electrons conserving the first adiabatic invariant. While these electrons may not contribute appreciably to current they alter the manner which quasi-neutrality is maintained through the acceleration region and hence the distribution of density and potential along the field line (Chiu and Schulz 1978; Sakanoi et al. 1995; Ergun et al. 2000). This lacuna is reflected in the surprising fact that none of the observational studies identified above were performed using measurements taken within the acceleration region itself. There are significant advantages for performing these analyses using measurements made within the acceleration region. These include avoiding the degradation of the spectrum at low altitudes traversed by rockets and removing the contribution from backscatter and secondary electrons at low altitudes to the primary electron spectrum. Measurements performed within in the acceleration region also reveal all the components of the electron and ion distributions which self-consistently carry J and support ϕ. Therefore significant advances could be made in subsequent studies by exploiting direct measurements from within the auroral acceleration such as those readily available from the FAST mission.

3.5 Radiation Belts

The radiation belts are the highest energy populations of charged particles in Earth's magnetosphere. The electron outer radiation belt is highly variable associated with magnetic storms[7], and disappearance and subsequent flux enhancements occur associated with magnetic storms (e.g. Miyoshi and Kataoka 2005).

Two different acceleration processes contribute to the energization of the outer belt electrons (e.g. Ebihara and Miyoshi 2011). One process is the radial diffusion. Through the conservation of the first adiabatic invariant, the electron energy increases when electrons move toward the Earth. The drift resonance with the MHD-fast mode waves, i.e. Ultra Low Frequency (ULF) pulsations is an elementary process for this acceleration (e.g. Elkington et al. 1999). If this process is dominant without significant source and loss process during the transport, the slope of the power-law distributions should be conserved. Another process is the wave-particle interactions. The cyclotron resonance with whistler mode chorus causes the non-adiabatic acceleration through violation of all adiabatic invariants (e.g. Summers et al. 1998; Miyoshi et al. 2003; Horne 2005). The resultant energy spectrum depends on the resonance conditions. If the resonance occurs with a wideband wave-number spectrum, the energy spectrum of the accelerated electrons should be a power law (Ma and Summers 1998),

[7] See the first footnote in Section 1 for 'storm'.

while non-linear wave-particle interactions cause different energy spectrum (Furuya et al. 2008).

Various data indicated that radiation belt electrons from 100 keV to 1.5 MeV can be modeled as a power-law spectrum in the outer radiation belt (e.g. Freeman et al. 1998; Burin des Roziers and Li 2006) although the spectrum can be more complex than a simple power-law (Baker et al. 1998). Freeman et al. (1998) derived time variations of the slope of the power-law spectrum. Typically the power-law index δ (as measured in differential flux) at geosynchrnous orbit ($R = 6.6$ R_E) is about 2. During the main phase of a storm, the outer belt flux decreases and the energy spectrum becomes soft. The power law index δ is 4 – 5 during the main phase. During the recovery phase, the flux of sub-relativistic and relativistic energy electrons gradually increases. During the period, the energy spectrum becomes hard and the power-law index recovers to the pre-storm level.

Similar variations of the power-law index are observed at different locations. Li et al. (1999) derived the time variation of energy spectrum using the GPS satellite at $R = 4.2$. Assuming a power-law form, they measured the slope between data points in the 0.4 – 0.8 MeV and 0.8 – 1.6 MeV ranges. The power-law index δ was 4.6 during the main phase and then became as small as 1.4, associated with the flux enhancement during the recovery phase. Miyoshi et al. (2003) derived spatial-temporal evolutions of the energy spectrum in the 30 – 300 keV range during the storm time. They found that the spectrum hardening takes place first in the inner part of the outer belt, and then the hard energy spectrum can be seen at the outer part of the outer belt. This indicates the non-adiabatic acceleration process occurs in the inner part of the outer belt, which are different from the radial diffusion.

4 Power Laws in Other Environment

In this section, we review power-law spectra in other regions such as solar energetic particles, shocks, magnetosheath, and the solar wind. Figure 13 summarizes the reported values of δ.

4.1 Solar Energetic Particles (SEPs)

Solar Energetic Particles (SEPs) are the particles detected in interplanetary space in association with solar eruptive events such as flares and coronal mass ejections (CMEs). Typically, SEP events are classified into ‘gradual’ and ‘impulsive’ events depending on the observed time profile of the SEP fluxes (Figure 14) (e.g. Reames 1999). While gradual and impulsive events are generally attributed to particle acceleration by CME-driven shocks and solar flares, respectively, the more precise and detailed origins of both types of SEPs (including the possibility of mixed sources) are still debated. In fact, there have been numerous studies of SEPs (including protons, heavy ions, and electrons) and it is beyond the scope of this paper to review further details of SEPs. Readers are referred to recent reviews (e.g. Verkhoglyadova et al. 2015; Desai and Giacalone 2016; Kahler and Ling 2017; Klein and Dalla 2017) and references therein. In this section, we will focus only on electrons during SEP events.

During a gradual SEP event (the typical duration of which is several days), the particle flux can enhance locally at and around the passage of an interplanetary shock (CME-driven shock) with a typical duration of hours (See, for example, the flux enhancements at the vertical lines in Figure 14 right panels). Such a local enhancement is historically referred to as Energetic Storm Particles (ESPs) and indicates particle acceleration and trapping by the traveling interplanetary shock, although all particles in the intensity-time profiles of an SEP

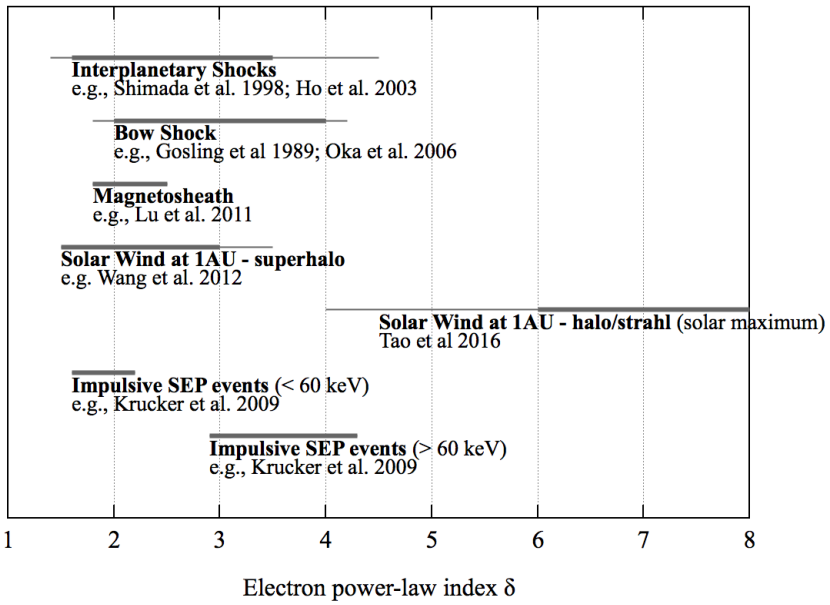

Fig. 13 An overview of electron power-law index δ in other environment such as shocks, solarwind and solar energetic particles (SEPs). The solar wind halo/strahl components exhibit softer ($\delta >8$) spectra during solar minimum and is not shown.

event (not just ESPs) could be accelerated by the shock. We will describe energetic electron events that are clearly associated with shocks (including ESP events) in Section 4.2 where both interplanetary shocks and Earth's bow shock are discussed.

Energetic electrons (that are not necessarily focused on ESPs and shocks) have provided important information for a better understanding of SEPs (e.g. Desai and Giacalone 2016; Klein and Dalla 2017, and references therein). For example, it has been reported that the relative peak intensity of energetic (> 0.5 MeV) electrons (i.e., electron-proton ratio) is substantially higher in relatively smaller events of gradual SEPs (with the proton intensity < 3 cm^{-2}s^{-1}sr^{-1}), unless the SEP events are poorly connected to the observer (e.g. Cliver and Ling 2007). Therefore, it was argued that the gradual SEP events with relatively high intensities of electrons are attributed to acceleration in solar flares rather than acceleration in CME-driven shocks. In fact, at least in the specific example in Fig. 14, energetic electrons in a gradual SEP event show an impulsive time-profile in the early phase. SEP electrons have also been studied in terms of anisotropy (e.g. Dresing et al. 2014), spatial distribution in the heliospheric longitude direction (e.g. Klassen et al. 2016), and mean free path (e.g. Agueda et al. 2014).

The energy spectra of SEP electrons have also been studied and compared with hard X-ray spectra at flares (e.g. Krucker et al. 2007, 2008b, 2009). A statistical study of impulsive SEP events reported that electron energy spectra (measured at 1 AU by Wind) typically exhibit a double power-law with a break around 60 keV (Krucker et al. 2009), although the origin of the double-power-law form is unclear. They reported that the average power-law indices below and above the break energy are $\delta_{\rm low} = 1.9 \pm 0.3$ and $\delta_{\rm high} = 3.6 \pm 0.7$, respectively. Both components are flatter/harder than those of hard X-ray emission from flares (See Figures 3 and 13). They also reported that the number of electrons measured during the impulsive

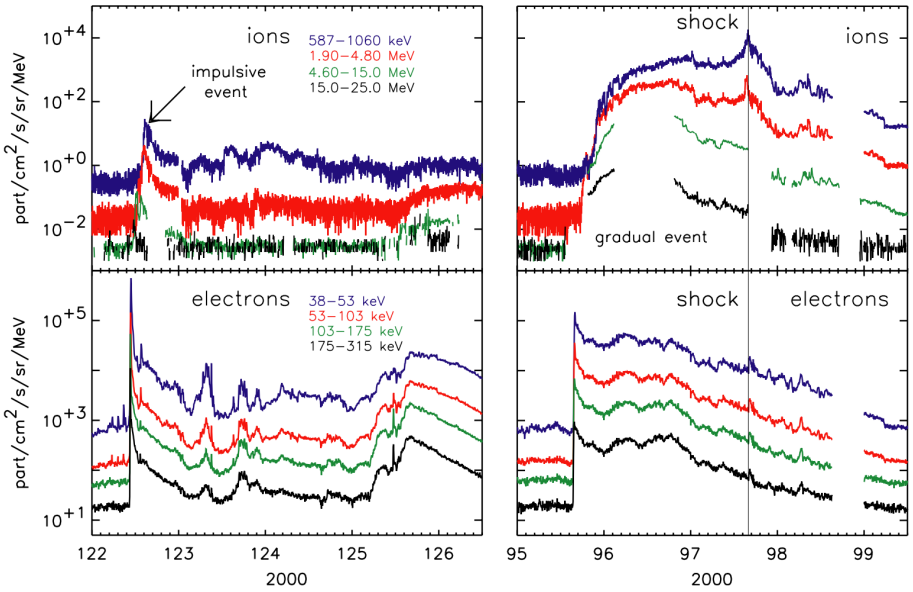

Fig. 14 Typical profiles of impulsive (left) and gradual (right) Solar Energetic Particle (SEP) events for ions (upper) and electrons (lower) as measured by ACE/EPAM, adapted from Lario (2005) ©COSPAR. Reproduced with permission. The horizontal axes show Day-of-Year (DOY).

SEP event (presumably escaping from the solar origin) is much lower than the number of electrons at the flaring site, deduced from the hard X-ray measurements. Thus, they argued that the electron population at the sun and near Earth are different and might be produced by different acceleration mechanisms. They also suggested that, alternatively, the escape from the sun is energy-dependent. Note, however, that Krucker et al. (2007) find a strong correlation of γ (flare) and δ (SEP) for impulsive events with close temporal correlation between the hard X-ray burst and the *in situ* electron events, the so-called prompt events. This is an important argument to keep in mind, since it hints at a common origin of both populations for the subset of prompt events (Krucker et al. 2009).

4.2 Shocks and Sheaths

Particles are accelerated to high energies by shocks. In the standard 'diffusive shock acceleration' (DSA) model, the power-law index s of shock-accelerated particles $f(p) \propto p^{-s}$ would be

$$s = \frac{3r}{r-1} \tag{15}$$

where r is the shock compression ratio. In sub-relativistic shocks in the heliosphere, r is no larger than $\sim$4 and so s is 4 or larger or δ is 1 or larger. Even if the shock were weak, say r = 1.4, the spectrum is still hard (flat) with $\delta \sim$4. This already implies that shocks in the heliosphere produce hard (flat) spectra.

In fact, *in situ* measurements of proton energy spectra at interplanetary shocks showed δ = 1 – 4 in the energy range 40 – 1000 keV (e.g. Scholer et al. 1983; van Nes et al. 1984). The particle and magnetic/electric field data at interplanetary shocks were used to test the diffusive

shock acceleration (DSA) theory (e.g. Kennel et al. 1984). However, not all of interplanetary shocks show the features predicted by DSA such as a power-law energy spectrum and an exponential increase of particle flux prior to the shock arrival (e.g. van Nes et al. 1984; Lario 2003; Lario et al. 2005; Fisk and Gloeckler 2012). Even when they show a power-law energy spectrum, the power-law index often deviates from the prediction by Equation 15. It is not clear exactly when or in which conditions ions show significant flux increase at and around shock fronts and how the power-law index could be understood. However, when shocks exhibit a power law with substantially enhanced fluxes, the power-law index δ seems to fall somewhere between 1 and 4.

Unlike ions, electrons show the predicted, exponential flux increase on the upstream only in limited cases. Using Geotail, Shimada et al. (1998) reported the power-law index $\delta = 1.4 – 1.5$ at an interplanetary shock and Oka et al. (2009) reported $\delta \sim 3.3$ at Earth's bow shock. Focusing on the power-law index, Ho et al. (2003) reported that, most of their 28 interplanetary shock events showed a power law with δ between 1.5 and 4.5 in the $>$38 keV range (See also Ho et al. (2008)). Just like the ion case, Ho et al. (2003) argued that the power-law indices are not well reproduced by the formula Eq. (15). In the lower energy range ($>$ 2 keV), electrons show a localized 'spiky' enhancement or almost no enhancement at interplanetary shocks (e.g. Tsurutani and Lin 1985; Lario 2003; Lario et al. 2005). Electrons at Earth's quasi-perpendicular bow shock also show a spiky enhancement localized at the shock transition layer. Despite the profile inconsistent with DSA, power-law energy spectra do form within the transition layer, indicating electrons can be accelerated by a mechanism very different from the classical DSA scenario (Gosling et al. 1989; Oka et al. 2006). In case studies by Gosling et al. (1989), δ was reported to be between $2 – 3$. In a statistical study by Oka et al. (2006), δ ranged from 2 to 4.

The similar power-law spectra have been observed on the downstream side of the shock front or Earth's magnetosheath. A caveat is that the non-thermal electrons tend to exhibit perpendicular anisotropy, which could be due to escape of field-aligned electrons from the acceleration region (i.e., the shock transition layer) (Feldman et al. 1983b; Gosling et al. 1989). In a long duration observation of Earth's magnetosheath, Lu et al. (2011) analyzed pitch-angle averaged electron energy spectra and obtained electron power-law indices $\Gamma = 2.8 – 3.5$ ($\delta = 1.8 – 2.5$). They argued, based on simulations, that a soft power law (with large δ) would evolve into harder spectra through excitation of whistler waves. (Lu et al. 2010).

To summarize, collisionless shocks in the heliosphere produce a power-law energy spectrum with $\delta < 4$. Similar power-law distributions have been observed in Earth's magnetosheath.

4.3 Quiet-Time Solar Wind

It has been reported that the solar wind ions in interplanetary space exhibit a non-thermal tail even when there is no significant disturbance such as shocks, magnetic clouds, counter-streaming electrons and magnetic holes (e.g. Gloeckler 2000; Fisk and Gloeckler 2006). The non-thermal tail can often be modeled as a power law with an exponential roll-off, indicating there is a limit to the maximum energy particles can acquire. More importantly, the power-law index δ seems to be $\sim$1.5 in many cases. This is the smallest power-law index a kappa distribution can take (Section 1.3). It was argued that such a hard and universal power-law index can be explained by a 'pump mechanism' in which particles are accelerated by a local compression in a turbulent medium but escape by spatial diffusion before the local

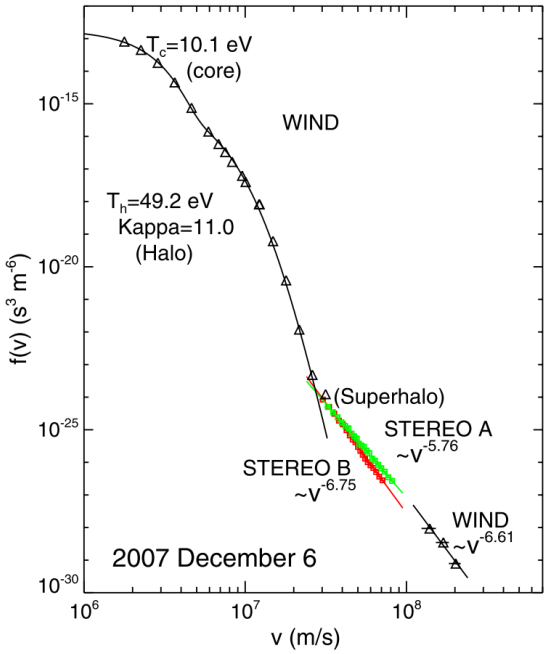

Fig. 15 Electron velocity distribution in a time period of quiet solar wind, adapted from Wang et al. (2012). The solid curves represent the fit by a combined Maxwellian and kappa distribution (for core-halo components) and a power-law (for super-halo component).

compression turns into an expansion, which would decelerate the accelerated particles (e.g. Fisk and Gloeckler 2006, 2014).

Non-thermal electrons have also been observed in the quiet-time solar wind (Figure 15). In addition to the 'core' component with the temperature of a few to ∼10 eV, there is a hotter 'halo' component with the temperature of several tens of eV (e.g. Marsch 2006). This halo component is often isotropic and may have a non-thermal tail, which could be fitted by the kappa distribution. However, Tao et al. (2016) reported that the tail (at 1 AU) is generally steep and the power-law index δ (or κ) is typically between 4 and 16. They also reported that the spectral slope depends on the solar activity and that the tails are substantially harder (flatter) during the solar maximum. The 'strahl' electrons are in an energy range similar to those of the halo electrons but they are streaming anti-sunward along the interplanetary magnetic field. The power-law spectra of the strahl electrons look similar to those of the isotropic halo component (Tao et al. 2016).

Both the halo and strahl components can evolve during the propagation of the solar wind. The relative number of stahl electrons is decreasing with radial distance from the sun, whereas the relative number of halo electrons is increasing (e.g. Maksimovic 2005; Štverák et al. 2009). It is often argued that the strahl component represents the escaping heat flux from the solar corona and that it eventually evolves to become the halo component via pitch angle scattering in the solar wind (e.g. Feldman et al. 1975; Štverák et al. 2009). In terms of the power-law index, Štverák et al. (2009) reported that, for both halo and strahl components in the slow solar wind, δ is large, ~ 9, at ~ 0.3 AU and the spectra gradually become hard $\delta \sim 2-4$ beyond 1 AU (See also Pierrard et al. 2016).

The super-halo component (at 1 AU) (e.g. Lin 1998; Wang et al. 2012) more generally exhibits a harder power law. This component is within the energy range of order tens to hundreds of keV, similar to the energy range of those electrons we have reviewed in Sections 2 and 3. For the super-halo component, the typical values of the power-law index s of $f(v) \propto v^{-\gamma}$ are 5 – 9 (Wang et al. 2012) so that $\delta = 1.5 - 3.5$.

5 Summary and Discussion

5.1 Solar Flares vs Earth's Magnetotail

There have already been many comparative studies of solar flares and terrestrial substorms from various points of view (e.g. Obayashi 1975; Bratenahl and Baum 1976; Terasawa et al. 2000; Bhattacharjee 2004; Lin et al. 2008; Birn and Hesse 2009; Tsurutani et al. 2009). These studies have discussed the basic similarities and differences in terms of (1) plasma parameters/environments, (2) morphologies of the phenomena and (3) the physics of magnetic reconnection. This review is an extension of the comparative studies to the realm of particle acceleration and non-thermal features in the possible key regions of solar flares (Section 2) and Earth's magnetotail (Section 3).

As compiled in Figures 3, 9 and 10, the power-law index δ takes on a wide variety of values in solar flares and Earth's magnetotail. Nevertheless, we find a notable resemblance between the δ values in solar flares and those in Earth's magnetotail when δ is measured close to the reconnection site.

5.1.1 Regions close to Reconnection Site

In order to examine the possible consequence of magnetic reconnection, we examine data from regions/structures that are closest to magnetic reconnection. For solar flares, the above-the-looptop (ALT) sources are the closest X-ray sources to the reconnection site (as expected in the standard model). Due to the limited energy coverage (typically 15 – 80 keV), different spectral models can be used for the ALT source, as shown in Figure 16. Figure 16 does not show δ values of the double coronal source events because, as far as we are aware, there have been only two studies that estimated the power-law index; and those two studies reported rather dissimilar ranges of values. Future studies will need to establish the typical δ values of the secondary, upper coronal source. Another caveat is that many cases of hard X-ray emission from the corona show a wide range of values of the power-law index δ and it can be as small as $\sim$2 (Section 2). Only in rare cases, the non-thermal source exhibits a clear 'above-the-looptop' configuration at roughly 20 – 60 Mm from the solar surface and is well separated from the lower-energy source by 10 – 20 Mm. The typical distance d between the lower and higher energy sources are smaller, $|d| < 2$, and the source height is also closer to the solar surface, 4 – 20 Mm.

For Earth's magnetotail, the collapsing region appears to be the counterpart of the solar hard X-ray above-the-looptop (ALT) source. We also note that reconnection outflows typically experience braking (and bouncing) at radial distances between $\sim$8 and $\sim$12 R_E in the collapsing region. (Thus, this specific region in the collapsing region is sometimes referred to as the 'flow-braking region'.) During magnetotail reconnection, various features such as 'fast flows', 'dipolarizing flux bundles', and 'dipolarization fronts' are observed not only in the collapsing region (between $\sim$8 and $\sim$12 R_E) but also throughout the plasma sheet including the region very close to (or even within) the Hall region (or ion-scale diffusion region). The

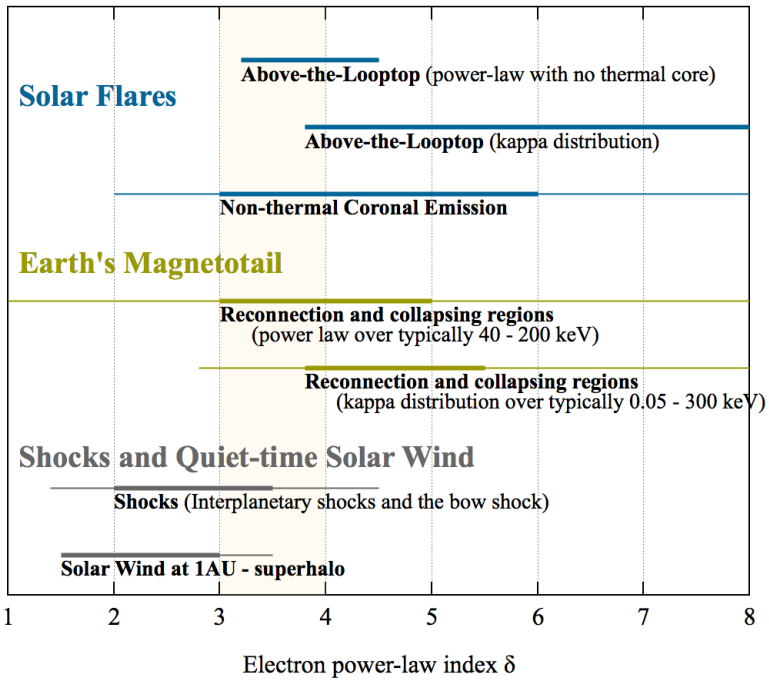

Fig. 16 An overview of electron power-law index δ in the regions close to magnetic reconnection and in shocks and quiet-time solar wind. The orange shade in the $3 < \delta < 4$ range highlights the result that, in many cases, the power-law spectra in solar flares and Earth's magnetotail plasma sheet are softer (steeper) while those of shocks and the solar wind are relatively harder (flatter). As described in Section 2, the 'above-the-looptop' source is a special case of non-thermal coronal emission in which the higher energy source is located clearly anti-sunward from the lower energy source.

power-law index δ also appears to show the similar lower-limit 3 – 4 in both the collapsing and reconnection regions (Figures 9 and 10), as summarized in Fig. 16. Some studies show that the power-law index δ can be substantially smaller in the < 10 R_E range (e.g. Stepanova and Antonova 2015; Runov et al. 2015). However, such an inner region resembles more like the looptop region rather than the above-the-looptop (ALT) region. Also, the inner region is where the radiation-belt electrons are generated, while an analogous region to the radiation belts does not seem to exist in solar flares. Thus, it appears reasonable to avoid values from the inner magnetosphere when comparing with solar flare ALT source. We also note that the there may be a fast-mode shock in the ALT source and it may be fundamentally different from the collapsing (or flow-braking) region we see in the magnetotail (as a fast-mode shock have not been detected in the magnetotail).

With all these factors taken into account, it is evident in Figure 16 that electron power-law spectra in the regions close to reconnection are relatively soft and δ is larger than ~ 4 in many cases (or $\sim$3 depending on the spectral model and/or energy range). The roughly similar lower limit at 3 – 4 is interesting, despite the orders of magnitudes difference of plasma parameters (See Appendix A).

5.1.2 Regions away from Reconnection Site

For solar flares, the footpoint sources are in the chromosphere and are away from the reconnection site in the standard model. The typical δ values of the footpoint sources are 3.5 – 4.7 (Figure 3). This is comparable to the typical δ values of 3 – 5 of the non-thermal emission in the corona.

The magnetospheric analogue of the footpoint sources is the top-side ionosphere. These are the regions which emit the brightest extreme-ultraviolet (EUV) and X-rays (e.g. Borg et al. 2007, and references therein). As reviewed in Section 3.4, power-law tails do exist in and around the auroral region (in the altitude of less than $\sim$ 1000 km). Unlike the power-law indices in solar footpoint sources, the power-law indices in the aurora region takes a wide range of values. The variation is so large that the distribution can be very close to Maxwellian $\delta >$8. In some cases, the power-law spectra can be very hard with δ as small as $\sim$2. The spectra can be hard even in the high-latitude plasma sheet, geometrically corresponding to the location along the loop, somewhere between the footpoint and looptop regions in a solar flare loop.

5.2 Shocks vs Reconnection

Figure 16 also shows the δ values from shocks and quiet-time solar wind (as described in Section 4 and illustrated in Figure 13). It is evident that shocks produce electron energy spectra harder than those in solar flares and Earth's magnetotail where magnetic reconnection plays an important role in their dynamics. Although there can be an overlap in the $\delta =$ 3 – 4 range, the difference suggests that electron acceleration at shocks leads to a larger non-thermal fraction of electron energies when compared to magnetic reconnection (and associated processes).

This difference between the shocks (including the downstream regions) and reconnection-related region may provide a hint for solving the problem of electron acceleration mechanism in the above-the-looptop (ALT) source. It has been suggested that a fast-mode termination shock plays an important role for accelerating electrons in the ALT source (as described in Section 2.4.1), although the power-law spectrum is soft (as mentioned above). Even in the recent study of fast-mode termination shock by Chen et al. (2015), the power-law index as measured by RHESSI was $\delta \sim$ 4.5 - 6.2 (using the thin-target assumption; the spectra would be even softer for a thick-target assumption).

In contrast, *in situ* measurements in space have shown that a fast-mode shock produces a hard power-law ($\delta \sim 2 – 4$) even in a weak shock condition similar to that of the above-the-looptop source, i.e., low Alfvén Mach number ($\sim$ 2) and large shock angle ($> 80^{o}$) (Oka et al. 2006). However, the spectrum can be softer ($\delta < 4$) if the shock angle were smaller. Thus, the fact that solar flare observations show soft spectra in the ALT source suggests that the shock angle is sufficiently small ($< 80^{o}$) or the shock acceleration scenario does not apply. It is also very possible that the spatial resolution of the X-ray measurement is insufficiently low and that a (possibly hard) power-law spectrum at the shock may have been averaged out. Therefore, a significantly higher spatial resolution is crucial for future studies of the shock acceleration scenario.

5.3 Origin of Power-Law Tails in Earth's Magnetotail

We point out a possibility that electrons form a power-law tail outside of the magnetotail and that such a non-thermal component is transported into the magnetotail without a significant change of the spectral form. As reviewed in Section 3.3.1, power-law distributions are present in the magnetotail plasma sheet even during quiet times (e.g. Anderson 1965; Christon et al. 1989) and the power-law index δ does not necessarily change by activity or locations (e.g. Åsnes et al. 2008; Gabrielse et al. 2014; Wu et al. 2015). These observations indicate that the existence of power-law high-energy tails of particle distributions cannot be taken as evidence for their creation inside the magnetotail. It should be noted that non-thermal tails are already present in the solar wind and in the magnetosheath (as reviewed in Section 4) in the energy range above a few hundreds of eV and these tails may enter into the magnetotail.

In fact, it has been suggested the bulk of the solar wind (and magnetosheath) plasma is transported into the plasma sheet from the distant tail (e.g. Gosling et al. 1984), through dayside reconnection (e.g. Baker et al. 1996) and the flanks of the magnetotail (e.g. Terasawa et al. 1997), although there is a substantial contribution from the ionosphere to the near-Earth plasma sheet. Magnetic reconnection in the distant tail could be important for the plasma transport from the distant tail to the near-Earth tail, although the precise mechanism of transport remains an open question (e.g. Hultqvist et al. 1999). We also note that the average (kinetic) temperatures increase from the magnetosheath to the magnetotail by an order of magnitude, but the typical ion to electron temperature ratio remains almost constant (5 – 10) (e.g. Wang et al. 2012). This can be taken as evidence that the major entry mechanism (which is still debated) is consistent with adiabatic heating, which would keep the shape of the energy distributions unchanged, so that the quiet time populations in the tail may be considered as heated magnetosheath populations.

Such an external origin scenario of electron power-law tails does not contradict with the observations that electrons are energized significantly in the magnetotail. Non-thermal electrons that enter from the magnetosheath can further acquire energies in the magnetotail as indicated by particle flux increases, well documented in the magnetotail over a wide range of distances (as reviewed in Section 3). And the energization process may, but need not, involve a change in the power law index.

However, the precise origin of the electron power-law tails and their evolution in the magnetotail remain inconclusive, and the external origin scenario of electron power-law tails needs to be studied further. This is because, we have shown, through a review of various studies, that electron energy spectra in the plasma sheet are relatively softer ($\delta \sim 3$ – 5) than those in the solar wind and magnetosheath ($\delta \sim 2$ –4), suggesting different sources of the power-law tails. In fact, a statistical analysis reported that there is no clear correlation between energetic plasma sheet electrons (>38 keV) and solar wind electrons of comparable energies (Burin des Roziers et al. 2009b). Similarly, Luo et al. (2012) reported that, for most of their magnetopause crossing events (>70%), the fluxes and phase-space-densities of energetic ($>$ 38 keV) electrons in the magnetosheath were less than those in the magnetosphere. They suggested that the energetic electrons in the magnetosheath cannot be a direct source sufficient for the energetic electrons inside the magnetosphere. Also, detailed case studies of the reconnection diffusion region (including the Hall region and electron diffusion region) report that electrons are energized across the diffusion region (as reviewed Section 3.3.2), suggesting that the lobe electrons rather than magnetosheath electrons entering through the tail flanks are accelerated.

5.4 Possible Future Studies

Our review led us to suggest similar values of δ (around 3 – 5) in the regions close to magnetic reconnection in solar flares and Earth's magnetotail. However, it is desired to have a larger number of studies of δ (from both observational and theoretical points of view) to examine the generality or validity of this idea.

An issue we have encountered in this review is that different studies use different models, methodologies or techniques to derive the power-law index, possibly leading to inconsistent results or larger variations of the δ values. For example, while some observations have a limited coverage of the energy range or a limited number of data points in the energy range (ending up using only a single functional form), other observations have a wide energy-range coverage or many data points (ending up using a combination of different spectral models). Thus, it is desirable to carry out a more systematic and coordinated studies of power-law distributions using consistent methodologies and conditions for comparing particle spectra in different regions. For studies of solar flares, we propose more frequent use of the relativistic Bethe-Heitler bremsstrahlung cross-section as implemented in the RHESSI/OSPEX software for more convenient comparisions with electron distributions measured *in-situ*. We also support development of new instrumentations or techniques. In particular, future solar X-ray missions with focusing optics (currently being proposed in Unites States and Japan) would achieve higher sensitivities and larger dynamic ranges. For studies of the magnetotail, MMS completed its first main tail season ('Maha Phase') very recently (2017 fall). With the state-of-the-art measurements achieved by MMS (for example, large energy coverages combined with unprecedentedly high time resolution), we envision a substantial advancement of our understanding of the power-law tails (for both ions and electrons) in the magnetotail in the coming years.

From a theoretical point of view, we already have a variety of different particle acceleration mechanisms (as briefly summarized in Section 1.4 and thoroughly reviewed in other review papers). However, in order to quantitatively predict the power-law index δ, we need a more generalized model for the 'escape' process via, for example, diffusion, because it would make the energy spectrum softer than the hardest possible spectrum (i.e., $\delta = 1.5$) as described in Section 1.4. Because particles need to be trapped in a specific region to be accelerated, the modeling of the 'escape' process can be equivalent to the modeling of particle trapping in acceleration region. In flares, the fact that the non-thermal coronal source is generally isolated rather than spatially extended along the loop already indicates that a certain degree of trapping is at work in the (above-the-)looptop region (See also Section 2.5). Thus, there have been many theoretical studies of trapping and related transport of flare particles from different approaches (e.g. Minoshima et al. 2011; Li et al. 2012; Chen and Petrosian 2013; Kontar et al. 2014). For Earth's magnetotail, the basic behaviors of energetic electrons seem to be explained by the drift motion in and around the dipolarizing flux bundles (e.g. Birn et al. 2004, 2013; Gabrielse et al. 2016) (See also Section 3.3.3). However, some observations suggest a need for taking into account particle diffusion processes (e.g. Imada et al. 2008; Stepanova and Antonova 2015, and references therein).

A Plasma Parameter Regimes

Plasma parameter regimes in the solar corona and Earth's magnetotail generally do not overlap (Table 3). For example, magnetic field magnitudes in the corona (2 – 200 G) are $>$ 4 orders of magnitude larger than those in the lobe region of Earths magnetotail ($\sim$ 30 nT). Also, the number densities in the corona ($\sim 10^8$ cm^{-3})

Table 3 Typical plasma parameters in different regions. Note 1 MK $\sim$ 86 eV and 1 G = 10^5 nT. The solar flare looptop parameters are for the above-the-looptop events that showed large loop sizes $>$ 40 Mm. Many flares are smaller $\lesssim$20 Mm and the parameters may be different by orders of magnitude. For comparison, typical parameters at $H \sim 50$ Mm in the quiet-time corona are shown in the first column (Taken from Aschwanden et al. (1999) and references therein). The 'collapsing region' in this table refers to the current sheet center $B_{x,\mathrm{GSM}} \sim 0$ around $|X_{\mathrm{GSM}}|$ = 8 – 11 R_E after arrival of dipolarization fronts. The ion (proton) gyro radius is based on the temperature and magnetic field magnitude that are also listed in the table.

Physical quantities	Solar Corona (in quiet time at $H \sim 50$ Mm)	Solar Corona (large flare looptop)	Magnetotail (lobe)	Magnetotail (collapsing region)	Solar Wind (at 1 AU)
density (cm^{-3})	$\sim 10^8$	$10^{10} - 10^{11}$	< 0.01	0.1 – 1	1 – 10
temperature (MK)	$\sim$2	10 – 30	< 1	10 – 100	0.1
magnetic field (G)	2 – 200	$\gtrsim$100	10^{-4}	10^{-4}	$10^{-5} - 10^{-4}$
Alfvén speed (km/s)	400 – 40000	500 – 2000	> 2000	100 – 1000	20 - 100
plasma β	< 0.1	$\lesssim 1$	< 0.1	0.1 – 100	0.1 - 50
ion gyro radius (km)	$10^{-4} - 10^{-2}$	$< 10^{-3}$	< 100	100 – 1000	10 – 1000
electron plasma frequency (Hz)	10^8	$\sim 10^9$	10^3	$10^{-4} - 10^{-3}$	$10^{-5} - 10^{-4}$
electron gyro frequency (Hz)	$10^6 - 10^8$	$> 10^8$	$10^2 - 10^3$	$10^2 - 10^3$	$10^1 - 10^2$

are roughly 10 orders of magnitude larger than those in the magnetotail (0.01 cm^{-3}), and the corona can be somewhat collisional depending on particle energies especially in a flaring region.

Interestingly, the Alfvén speed V_A turns out to be similar, of the same order of magnitude, and the plasma beta β sometimes differ by only 1 – 2 orders of magnitude (Terasawa et al. 2000; Lin et al. 2008). A caveat is that the ion gyro radius is $\sim$ 5 orders of magnitude smaller in the solar coronal environment. Thus, if normalized by the ion gyro radius (or the thickness of a reconnecting current sheet [8]), the spatial scale of a solar flare is again many orders of magnitude larger than that of the magnetotail. Therefore, plasma conditions remain very different in solar flares and Earth's magnetotail.

Note that solar flares can occur in various spatial scales at different altitude (e.g. Shibata et al. 2007). If magnetic reconnection takes place in the chromosphere with a characteristic spatial scale of $\sim 10^3$ km or less, the environment would be dominated by partially ionized plasmas with frequent Coulomb collisions.

The guide field B_g (the magnetic field component perpendicular to the reconnection plane) is also an important parameter, especially from the reconnection physics point of view. It is zero when two magnetic field lines are approaching toward each other (to be reconnected) at exactly 180° angle. It is non-zero when the shear angle is less than 180°. In the near-Earth plasma sheet, say R$<$30R_E, B_g is often small and can be $\sim$0.1 B_0 where B_0 is the asymptotic value in the magnetotail lobe region. However, B_g/B_0 can be as large $\sim$1 in the distant magnetotail as well as in the solar corona.

B Non-Extensive Statistical Mechanics

Classical particle systems in thermal equilibrium have their phase-space distribution stabilized into a Maxwell-Boltzmann function. These systems are characterized by limited or no correlations among their particles' energies or individual phase-space. In contrast, space plasmas are particle systems frequently described by stationary states out of thermal equilibrium, namely, their distribution is stabilized into a function that is not given by the Maxwell-Boltzmann formulation and is typically described by a kappa distribution (See Section 1.3, Eq. (11)). These systems are characterized by long-range interactions that induce 'correlations' resulting to a collective behavior among particles.[9]

[8] Our experimence with particle-in-cell (PIC) simulations as well as Earth's magnetotail suggests that a current sheet needs to be as thin as the ion gyro radius before magnetic reconnection to take place.

[9] Correlations are represented by a collective behavior of plasma particles via electrostatic and/or electromagnetic fields and can keep space plasmas away from the thermal equilibrium (e.g. Livadiotis 2015).

Non-extensive statistical mechanics was introduced by Tsallis (1988) as a generalization of Boltzmann-Gibbs statistical mechanics. It has been applied to power-law distributions in various fields of natural and social science. Inspired by multifractals, Tsallis introduced a free parameter q and postulated that the entropy can be expressed as

$$S_q \equiv k_B \frac{1-\int f(v)^q dv}{q-1}, \tag{16}$$

where $f(v)$ is the probability function (This is a continuum limit in which intergral is used instead of sum of discretized volume element). In the limit of $q \to 1$, it reduces to the traditional Boltzmann-Gibbs entropy, $S_1 = -k_B \int f(v) \ln f(v) dv$. While Boltzmann-Gibbs entropy is extensive (or additive due to the logarithmic measure), Tsallis entropy is non-extensive, i.e., the entropy of the whole is not equal with the sum of the partial entropies of the parts. Note that the Boltzmann-Gibbs entropy is maximized under the constraints of canonical ensemble (i.e., normalization of the distribution, and fixed energy of the system) leading to the Maxwell-Boltzmann distribution. On the other hand, the maximization of Tsallis entropy under the constraints of the canonical ensemble leads to Tsallis distribution which is, in one-dimensional form,

$$f(v) \propto \left[1+(q-1)(\beta v^2)\right]^{-\frac{1}{q-1}}, \tag{17}$$

where β is a parameter related to the inverse of temperature and the q-index (e.g. Tsallis 1988; Tsallis et al. 1998). This distribution recovers the Maxwell-Boltzman distribution in the limit of $q \to 1$.

It was soon recognized that, with the transformation $\kappa = 1/(q-1)$, the Tsallis distribution corresponds to the empirically derived kappa distribution (Section 1.3, Eq. (11))[10]. The connection of kappa distributions with statistical mechanics, and specifically with the concept of non-extensive statistical mechanics, has been established by several authors (e.g. Treumann 1997; Milovanov and Zelenyi 2000; Leubner 2002; Livadiotis and McComas 2009). Livadiotis and McComas (2009) showed that the consistent connection of the theory and formalism of kappa distributions with non-extensive statistical mechanics is based on several fundamental physical notions and concepts, including that of temperature. For further details, see the 'historical comments' in Chapter 1 of Livadiotis (2017).

The κ parameter (that appears in the power-law index) is interwoven with the statistical correlation between the energy of the particles. It has been shown that a simple relation exists between the correlation ρ (ranging between 0 and 1) and κ, i.e., $\rho = (3/2)\kappa$ for 3 degrees of freedom per particle (Livadiotis and McComas 2011). The largest value of kappa is infinity, corresponding to the system residing at thermal equilibrium, where the particles are characterized by zero correlation. The smallest kappa is 3/2 and corresponds to the furthest state from thermal equilibrium, called anti-equilibrium, where the particle energies are highly correlated.

Finally, we mention that the relations of kappa with spectral indices may change in the presence of nonzero potential energies (Livadiotis 2015b), anisotropies of the velocity space (Chapter 10 of Livadiotis (2017)), and generalized formalisms of kappa distributions (e.g., the Lp-normed kappa distribution, Livadiotis (2016); Randol and Christian (2016)).

C Fermi Acceleration

Here we summarize very briefly the original theory by Fermi and its variants, following reviews by, for example, Tsuneta (2011). For a more complete review, readers are referred to literatures by, for example, Drury (1983); Blandford and Eichler (1987); Longair (1994) and Kulsrud (2005).

If we consider a particle with mass m and speed v in an acceleration region full of magnetic 'clouds', the particle energy gain by an elastic collision with a cloud (in 1D space) would be $\Delta E_\pm = (1/2)m(v \pm 2V)^2 - (1/2)mv^2 \sim \pm 2mvV$ where $V \ll v$ is the speed of the cloud and the positive and negative signs denote the

Thus, correlations can be present at different spatial scales. The smallest correlation length is represented by the Debye length (e.g. Livadiotis and McComas 2014) and the largest correlation length is represented by, perhaps, the minium wave number $k_{\min}$ of power spectral density, often discussed in the context of solar wind turbulence theory. Without any correlation, plasmas would be completely uniform with no characteristic spatial scale. As a result of correlations (and associated collective behaviors), space plasmas would reach a steady state represented by the kappa distribution. As a result of collisions, on the other hand, space plasmas would reach a steady state represented by the Maxwell distribution as collisions would destry correlations (e.g. Livadiotis 2015).

[10] As already noted in the footnote of Section 1.3, these slightly different forms of kappa distribution can be equivalent under a certain transformation.

head-on and head-tail collisions, respectively. Here, the probability of head-on and head-tail collisions can be expressed as

$$p_{\pm} = \frac{v \pm V}{2v}, \tag{18}$$

where $p_+ + p_- = 1$ and p_+ is slightly larger than p_-. Thus, the average energy gain by a collision becomes $\Delta E = p_+ \Delta E_+ + p_- \Delta E_- = 2mV^2$. Using the average collision time $\sim l/v$, where l is the typical distance between clouds, the energy gain per unit time becomes

$$\frac{dE}{dt} = \alpha E, \tag{19}$$

where $\alpha \equiv 4V^2/vl$. In a 3D configuration, $\alpha = (4/3)V^2/vl$ as described by, for example, Longair (1994) for the relativistic case. If the particle is relativistic $v \sim c$, α can be regarded as a constant so that solving Eq. 19 yields $E \propto \exp(\alpha t)$, indicating exponential energy increase. (The non-relativistic case will be described later.) Because of the dependence on V^2, this process is called **second-order Fermi** acceleration.

Particle thus accelerated will, at some point, escape from the acceleration region. If we define such a time scale $t_{\rm esc}$, the probability of a particle remaining in the acceleration region could be expressed as $P(t) = \exp(-t/t_{\rm esc})$. Then, $dN/dE = (dP/dt)(dt/dE)$ becomes a power law, as does the differential density $N(E)$

$$N(E) \propto E^{-\left(1+\frac{t_{\rm acc}}{t_{\rm esc}}\right)}, \tag{20}$$

where we have used the acceleration time scale $t_{\rm acc} \equiv \alpha^{-1}$ because of Equation (19). Therefore, the power-law index is a function of both acceleration (energization 'kick') and escape time scales (However, the quantity $\tau_{\rm acc}/\tau_{\rm esc}$ is assumed to be energy independent). The same power-law form can be derived if we consider the continuity equation in energy space

$$\frac{\partial N}{\partial t} + \frac{\partial}{\partial E}\left(\frac{dE}{dt}N\right) = q - \frac{N}{t_{\rm esc}} \tag{21}$$

where q is the source term. If we neglect the source term and use Equation (19), then we can readily obtain Equation (20).

This Fermi process would be more efficient if there were head-on collisions only (one can imagine a trapped particle bouncing between two walls approaching toward each other). In this case, the average energy gain by a collision becomes $\Delta E = 2mvV$. The average collision time could be $\sim 2l/v$ so that we again obtain Equation (19) but with $\alpha = 2V/l$, which is a constant in both relativistic and non-relativistic regimes. Because of the dependence on V this is known as **first-order Fermi** acceleration.

As for the non-relativistic case of the second-order Fermi acceleration, α in Eq. (19) is not a constant and the equation should be rewritten as

$$\frac{dE}{dt} = \alpha E^{\frac{1}{2}} \tag{22}$$

with the constant $\alpha = 2\sqrt{2m}V^2/l$. Using Equation (21), the differential density becomes

$$N(E) = E^{-0.5} \exp\left(-\sqrt{\frac{E}{E_0}}\right) \tag{23}$$

where $E_0 \equiv \alpha^2 t_{\rm esc}^2/4$ (e.g. Tsuneta 1995). This is an unrealistically hard power-law with an exponential cutoff at E_0. Thus, we expect first-order Fermi acceleration (instead of second-order) to be applicable in many cases of power-law observations reviewed in this paper. When acceleration occurs by a DC electric field (i.e., $m(dv/dt) = -eE$ with electric field E larger than the Dreicer electric field), Eq. (22) appears again with $\alpha = \sqrt{2/me}E$ if we allow $E = (1/2)mv^2$ (e.g. Tsuneta 1995). Thus, a DC electric field alone likely cannot explain the power-law spectra in solar flares as well as Earth's magnetotail because they are much softer (steeper).

Let us now consider what a 'cloud' could be or how particles receive an energization 'kick' in the acceleration region. The nature of the 'kick' can actually vary in different situations. The most widely known application of Fermi acceleration is the diffusive shock acceleration (DSA) whereby particles move back and forth across the shock front and receive energy 'kick' multiple times via collisions with magneto-hydrodynamic (MHD) waves, which are assumed to be convecting together with the plasma bulk flow. While waves are convected toward the same direction (i.e., downstream) with the speed V_1 and V_2 in the upstream and downstream regions, respectively, we can find a frame in which the upstream and downstream plasma converge toward each other with the speed $(V_1 - V_2)/2$, leading to first-order Fermi acceleration. Additional details of diffusive shock acceleration can be found in, for example, Blandford and Eichler (1987).

In solar flares and Earth's magnetotail, where the spatial scale of the acceleration region (or more precisely the magnetic field curvature radius) can be larger than the particle gyro-radius, particle motion may be described by a guiding-center approximation (e.g. Northrop 1963). In this approximation the rate of energy gain may be expressed

$$\frac{dE}{dt} = -\mu V_{||} \frac{\partial B}{\partial s} + m(v_{||} - V_{||})^2 \mathbf{V}_{\perp} \cdot \frac{\partial \mathbf{b}}{\partial s} + \mathscr{O}(l^2), \tag{24}$$

where $\mathbf{V}$ is the velocity of the 'cloud,' $\mathbf{b} = \mathbf{B}/B$, $\partial/\partial s = \mathbf{b} \cdot \nabla$, $\mu = m_e v_{\perp}^2/(2B)$, and l represents the smallness parameter, for instance, the ratio between gyro-radius and a macroscopic scale length (Northrop 1963). The first term on the right-hand side represents **Fermi Type A acceleration**, i.e., a reflection by a moving magnetic mirror, and includes the effect of betatron acceleration. The second term is **Fermi Type B acceleration**, or the 'slingshot' effect (Birn et al. 2004), which occurs when the lines of force are curved but the magnitude of $\mathbf{B}$ may be constant along the guiding center trajectory.

Figure 2 illustrates field-line configurations favorable for Fermi Type B acceleration. Fig. 2a shows the curved field line as illustrated in the original paper by Fermi (1949). Fig. 2b represents a situation in which the two ends of the field-line are fixed (or 'line-tied') (e.g., the collapsing magnetic fields in solar flares and Earth's magnetotail). While particles can undergo mirror reflection at the footpoints, in the observer's frame $\partial \mathbf{b}/\partial s = 0$ and Fermi Type B acceleration is dominant. In the frame co-moving with the 'looptop' (i.e., the intersection of the field line and the equatorial plane), Fermi Type A acceleration becomes important. Such a frame dependence has been reproduced in more realistic simulations of test-particles in dynamically evolving MHD fields of Earth's magnetotail (e.g. Birn et al. 2004, 2013). Fig. 2c shows a magnetic island in which the curved field-line in Fig. 2a is closed by another curved field-line on the opposite side. The dynamical (shrinking) motion of the magnetic island leads to particle energization (e.g. Kliem 1994) (as in the analogy of two walls approaching toward each other) and has drawn considerable attentions in recent years (e.g. Drake et al. 2006). Theoretically, there could also be a hybrid in which a magnetic island hits a fast-mode shock so that the gray region in Fig. 2b represents the shock (e.g. Nishizuka and Shibata 2013).

Acknowledgements We thank Vahé Petrosian for his comments on the power-law index conversions including Table 1. We thank Alexander Warmuth and Hugh Hudson for drawing our attention to some important papers on flares with unusually hard power-law spectra. We thank Shiyong Huang for drawing our attention to some important papers on energetic electrons in the magnetotail. We thank Christine Gabrielse for a clarification of her analysis. We thank Alfred Mallet for his comment on turbulence. We thank Fan Guo for his helpful comments about this manuscript.

This work was initiated and partly carried out with support from the International Space Science Institute (ISSI) in the framework of an International Team entitled 'Particle acceleration in solar flares and terrestrial substorms'. We particularly thank Lyndsay Fletcher for her contributions to this paper as a member of the ISSI team. The authors are indebted to ISSI and its staff in Bern, Switzerland, for the support of this activity. MO was supported by NASA grants NNX08AO83G at UC Berkeley and NNH16AC60I at Los Alamos National Laboratory (LANL). FE acknowledges partial support by NASA grant NNX17AK25G.

References

M. Ackermann, A. Allafort, L. Baldini, G. Barbiellini, D. Bastieri, R. Bellazzini, E. Bissaldi, R. Bonino, E. Bottacini, J. Bregeon, P. Bruel, R. Buehler, R.A. Cameron, M. Caragiulo, P.A. Caraveo, E. Cavazzuti, C. Cecchi, E. Charles, S. Ciprini, F. Costanza, S. Cutini, F. D'Ammando, F. de Palma, R. Desiante, S.W. Digel, N.D. Lalla, M.D. Mauro, L.D. Venere, P.S. Drell, C. Favuzzi, Y. Fukazawa, P. Fusco, F. Gargano, N. Giglietto, F. Giordano, M. Giroletti, I.A. Grenier, L. Guillemot, S. Guiriec, T. Jogler, G. Jóhannesson, L. Kashapova, S. Krucker, M. Kuss, G.L. Mura, S. Larsson, L. Latronico, J. Li, W. Liu, F. Longo, F. Loparco, P. Lubrano, J.D. Magill, S. Maldera, A. Manfreda, M.N. Mazziotta, W. Mitthumsiri, T. Mizuno, M.E. Monzani, A. Morselli, I.V. Moskalenko, M. Negro, E. Nuss, T. Ohsugi, N. Omodei, E. Orlando, V. Pal'shin, D. Paneque, J.S. Perkins, M. Pesce-Rollins, V. Petrosian, F. Piron, G. Principe, S. Rainò, R. Rando, M. Razzano, O. Reimer, F.R. da Costa, C. Sgrò, D. Simone, E.J. Siskind, F. Spada, G. Spandre, P. Spinelli, H. Tajima, J.B. Thayer, D.F. Torres, E. Troja, G. Vianello, Fermi -LAT Observations of High-energy Behind-the-limb Solar Flares. Astrophys. J. **835**(2), 219 (2017). doi:10.3847/1538-4357/835/2/219. http://stacks.iop.org/0004-637X/835/i=2/a=219?key=crossref.91dc818a387d47db42b229ff3fe731af

N. Agueda, K.-L. Klein, N. Vilmer, R. Rodríguez-Gasén, O.E. Malandraki, A. Papaioannou, M. Subirà, B. Sanahuja, E. Valtonen, W. Dröge, A. Nindos, B. Heber, S. Braune, I.G. Usoskin, D. Heynderickx, E. Talew, R. Vainio, Release timescales of solar energetic particles in the low corona. Astron. Astrophys. **570**(A5), 5 (2014). doi:10.1051/0004-6361/201423549. http://www.aanda.org/10.1051/0004-6361/201423549

D. Alexander, T.R. Metcalf, Energy dependence of electron trapping in a solar flare. Sol. Phys. **210**(1/2), 323–340 (2002). doi:10.1023/A:1022457413628. http://link.springer.com/chapter/10.1007/978-94-017-3452-3_18 http://link.springer.com/10.1023/A:1022457413628

K.A. Anderson, Energetic electron fluxes in the tail of the geomagnetic field. J. Geophys. Res. **70**(19), 4741–4763 (1965). doi:10.1029/JZ070i019p04741. http://doi.wiley.com/10.1029/JZ070i019p04741

V. Angelopoulos, The THEMIS Mission. Space Sci. Rev. **141**, 5–34 (2008). doi:10.1007/s11214-008-9336-1. http://www.springerlink.com/index/10.1007/s11214-008-9336-1

V. Angelopoulos, W. Baumjohann, C.F. Kennel, F.V. Coroniti, M.G. Kivelson, R.J. Walker, G. Paschmann, Bursty Bulk Flows in the Inner Central Plasma Sheet flows. J. Geophys. Res. Sp. Phys. **97**(A4), 4027–4039 (1992)

Y. Asano, R. Nakamura, I. Shinohara, M. Fujimoto, T. Takada, W. Baumjohann, C.J. Owen, a.N. Fazakerley, A. Runov, T. Nagai, E.a. Lucek, H. Rème, Electron flat-top distributions around the magnetic reconnection region. J. Geophys. Res. Sp. Phys. **113**(A1), 01207 (2008). doi:10.1029/2007JA012461. http://doi.wiley.com/10.1029/2007JA012461

Y. Asano, I. Shinohara, A. Retinò, P.W. Daly, E.a. Kronberg, T. Takada, R. Nakamura, Y.V. Khotyaintsev, A. Vaivads, T. Nagai, W. Baumjohann, a.N. Fazakerley, C.J. Owen, Y. Miyashita, E.a. Lucek, H. Rème, Electron acceleration signatures in the magnetotail associated with substorms. J. Geophys. Res. Sp. Phys. **115**, 05215 (2010). doi:10.1029/2009JA014587. http://www.agu.org/pubs/crossref/2010/2009JA014587.shtml

M.J. Aschwanden, *Physics of the Solar Corona*. Springer Praxis Books (Springer Berlin Heidelberg, ???, 2005). ISBN 978-3-540-30765-5. doi:10.1007/3-540-30766-4. http://link.springer.com/10.1007/3-540-30766-4

M.J. Aschwanden, Y. Xu, J. Jing, GLOBAL ENERGETICS OF SOLAR FLARES. I. MAGNETIC ENERGIES. Astrophys. J. **797**, 50 (2014). doi:10.1088/0004-637X/797/1/50. http://stacks.iop.org/0004-637X/797/i=1/a=50?key=crossref.8f2c7814cc268eec2cbb20c7d5aaba00

M.J. Aschwanden, L. Fletcher, T. Sakao, T. Kosugi, H. Hudson, Deconvolution of Directly Precipitating and Trapprecipitating Electrons in Solar Flare Hard XRays. III. Yohkoh Hard XRay Telescope Data Analysis. Astrophys. J. **517**(2), 977–989 (1999). doi:10.1086/307230. http://ads.nao.ac.jp/abs/1999ApJ...517..977A%5Cnhttp://iopscience.iop.org/0004-637X/517/2/977/pdf/39391.web.pdf http://stacks.iop.org/0004-637X/517/i=2/a=977

S.M. Ashford, K.A. Anderson, R.P. Lin, J.R. Sommers, J.L. Phillips, Energetic solar particle dropouts detected by Ulysses at 1.63 AU: A possible encounter with the Earth's distant magnetotail. J. Geophys. Res. Sp. Phys. **103**(A5), 9535–9543 (1998). doi:10.1029/97JA02864. http://doi.wiley.com/10.1029/97JA02864

A. Åsnes, R.W.H. Friedel, B. Lavraud, G.D. Reeves, M.G.G.T. Taylor, P. Daly, Statistical properties of tail plasma sheet electrons above 40 keV. J. Geophys. Res. Sp. Phys. **113**(A3), (2008). doi:10.1029/2007JA012502. http://doi.wiley.com/10.1029/2007JA012502

H. Aurass, B. Vršnak, G. Mann, Shock-excited radio burst from reconnection outflow jet? Astron. Astrophys. **384**(1), 273–281 (2002). doi:10.1051/0004-6361:20011735. http://www.edpsciences.org/10.1051/0004-6361:20011735

H. Aurass, G. Mann, Radio Observation of Electron Acceleration at Solar Flare Reconnection Outflow Termination Shocks. Astrophys. J. **615**(1), 526–530 (2004). doi:10.1086/424374. http://stacks.iop.org/0004-637X/615/i=1/a=526

D.N. Baker, E.C. Stone, Energetic electron anisotropies in the magnetotail: Identification of open and closed field lines. Geophys. Res. Lett. **3**(9), 557–560 (1976). doi:10.1029/GL003i009p00557. http://doi.wiley.com/10.1029/GL003i009p00557

D.N. Baker, R.D. Belian, P.R. Higbie, E.W. Hones, High-energy magnetospheric protons and their dependence on geomagnetic and interplanetary conditions. J. Geophys. Res. **84**(A12), 7138 (1979). doi:10.1029/JA084iA12p07138

D.N. Baker, P. Stauning, E.W. Hones, P.R. Higbie, R.D. Belian, Near-equatorial, high-resolution measurements of electron precipitation at L 6.6. J. Geophys. Res. **86**(A4), 2295 (1981). doi:10.1029/JA086iA04p02295. http://doi.wiley.com/10.1029/JA086iA04p02295

D.N. Baker, T.I. Pulkkinen, V. Angelopoulos, W. Baumjohann, R.L. McPherron, Neutral line model of substorms: Past results and present view. J. Geophys. Res. Sp. Phys. **101**(A6), 12975–13010 (1996). doi:10.1029/95JA03753. http://www.agu.org/pubs/crossref/1996/95JA03753.shtml http://doi.wiley.com/10.1029/95JA03753

D.N. Baker, X. Li, J.B. Blake, S. Kanekal, Strong electron acceleration in the Earth's magnetosphere. Adv. Sp. Res. **21**(4), 609–613 (1998). doi:10.1016/S0273-1177(97)00970-8. http://www.sciencedirect.com/science/article/pii/S0273117797009708 http://linkinghub.elsevier.com/retrieve/pii/S0273117797009708

S.J. Bame, J.R. Asbridge, H.E. Felthauser, R.A. Olson, I.B. Strong, Electrons in the Plasma Sheet of the Earth's Magnetic Tail. Phys. Rev. Lett. **16**(4), 138–142 (1966). doi:10.1103/PhysRevLett.16.138. https://link.aps.org/doi/10.1103/PhysRevLett.16.138

S.J. Bame, J.R. Asbridge, H.E. Felthauser, E.W. Hones, I.B. Strong, Characteristics of the plasma sheet in the Earth's magnetotail. J. Geophys. Res. **72**(1), 113 (1967). doi:10.1029/JZ072i001p00113. http://doi.wiley.com/10.1029/JZ072i001p00113

M. Battaglia, A.O. Benz, Exploring the connection between coronal and footpoint sources in a thin-thick target solar flare model. Astron. Astrophys. **466**(2), 713–716 (2007). doi:10.1051/0004-6361:20077144. http://www.aanda.org/10.1051/0004-6361:20077144

M. Battaglia, P.C. Grigis, A.O. Benz, Size dependence of solar X-ray flare properties. Astron. Astrophys. **439**(2), 737–747 (2005). doi:10.1051/0004-6361:20053027. http://www.aanda.org/10.1051/0004-6361:20053027

M. Battaglia, A.O. Benz, Relations between concurrent hard X-ray sources in solar flares **760**, 11 (2006). doi:10.1051/0004-6361:20065233. `http://arxiv.org/abs/astro-ph/0606353`

M. Battaglia, E.P. Kontar, HARD X-RAY FOOTPOINT SIZES AND POSITIONS AS DIAGNOSTICS OF FLARE ACCELERATED ENERGETIC ELECTRONS IN THE LOW SOLAR ATMOSPHERE. Astrophys. J. **735**(1), 42 (2011). doi:10.1088/0004-637X/735/1/42. http://arxiv.org/abs/1104.2997%0Ahttp://dx.doi.org/10.1088/0004-637X/735/1/42 http://stacks.iop.org/0004-637X/735/i=1/a=42?key=crossref.445b7c8d6b3e0226e62c23f6131a35cf

M. Battaglia, G. Motorina, E.P. Kontar, Multithermal Representation of the Kappa-Distribution of Solar Flare Electrons and Application To Simultaneous X-Ray and Euv Observations. Astrophys. J. **815**(1), 73 (2015). doi:10.1088/0004-637X/815/1/73. http://stacks.iop.org/0004-637X/815/i=1/a=73?key=crossref.2a85d130c4d23b7f39fa7cc06c9ed30c

A.O. Benz, *Plasma astrophysics: Kinetic processes in solar and stellar coronae* (Kluwer Academic Pubilshers, Boston, 1993), p. 299. ISBN 0792324293

A.O. Benz, Flare Observations. Living Rev. Sol. Phys. **14**(1), 2 (2017). doi:10.1007/s41116-016-0004-3. http://link.springer.com/10.1007/s41116-016-0004-3

A. Bhattacharjee, Impulsive Magnetic Reconnection in the Earth'S Magnetotail and the Solar Corona. Annu. Rev. Astron. Astrophys. **42**(1), 365–384 (2004). doi:10.1146/annurev.astro.42.053102.134039. http://www.annualreviews.org/doi/abs/10.1146/annurev.astro.42.053102.134039

N.H. Bian, a.G. Emslie, D.J. Stackhouse, E.P. Kontar, THE FORMATION OF KAPPA-DISTRIBUTION ACCELERATED ELECTRON POPULATIONS IN SOLAR FLARES. Astrophys. J. **796**(2), 142 (2014). doi:10.1088/0004-637X/796/2/142. http://stacks.iop.org/0004-637X/796/i=2/a=142?key=crossref.6ca523cba174623a1cc290b61b1e3e32

J. Birn, M.F. Thomsen, J.E. Borovsky, G.D. Reeves, D.J. McComas, R.D. Belian, Characteristic plasma properties during dispersionless substorm injections at geosynchronous orbit. J. Geophys. Res. Sp. Phys. **102**(A2), 2309–2324 (1997). doi:10.1029/96JA02870. http://doi.wiley.com/10.1029/96JA02870

J. Birn, R. Nakamura, E.V. Panov, M. Hesse, Bursty bulk flows and dipolarization in MHD simulations of magnetotail reconnection. J. Geophys. Res. Sp. Phys. **116**(A1), (2011). doi:10.1029/2010JA016083. http://doi.wiley.com/10.1029/2010JA016083

J. Birn, M. Hesse, Reconnection in substorms and solar flares: Analogies and differences. Ann. Geophys. **27**, 1067–1078 (2009). ISBN 1432-0576. doi:10.5194/angeo-27-1067-2009

J. Birn, A. Runov, M. Hesse, Energetic electrons in dipolarization events: Spatial properties and anisotropy. J. Geophys. Res. Sp. Phys. **119**(5), 3604–3616 (2014). ISBN 2169-9402. doi:10.1002/2013JA019738. http://doi.wiley.com/10.1002/2013JA019738

J. Birn, M.F. Thomsen, M. Hesse, Electron acceleration in the dynamic magnetotail: Test particle orbits in three-dimensional magnetohydrodynamic simulation fields. Phys. Plasmas **11**(5), 1825–1833 (2004). doi:10.1063/1.1704641

J. Birn, a.V. Artemyev, D.N. Baker, M. Echim, M. Hoshino, L.M. Zelenyi, Particle Acceleration in the Magnetotail and Aurora. Space Sci. Rev. **173**(1-4), 49–102 (2012). doi:10.1007/s11214-012-9874-4. http://www.springerlink.com/index/10.1007/s11214-012-9874-4 http://link.springer.com/10.1007/s11214-012-9874-4

J. Birn, M. Hesse, R. Nakamura, S. Zaharia, Particle acceleration in dipolarization events. J. Geophys. Res. Sp. Phys. **118**(October 2012), 1960–1971 (2013). doi:10.1002/jgra.50132

R. Blandford, D. Eichler, Particle acceleration at astrophysical shocks: A theory of cosmic ray origin. Phys. Rep. **154**(1), 1–75 (1987). doi:10.1016/0370-1573(87)90134-7. http://linkinghub.elsevier.com/retrieve/pii/0370157387901347

A.L. Borg, N. Østgaard, A. Pedersen, M. Øieroset, T.D. Phan, G. Germany, A. Aasnes, W. Lewis, J. Stadsnes, E.A. Lucek, H. Rème, C. Mouikis, Simultaneous observations of magnetotail reconnection and bright X-ray aurora on 2 October 2002. J. Geophys. Res. Sp. Phys. **112**(6), 1–9 (2007). doi:10.1029/2006JA011913

A. Bratenahl, P.J. Baum, On flares, substorms, and the theory of impulsive flux transfer events. Sol. Phys. **47**, 345–360 (1976). doi:10.1007/BF00152273

J.C. Brown, The deduction of energy spectra of non-thermal electrons in flares from the observed dynamic spectra of hard X-ray bursts. Sol. Phys. **18**(3), 489–502 (1971). doi:10.1007/BF00149070.

http://link.springer.com/10.1007/BF00149070

J.L. Burch, R. Torbert, T.D. Phan, L.-J. Chen, T.E. Moore, R.E. Ergun, J.P. Eastwood, D.J. Gershman, P.A. Cassak, M.R. Argall, S. Wang, M. Hesse, C.J. Pollock, B.L. Giles, R. Nakamura, B.H. Mauk, S.A. Fuselier, C.T. Russell, R.J. Strangeway, J.F. Drake, M.A. Shay, Y.V. Khotyaintsev, P.-A. Lindqvist, G. Marklund, F.D. Wilder, D.T. Young, K. Torkar, J. Goldstein, J.C. Dorelli, L.A. Avanov, M. Oka, D.N. Baker, A.N. Jaynes, K.A. Goodrich, I.J. Cohen, D.L. Turner, J.F. Fennell, J.B. Blake, J. Clemmons, M. Goldman, D. Newman, S.M. Petrinec, K.J. Trattner, B. Lavraud, P.H. Reiff, W. Baumjohann, W. Magnes, M. Steller, W. Lewis, Y. Saito, V. Coffey, M. Chandler, Electron-scale measurements of magnetic reconnection in space. Science (80-.). **352**(6290), 2939 (2016). doi:10.1126/science.aaf2939. http://www.sciencemag.org/cgi/doi/10.1126/science.aaf2939

E. Burin des Roziers, X. Li, Specification of >2 MeV geosynchronous electrons based on solar wind measurements. Sp. Weather **4**(6), (2006). doi:10.1029/2005SW000177. http://doi.wiley.com/10.1029/2005SW000177

E. Burin des Roziers, X. Li, D.N. Baker, T.A. Fritz, R.L. McPherron, I. Dandouras, Cluster observations of energetic electron flux variations within the plasma sheet. J. Geophys. Res. Sp. Phys. **114**(A11), (2009a). ISBN 0148-0227. doi:10.1029/2009JA014239. http://doi.wiley.com/10.1029/2009JA014239

E. Burin des Roziers, X. Li, D.N. Baker, T.A. Fritz, R. Friedel, T.G. Onsager, I. Dandouras, Energetic plasma sheet electrons and their relationship with the solar wind: A Cluster and Geotail study. J. Geophys. Res. Sp. Phys. **114**(A2), (2009b). doi:10.1029/2008JA013696. http://doi.wiley.com/10.1029/2008JA013696

A.M. Bykov, G.D. Fleishman, PARTICLE ACCELERATION BY STRONG TURBULENCE IN SOLAR FLARES: THEORY OF SPECTRUM EVOLUTION. Astrophys. J. **692**(1), 45–49 (2009). doi:10.1088/0004-637X/692/1/L45. http://stacks.iop.org/1538-4357/692/i=1/a=L45?key=crossref.fbc263a89e00489d173ac156eccc079d

A. Caspi, R.P. Lin, RHESSI LINE AND CONTINUUM OBSERVATIONS OF SUPER-HOT FLARE PLASMA. Astrophys. J. **725**(2), 161–166 (2010). doi:10.1088/2041-8205/725/2/L161. http://stacks.iop.org/2041-8205/725/i=2/a=L161?key=crossref.ed6e76acca2df640de6480bdcd36dd25

A. Caspi, S. Krucker, R.P. Lin, Statistical Properties of Super-Hot Solar Flares. Astrophys. J. **781**(1), 43 (2014). doi:10.1088/0004-637X/781/1/43. http://stacks.iop.org/0004-637X/781/i=1/a=43?key=crossref.7ca78824b32d7be241bfbe65748e5cd8

Y.F. Chateau, N. Meyer-Vernet, Electrostatic noise in non-Maxwellian plasmas: Flat-top distribution function. J. Geophys. Res. Sp. Phys. **94**(A11), 15407 (1989). doi:10.1029/JA094iA11p15407. http://doi.wiley.com/10.1029/JA094iA11p15407

B. Chen, T.S. Bastian, C. Shen, D.E. Gary, S. Krucker, L. Glesener, Particle acceleration by a solar flare termination shock. Science (80-.). **350**(6265), 1238–1242 (2015). doi:10.1126/science.aac8467. http://www.sciencemag.org/cgi/doi/10.1126/science.aac8467

L.-J. Chen, A. Bhattacharjee, P.a. Puhl-Quinn, H. Yang, N. Bessho, S. Imada, S. Mühlbachler, P.W. Daly, B. Lefebvre, Y. Khotyaintsev, A. Vaivads, A. Fazakerley, E. Georgescu, Observation of energetic electrons within magnetic islands. Nat. Phys. **4**(1), 19–23 (2007). doi:10.1038/nphys777. http://www.nature.com/doifinder/10.1038/nphys777

L.-J. Chen, N. Bessho, B. Lefebvre, H. Vaith, a. Åsnes, O. Santolik, A. Fazakerley, P. Puhl-Quinn, A. Bhattacharjee, Y. Khotyaintsev, P. Daly, R. Torbert, Multispacecraft observations of the electron current sheet, neighboring magnetic islands, and electron acceleration during magnetotail reconnection. Phys. Plasmas **16**(5), 056501 (2009). doi:10.1063/1.3112744. http://scitation.aip.org/content/aip/journal/pop/16/5/10.1063/1.3112744

Q. Chen, V. Petrosian, DETERMINATION OF STOCHASTIC ACCELERATION MODEL CHARACTERISTICS IN SOLAR FLARES. Astrophys. J. **777**(1), 33 (2013). doi:10.1088/0004-637X/777/1/33. http://stacks.iop.org/0004-637X/777/i=1/a=33?key=crossref.33c6cd96273a6617cf116461ada198c1

Y. Chen, Z. Wu, W. Liu, R.A. Schwartz, D. Zhao, B. Wang, G. Du, Double-coronal X-Ray and Microwave Sources Associated with a Magnetic Breakout Solar Eruption. Astrophys. J. **843**(1), 8 (2017). doi:10.3847/1538-4357/aa7462. http://stacks.iop.org/0004-637X/843/i=1/a=8?key=crossref.e129ab2e0957ea92ecbb8bc3ff921bab

Y.T. Chiu, M. Schulz, Self-consistent particle and parallel electrostatic field distributions in the magnetospheric-ionospheric auroral region. J. Geophys. Res. **83**(A2), 629 (1978). doi:10.1029/JA083iA02p00629. http://doi.wiley.com/10.1029/JA083iA02p00629

S. Christe, I.G. Hannah, S. Krucker, J. McTiernan, R.P. Lin, RHESSI Microflare Statistics. I. FlareFinding and Frequency Distributions. Astrophys. J. **677**(2), 1385–1394 (2008). doi:10.1086/529011. http://stacks.iop.org/0004-637X/677/i=2/a=1385

S.P. Christon, D.G. Mitchell, D.J. Williams, L.A. Frank, C.Y. Huang, T.E. Eastman, Energy spectra of plasma sheet ions and electrons from 50 eV/ e to 1 MeV during plasma temperature transitions. J. Geophys. Res. Sp. Phys. **93**(A4), 2562 (1988). doi:10.1029/JA093iA04p02562.

http://doi.wiley.com/10.1029/JA093iA04p02562
S.P. Christon, D.J. Williams, D.G. Mitchell, L.A. Frank, C.Y. Huang, Spectral characteristics of plasma sheet ion and electron populations during undisturbed geomagnetic conditions. J. Geophys. Res. **94**(A10), 13409 (1989). doi:10.1029/JA094iA10p13409. http://doi.wiley.com/10.1029/JA094iA10p13409
S.P. Christon, D.J. Williams, D.G. Mitchell, C.Y. Huang, L.A. Frank, Spectral characteristics of plasma sheet ion and electron populations during disturbed geomagnetic conditions. J. Geophys. Res. **96**(A1), 1 (1991). doi:10.1029/90JA01633. http://doi.wiley.com/10.1029/90JA01633
E.W. Cliver, A.G. Ling, Electrons and Protons in Solar Energetic Particle Events. Astrophys. J. **658**(2), 1349–1356 (2007). doi:10.1086/511737. http://stacks.iop.org/0004-637X/658/i=2/a=1349
J.T. Dahlin, J.F. Drake, M. Swisdak, Electron acceleration in three-dimensional magnetic reconnection with a guide field. Phys. Plasmas **22**(10), 100704 (2015). ISBN 0565010565. doi:10.1063/1.4933212. http://aip.scitation.org/doi/10.1063/1.4933212
A.G. Daou, D. Alexander, Hard X-Ray Asymmetry Limits in Solar Flare Conjugate Footpoints. Astrophys. J. **832**(1), 63 (2016). doi:10.3847/0004-637X/832/1/63. http://stacks.iop.org/0004-637X/832/i=1/a=63?key=crossref.fcb005d19d51d42fd51bb22a070d9fc9
X. Deng, M. Ashour-Abdalla, M. Zhou, R. Walker, M. El-Alaoui, V. Angelopoulos, R.E. Ergun, D. Schriver, Wave and particle characteristics of earthward electron injections associated with dipolarization fronts. J. Geophys. Res. Sp. Phys. **115**(A9), (2010). doi:10.1029/2009JA015107. http://doi.wiley.com/10.1029/2010JA016188 http://doi.wiley.com/10.1029/2009JA015107
M. Desai, J. Giacalone, Large gradual solar energetic particle events. Living Rev. Sol. Phys. **13**(1), 3 (2016). ISBN 2367-3648. doi:10.1007/s41116-016-0002-5. http://link.springer.com/10.1007/s41116-016-0002-5
E.E. Dors, C.A. Kletzing, Effects of suprathermal tails on auroral electrodynamics. J. Geophys. Res. Sp. Phys. **104**(A4), 6783–6796 (1999). doi:10.1029/1998JA900135. http://doi.wiley.com/10.1029/1998JA900135
J.F. Drake, M. Opher, M. Swisdak, J.N. Chamoun, A MAGNETIC RECONNECTION MECHANISM FOR THE GENERATION OF ANOMALOUS COSMIC RAYS. Astrophys. J. **709**(2), 963–974 (2010). doi:10.1088/0004-637X/709/2/963. http://stacks.iop.org/0004-637X/709/i=2/a=963?key=crossref.c4d29f5a8027b832840cc570881146b3
J.F. Drake, M. Swisdak, H. Che, M.A. Shay, Electron acceleration from contracting magnetic islands during reconnection. Nature **443**(7111), 553–6 (2006). doi:10.1038/nature05116. http://www.ncbi.nlm.nih.gov/pubmed/17024088
N. Dresing, R. Gómez-Herrero, B. Heber, A. Klassen, O. Malandraki, W. Dröge, Y. Kartavykh, Statistical survey of widely spread out solar electron events observed with STEREO and ACE with special attention to anisotropies. Astron. Astrophys. **567**, 27 (2014). doi:10.1051/0004-6361/201423789. http://www.aanda.org/10.1051/0004-6361/201423789
L.O. Drury, An introduction to the theory of diffusive shock acceleration of energetic particles in tenuous plasmas. Reports Prog. Phys. **46**(8), 973–1027 (1983). doi:10.1088/0034-4885/46/8/002. http://stacks.iop.org/0034-4885/46/i=8/a=002?key=crossref.b70b24cdb95f439137f0b14883bca142
A.Y. Duan, J.B. Cao, M. Dunlop, Z.Q. Wang, Energetic electron bursts in the plasma sheet and their relation with BBFs. J. Geophys. Res. Sp. Phys. **119**(11), 8902–8915 (2014). ISBN 2169-9402. doi:10.1002/2014JA020169. http://doi.wiley.com/10.1002/2014JA020169
J. Dudík, E. Dzifčáková, N. Meyer-Vernet, G. Del Zanna, P.R. Young, A. Giunta, B. Sylwester, J. Sylwester, M. Oka, H.E. Mason, C. Vocks, L. Matteini, S. Krucker, D.R. Williams, Š. Mackovjak, Nonequilibrium Processes in the Solar Corona, Transition Region, Flares, and Solar Wind (Invited Review). Sol. Phys. **292**(8), 100 (2017). doi:10.1007/s11207-017-1125-0. http://arxiv.org/abs/1706.03396 http://link.springer.com/10.1007/s11207-017-1125-0
C.T. Dum, Anomalous heating by ion sound turbulence. Phys. Fluids **21**(6), 945 (1978). doi:10.1063/1.862338. http://scitation.aip.org/content/aip/journal/pof1/21/6/10.1063/1.862338
J.P. Eastwood, T.D. Phan, J.F. Drake, M.A. Shay, a.L. Borg, B. Lavraud, M.G.G.T. Taylor, Energy Partition in Magnetic Reconnection in Earth's Magnetotail. Phys. Rev. Lett. **110**(22), 225001 (2013). doi:10.1103/PhysRevLett.110.225001. http://link.aps.org/doi/10.1103/PhysRevLett.110.225001 https://link.aps.org/doi/10.1103/PhysRevLett.110.225001
Y. Ebihara, Y. Miyoshi, *The Dynamic Magnetosphere* (Springer, Dordrecht, 2011), pp. 257–269. ISBN 978-94-007-0500-5. doi:10.1007/978-94-007-0501-2. http://link.springer.com/10.1007/978-94-007-0501-2
F. Effenberger, F.R. da Costa, M. Oka, P. Saint-Hilaire, W. Liu, V. Petrosian, L. Glesener, S. Krucker, Hard X-Ray Emission from Partially Occulted Solar Flares: RHESSI Observations in Two Solar Cycles. Astrophys. J. **835**(2), 124 (2017). doi:10.3847/1538-4357/835/2/124. http://arxiv.org/abs/1612.02856%0Ahttp://adsabs.harvard.edu/abs/2016arXiv161202856E http://stacks.iop.org/0004-637X/835/i=2/a=124?key=crossref.335c0a7c6f2db81a7daef6de55928092
J. Egedal, M. Øieroset, W. Fox, R.P. Lin, In Situ Discovery of an Electrostatic Potential, Trapping Electrons and Mediating Fast Reconnection in the Earth's Magnetotail. Phys. Rev. Lett. **94**(2), 025006 (2005).

doi:10.1103/PhysRevLett.94.025006. http://link.aps.org/doi/10.1103/PhysRevLett.94.025006

J. Egedal, A. Lê, N. Katz, L.-J. Chen, B. Lefebvre, W. Daughton, A. FAZAKERLEY, Cluster observations of bidirectional beams caused by electron trapping during antiparallel reconnection. J. Geophys. Res. Sp. Phys. **115**(A3), 03214 (2010). doi:10.1029/2009JA014650. http://doi.wiley.com/10.1029/2009JA014650 http://discovery.ucl.ac.uk/1302979/

J. Egedal, W. Daughton, A. Le, a.L. Borg, Double layer electric fields aiding the production of energetic flat-top distributions and superthermal electrons within magnetic reconnection exhausts. Phys. Plasmas **22**(10), 101208 (2015). doi:10.1063/1.4933055. http://scitation.aip.org/content/aip/journal/pop/22/10/10.1063/1.4933055

S.R. Elkington, M.K. Hudson, A.A. Chan, Acceleration of relativistic electrons via drift-resonant interaction with toroidal-mode Pc-5 ULF oscillations. Geophys. Res. Lett. **26**(21), 3273–3276 (1999). doi:10.1029/1999GL003659. http://doi.wiley.com/10.1029/1999GL003659

R.C. Elphic, J.W. Bonnell, R.J. Strangeway, L. Kepko, R.E. Ergun, J.P. McFadden, C.W. Carlson, W. Peria, C.A. Cattell, D. Klumpar, E. Shelley, W. Peterson, E. Moebius, L. Kistler, R. Pfaff, The auroral current circuit and field-aligned currents observed by FAST. Geophys. Res. Lett. **25**(12), 2033–2036 (1998). doi:10.1029/98GL01158. http://onlinelibrary.wiley.com/doi/10.1029/98GL01158/full http://doi.wiley.com/10.1029/98GL01158

A.G. Emslie, Energy partition in two solar flare/CME events. J. Geophys. Res. **109**(A10), 10104 (2004). doi:10.1029/2004JA010571. http://doi.wiley.com/10.1029/2004JA010571

A.G. Emslie, E.P. Kontar, S. Krucker, R.P. Lin, RHESSI Hard X-Ray Imaging Spectroscopy of the Large Gamma-Ray Flare of 2002 July 23. Astrophys. J. **595**(2), 107–110 (2003). doi:10.1086/378931. http://stacks.iop.org/1538-4357/595/i=2/a=L107

a.G. Emslie, B.R. Dennis, a.Y. Shih, P.C. Chamberlin, R.a. Mewaldt, C.S. Moore, G.H. Share, A. Vourlidas, B.T. Welsch, GLOBAL ENERGETICS OF THIRTY-EIGHT LARGE SOLAR ERUPTIVE EVENTS. Astrophys. J. **759**(1), 71 (2012). doi:10.1088/0004-637X/759/1/71. http://stacks.iop.org/0004-637X/759/i=1/a=71?key=crossref.1c3191e7ead00c1d25dfd8ceb08a0ea1

R.E. Ergun, C.W. Carlson, J.P. McFadden, F.S. Mozer, R.J. Strangeway, parallel electric fields in discrete arcs. Geophys. Res. Lett. **27**(24), 4053–4056 (2000). doi:10.1029/2000GL003819. http://doi.wiley.com/10.1029/2000GL003819

K.N. Erickson, R.L. Swanson, R.J. Walker, J.R. Winckler, A study of magnetosphere dynamics during auroral electrojet events by observations of energetic electron intensity changes at synchronous orbit. J. Geophys. Res. **84**(A3), 931 (1979). doi:10.1029/JA084iA03p00931. http://doi.wiley.com/10.1029/JA084iA03p00931

C.Y. Fan, G. Gloeckler, D. Hovestadt, Energy Spectra and Charge States of H, He, and Heavy Ions Observed in the Earth's Magnetosheath and Magnetotail. Phys. Rev. Lett. **34**(8), 495–498 (1975). doi:10.1103/PhysRevLett.34.495. https://link.aps.org/doi/10.1103/PhysRevLett.34.495

W.C. Feldman, J.R. Asbridge, S.J. Bame, M.D. Montgomery, S.P. Gary, Solar wind electrons. J. Geophys. Res. **80**(31), 4181–4196 (1975). doi:10.1029/JA080i031p04181. http://doi.wiley.com/10.1029/JA080i031p04181

W.C. Feldman, S.J. Bame, S.P. Gary, J.T. Gosling, D. McComas, M.F. Thomsen, G. Paschmann, N. Sckopke, M.M. Hoppe, C.T. Russell, Electron Heating Within the Earth's Bow Shock. Phys. Rev. Lett. **49**(3), 199–201 (1982). doi:10.1103/PhysRevLett.49.199. http://link.aps.org/doi/10.1103/PhysRevLett.49.199 https://link.aps.org/doi/10.1103/PhysRevLett.49.199

W.C. Feldman, R.C. Anderson, S.J. Bame, J.T. Gosling, R.D. Zwickl, E.J. Smith, Electron velocity distributions near interplantary shocks. J. Geophys. Res. Sp. Phys. **88**(A12), 9949 (1983a). doi:10.1029/JA088iA12p09949. http://doi.wiley.com/10.1029/JA088iA12p09949

W.C. Feldman, R.C. Anderson, S.J. Bame, S.P. Gary, J.T. Gosling, D.J. Mccomas, M.F. Thomsen, G. Paschmann, M.M. Hoppe, Electron velocity distributions near the earth's bow shock. J. Geophys. Res. **88**(A1), 96–110 (1983b). ISBN doi:10.1029/JA088iA01p00096. doi:10.1029/JA088iA01p00096. http://doi.wiley.com/10.1029/JA088iA01p00096

E. Fermi, On the Origin of the Cosmic Radiation. Phys. Rev. **75**(8), 1169–1174 (1949). doi:10.1103/PhysRev.75.1169. https://link.aps.org/doi/10.1103/PhysRev.75.1169

L.A. Fisk, G. Gloeckler, The case for a common spectrum of particles accelerated in the heliosphere: Observations and theory. J. Geophys. Res. Sp. Phys. **119**(11), 8733–8749 (2014). doi:10.1002/2014JA020426. http://doi.wiley.com/10.1002/2014JA020426

L.A. Fisk, G. Gloeckler, The Common Spectrum for Accelerated Ions in the Quiet-Time Solar Wind. Astrophys. J. **640**(1), 79–82 (2006). doi:10.1086/503293. http://stacks.iop.org/1538-4357/640/i=1/a=L79

L.a. Fisk, G. Gloeckler, Particle Acceleration in the Heliosphere: Implications for Astrophysics. Space Sci. Rev. **173**(1-4), 433–458 (2012). doi:10.1007/s11214-012-9899-8. http://link.springer.com/10.1007/s11214-012-9899-8

G.D. Fleishman, Y. Xu, G.N. Nita, D.E. Gary, VALIDATION OF THE CORONAL THICK TARGET SOURCE MODEL. Astrophys. J. **816**(2), 62 (2016). doi:10.3847/0004-637X/816/2/62. http://stacks.iop.org/0004-637X/816/i=2/a=62?key=crossref.d42f7a9a972fa0179cc4c81317fcd830

L. Fletcher, B.R. Dennis, H.S. Hudson, S. Krucker, K. Phillips, A.M. Veronig, M. Battaglia, L. Bone, A. Caspi, Q. Chen, P. Gallagher, P.T. Grigis, H. Ji, W. Liu, R.O. Milligan, M. Temerin, An Observational Overview of Solar Flares. Space Sci. Rev. **159**(1-4), 19–106 (2011). doi:10.1007/s11214-010-9701-8. http://www.springerlink.com/index/10.1007/s11214-010-9701-8 http://link.springer.com/10.1007/s11214-010-9701-8

C. Forsyth, M. Lester, S.W.H. Cowley, I. Dandouras, A.N. Fazakerley, R.C. Fear, H.U. Frey, A. Grocott, A. Kadokura, E. Lucek, H. Rème, S.E. Milan, J. Watermann, Observed tail current systems associated with bursty bulk flows and auroral streamers during a period of multiple substorms. Ann. Geophys. **26**(1), 167–184 (2008). ISBN 1432-0576. doi:10.5194/angeo-26-167-2008. www.ann-geophys.net/26/167/2008/ http://www.ann-geophys.net/26/167/2008/

L.A. Frank, On the local-time dependence of outer radiation zone electron (E>1.6 Mev) intensities near the magnetic equator. J. Geophys. Res. **70**(17), 4131–4138 (1965). doi:10.1029/JZ070i017p04131. http://doi.wiley.com/10.1029/JZ070i017p04131

J.˜.W. Freeman, T.˜.P. O'Brien, A.˜.a. Chan, R.˜.a. Wolf, Energetic electrons at geostationary orbit during the November 3-4, 1993 storm: Spatial/temporal morphology, characterization by a power law spectrum and, representation by an artificial neural network. J. Geophys. Res. Sp. Phys. **103**(A11), 26251–26260 (1998). ISBN 0148-0227. doi:10.1029/97JA03268. http://doi.wiley.com/10.1029/97JA03268

M. Fridman, J. Lemaire, Relationship between auroral electrons fluxes and field aligned electric potential difference. J. Geophys. Res. **85**(A2), 664 (1980). doi:10.1029/JA085iA02p00664. http://doi.wiley.com/10.1029/JA085iA02p00664

K.J. Frost, B.R. Dennis, Evidence from Hard X-Rays for Two-Stage Particle Acceleration in a Solar Flare. Astrophys. J. **165**, 655 (1971). doi:10.1086/150932. http://adsabs.harvard.edu/doi/10.1086/150932

H.S. Fu, Y.V. Khotyaintsev, M. André, A. Vaivads, Fermi and betatron acceleration of suprathermal electrons behind dipolarization fronts. Geophys. Res. Lett. **38**(16), (2011). doi:10.1029/2011GL048528. http://www.agu.org/pubs/crossref/2011/2011GL048528.shtml http://doi.wiley.com/10.1029/2011GL048528

H.S. Fu, Y.V. Khotyaintsev, A. Vaivads, A. Retinò, M. André, Energetic electron acceleration by unsteady magnetic reconnection. Nat. Phys. **9**(7), 426–430 (2013). ISBN 1745-2473. doi:10.1038/nphys2664. http://www.nature.com/doifinder/10.1038/nphys2664

K. Fujimoto, Wave activities in separatrix regions of magnetic reconnection. Geophys. Res. Lett. **41**(8), 2721–2728 (2014). doi:10.1002/2014GL059893. http://doi.wiley.com/10.1002/2014GL059893

M. Fujimoto, M.S. Nakamura, I. Shinohara, T. Nagai, T. Mukai, Y. Saito, T. Yamamoto, S. Kokubun, Observations of earthward streaming electrons at the trailing boundary of a plasmoid. Geophys. Res. Lett. **24**(22), 2893–2896 (1997). doi:10.1029/97GL02821. http://doi.wiley.com/10.1029/97GL02821

N. Furuya, Y. Omura, D. Summers, Relativistic turning acceleration of radiation belt electrons by whistler mode chorus. J. Geophys. Res. Sp. Phys. **113**(A4), (2008). doi:10.1029/2007JA012478. http://doi.wiley.com/10.1029/2007JA012478

C. Gabrielse, V. Angelopoulos, A. Runov, D.L. Turner, Statistical characteristics of particle injections throughout the equatorial magnetotail. J. Geophys. Res. Sp. Phys. **119**(4), 2512–2535 (2014). doi:10.1002/2013JA019638. http://doi.wiley.com/10.1002/2013JA019638

C. Gabrielse, C. Harris, V. Angelopoulos, A. Artemyev, A. Runov, The role of localized inductive electric fields in electron injections around dipolarizing flux bundles. J. Geophys. Res. Sp. Phys. **121**(10), 9560–9585 (2016). ISBN 2169-9402. doi:10.1002/2016JA023061. http://doi.wiley.com/10.1002/2016JA023061

G. Gloeckler, Sources, injection and acceleration of heliospheric ion populations, in *AIP Conf. Proc.*, vol. 528 (AIP, ???, 2000), pp. 221–228. doi:10.1063/1.1324316. http://aip.scitation.org/doi/abs/10.1063/1.1324316

J.T. Gosling, D.N. Baker, S.J. Bame, E.W. Hones, D.J. McComas, R.D. Zwickl, J.A. Slavin, E.J. Smith, B.T. Tsurutani, Plasma entry into the distant tail lobes: ISEE-3. Geophys. Res. Lett. **11**(10), 1078–1081 (1984). doi:10.1029/GL011i010p01078. http://doi.wiley.com/10.1029/GL011i010p01078

J.T. Gosling, M.F. Thomsen, S.J. Bame, C.T. Russell, Suprathermal electrons at Earth's bow shock. J. Geophys. Res. Sp. Phys. **94**(A8), 10011–10025 (1989). doi:10.1029/JA094iA08p10011. http://doi.wiley.com/10.1029/JA094iA08p10011

P.C. Grigis, A.O. Benz, The spectral evolution of impulsive solar X-ray flares. Astron. Astrophys. **426**(3), 1093–1101 (2004). doi:10.1051/0004-6361:20041367. http://www.aanda.org/10.1051/0004-6361:20041367

P.C. Grigis, A.O. Benz, The Evolution of Reconnection along an Arcade of Magnetic Loops. Astrophys. J. **625**(2), 143–146 (2005). doi:10.1086/431147. http://stacks.iop.org/1538-4357/625/i=2/a=L143

P.C. Grigis, A.O. Benz, Electron Acceleration in Solar Flares: Theory of Spectral Evolution. Astron. Astrophys. **458**(2), 641–651 (2006). doi:10.1051/0004-6361:20065809. http://arxiv.org/abs/astro-

ph/0606339%5Cnhttp://dx.doi.org/10.1051/0004-6361:20065809
F. Guo, H. Li, W. Daughton, Y.-H. Liu, Formation of Hard Power Laws in the Energetic Particle Spectra Resulting from Relativistic Magnetic Reconnection. Phys. Rev. Lett. **113**(15), 155005 (2014). doi:10.1103/PhysRevLett.113.155005. http://link.aps.org/doi/10.1103/PhysRevLett.113.155005
J. Guo, A.G. Emslie, E.P. Kontar, F. Benvenuto, A.M. Massone, M. Piana, Determination of the acceleration region size in a loop-structured solar flare. Astron. Astrophys. **543**, 53 (2012a). doi:10.1051/0004-6361/201219341. http://www.aanda.org/10.1051/0004-6361/201219341
J. Guo, A. Gordon Emslie, A.M. Massone, M. Piana, PROPERTIES OF THE ACCELERATION REGIONS IN SEVERAL LOOP-STRUCTURED SOLAR FLARES. Astrophys. J. **755**(1), 32 (2012b). doi:10.1088/0004-637X/755/1/32. http://stacks.iop.org/0004-637X/755/i=1/a=32?key=crossref.6a5abae4f14d816b6fbfef30324cb213
I.G. Hannah, S. Christe, S. Krucker, G.J. Hurford, H.S. Hudson, R.P. Lin, RHESSI MICROFLARE STATISTICS . II . X-RAY IMAGING , SPECTROSCOPY , AND ENERGY DISTRIBUTIONS. Astrophys. J. Lett. **677**, 704–718 (2008)
I.G. Hannah, H.S. Hudson, G.J. Hurford, R.P. Lin, Constraining the Hard X Ray Properties of the Quiet Sun qith New RHESSI Observations. Astrophys. J. **724**(1), 487–492 (2010). doi:10.1088/0004-637X/724/1/487. http://arxiv.org/abs/1009.2918%5Cnpapers3://publication/doi/10.1088/0004-637X/724/1/487 http://stacks.iop.org/0004-637X/724/i=1/a=487?key=crossref.d631aca04d40f1ef158c831a4f892d56
A. Hasegawa, K. Mima, M. Duong-Van, Plasma distribution function in a superthermal radiation field. Phys. Rev. Lett. **54**(24), 2608–2610 (1985). doi:10.1103/PhysRevLett.54.2608
M. Hesse, J. Birn, On dipolarization and its relation to the substorm current wedge. J. Geophys. Res. **96**(A11), 19417 (1991). ISBN 0148-0227. doi:10.1029/91JA01953. http://doi.wiley.com/10.1029/91JA01953
G.C. Ho, D. Lario, R.B. Decker, E.C. Roelof, M. Desai, C.W. Smith, Energetic Electrons Associated with Transient Interplanetary Shocks : Evidence for Weak Interaction, in *28th Int. Cosm. Ray Conf.* (Universal Academy Press, Inc., ???, 2003), pp. 3689–3692
G.C. Ho, D. Lario, R.B. Decker, C.W. Smith, Q. Hu, G. Li, Q. Hu, O. Verkhoglyadova, G.P. Zank, R.P. Lin, J. Luhmann, Transient Shocks and Associated Energetic Particle Distributions Observed by ACE during Cycle 23, in *AIP Conf. Proc.*, vol. 1039 (AIP, ???, 2008), pp. 184–189. ISBN 9780735405660. doi:10.1063/1.2982443. http://aip.scitation.org/doi/abs/10.1063/1.2982443
G.D. Holman, Scientific considerations for future spectroscopic measurements from space of activity on the Sun. J. Geophys. Res. Sp. Phys. **121**(12), 11667–11697 (2016). doi:10.1002/2016JA022651
G.D. Holman, L. Sui, R.A. Schwartz, A.G. Emslie, Electron Bremsstrahlung Hard X-Ray Spectra, Electron Distributions, and Energetics in the 2002 July 23 Solar Flare. Astrophys. J. **595**(2), 97–101 (2003). doi:10.1086/378488. http://stacks.iop.org/1538-4357/595/i=2/a=L97
G.D. Holman, M.J. Aschwanden, H. Aurass, M. Battaglia, P.C. Grigis, E.P. Kontar, W. Liu, P. Saint-Hilaire, V.V. Zharkova, Implications of X-ray Observations for Electron Acceleration and Propagation in Solar Flares. Space Sci. Rev. **159**(1-4), 107–166 (2011). doi:10.1007/s11214-010-9680-9. http://www.springerlink.com/index/10.1007/s11214-010-9680-9 http://link.springer.com/10.1007/s11214-010-9680-9
E.W. Hones, Substorm processes in the magnetotail: Comments on On hot tenuous plasmas, fireballs, and boundary layers in the Earth's magnetotail' by L. A. Frank, K. L. Ackerson, and R. P. Lepping. J. Geophys. Res. **82**(35), 5633–5640 (1977). doi:10.1029/JA082i035p05633. http://www.agu.org/pubs/crossref/1977/JA082i035p05633.shtml http://doi.wiley.com/10.1029/JA082i035p05633
E.W. Hones, I.D. Palmer, P.R. Higbie, Energetic protons of magnetospheric origin in the plasma sheet associated with substorms. J. Geophys. Res. **81**(22), 3866–3874 (1976). doi:10.1029/JA081i022p03866. http://doi.wiley.com/10.1029/JA081i022p03866
E.W. Hones, Transient phenomena in the magnetotail and their relation to substorms. Space Sci. Rev. **23**(3), 393–410 (1979). doi:10.1007/BF00172247. http://link.springer.com/10.1007/BF00172247
R.B. Horne, Timescale for radiation belt electron acceleration by whistler mode chorus waves. J. Geophys. Res. **110**(A3), 03225 (2005). ISBN 2156-2202. doi:10.1029/2004JA010811. http://doi.wiley.com/10.1029/2004JA010811
M. Hoshino, T. Mukai, T. Terasawa, I. Shinohara, Suprathermal electron acceleration in magnetic reconnection. J. Geophys. Res. Sp. Phys. **106**(A11), 25979–25997 (2001). ISBN 0148-0227. doi:10.1029/2001JA900052. http://doi.wiley.com/10.1029/2001JA900052
P. Hoyng, A. Duijveman, A. Boelee, C. de Jager, M. Galama, R. Hoekstra, J. Imhof, H. Lafleur, M.E. Machado, R. Fryer, Hard X-ray imaging of two flares in active region 2372. Astrophys. J. **244**, 153 (1981a). doi:10.1086/183501. http://adsabs.harvard.edu/doi/10.1086/183501
P. Hoyng, A. Duijveman, M.E. Machado, D.M. Rust, Z. Svestka, A. Boelee, C. de Jager, K.T. Frost, H. Lafleur, G.M. Simnett, H.F. van Beek, B.E. Woodgate, Origin and Location of the Hard

X-Ray Emission in a Two-Ribbon Flare. Astrophys. J. **246**, 155 (1981b). doi:10.1086/183574. http://adsabs.harvard.edu/doi/10.1086/183574

S.Y. Huang, A. Vaivads, Y.V. Khotyaintsev, M. Zhou, H.S. Fu, A. Retinò, X.H. Deng, M. André, C.M. Cully, J.S. He, F. Sahraoui, Z.G. Yuan, Y. Pang, Electron acceleration in the reconnection diffusion region: Cluster observations. Geophys. Res. Lett. **39**(11), (2012a). ISBN 1944-8007. doi:10.1029/2012GL051946. http://doi.wiley.com/10.1029/2012GL051946

S.Y. Huang, M. Zhou, F. Sahraoui, A. Vaivads, X.H. Deng, M. André, J.S. He, H.S. Fu, H.M. Li, Z.G. Yuan, D.D. Wang, Observations of turbulence within reconnection jet in the presence of guide field. Geophys. Res. Lett. **39**(11), 4–9 (2012b). doi:10.1029/2012GL052210

B. Hultqvist, M. André, S.P. Christon, G. Paschmann, D.G. Sibeck, Contributions of different source and loss processes to the plasma content of the magnetosphere. Space Sci. Rev. **88**(1/2), 355–372 (1999). doi:10.1023/A:1005260002333. http://link.springer.com/10.1023/A:1005260002333

S. Imada, M. Hoshino, T. Mukai, The dawn-dusk asymmetry of energetic electron in the Earth's magnetotail: Observation and transport models. J. Geophys. Res. Sp. Phys. **113**(A11), (2008). doi:10.1029/2008JA013610. http://doi.wiley.com/10.1029/2008JA013610

S. Imada, M. Hoshino, T. Mukai, Average profiles of energetic and thermal electrons in the magnetotail reconnection regions. Geophys. Res. Lett. **32**, 09101 (2005). doi:10.1029/2005GL022594. http://www.agu.org/pubs/crossref/2005/2005GL022594.shtml

S. Imada, R. Nakamura, P.W. Daly, M. Hoshino, W. Baumjohann, S. Mühlbachler, A. Balogh, H. Rème, Energetic electron acceleration in the downstream reconnection outflow region. J. Geophys. Res. Sp. Phys. **112**, 03202 (2007). doi:10.1029/2006JA011847. http://www.agu.org/pubs/crossref/2007/2006JA011847.shtml

S. Imada, M. Hirai, M. Hoshino, T. Mukai, Favorable conditions for energetic electron acceleration during magnetic reconnection in the Earth's magnetotail. J. Geophys. Res. Sp. Phys. **116**, 08217 (2011). doi:10.1029/2011JA016576. http://www.agu.org/pubs/crossref/2011/2011JA016576.shtml

D.S. Intriligator, H.R. Collard, J.D. Mihalov, O.L. Vaisberg, J.H. Wolfe, Evidence for Earth magnetospheric tail associated phenomena at 3100 R E. Geophys. Res. Lett. **6**(7), 585–588 (1979). doi:10.1029/GL006i007p00585. http://doi.wiley.com/10.1029/GL006i007p00585

S. Ishikawa, S. Krucker, T. Takahashi, R.P. Lin, ON THE RELATION OF ABOVE-THE-LOOP AND FOOTPOINT HARD X-RAY SOURCES IN SOLAR FLARES. Astrophys. J. **737**(2), 48 (2011). doi:10.1088/0004-637X/737/2/48. http://stacks.iop.org/0004-637X/737/i=2/a=48?key=crossref.fded65af29cf5e58e0f9a501724af030

S.-n. Ishikawa, S. Krucker, M. Ohno, R.P. Lin, SUZAKU /WAM AND RHESSI OBSERVATIONS OF NON-THERMAL ELECTRONS IN SOLAR MICROFLARES. Astrophys. J. **765**(2), 143 (2013). doi:10.1088/0004-637X/765/2/143. http://stacks.iop.org/0004-637X/765/i=2/a=143?key=crossref.063f7b98a33145fe56473988e3310e8c

C. Jacquey, J.A. Sauvaud, J. Dandouras, Location and propagation of the magnetotail current disruption during substorm expansion: Analysis and simulation of an ISEE multi-onset event. Geophys. Res. Lett. **18**(3), 389–392 (1991). ISBN 0094-8276. doi:10.1029/90GL02789. http://doi.wiley.com/10.1029/90GL02789

P. Janhunen, A. Olsson, The current-voltage relationship revisited: exact and approximate formulas with almost general validity for hot magnetospheric electrons for bi-Maxwellian and kappa distributions. Ann. Geophys. **16**(3), 292–297 (1998). ISBN 0992-7689. doi:10.5194/angeo-16-292-1998. http://www.ann-geophys.net/16/292/1998/

S.R. Kaeppler, M.J. Nicolls, A. Strømme, C.A. Kletzing, S.R. Bounds, Observations in the e region ionosphere of kappa distribution functions associated with precipitating auroral electrons and discrete aurorae. J. Geophys. Res. A Sp. Phys. **119**(12), 10164–10183 (2014). doi:10.1002/2014JA020356

S.W. Kahler, A.G. Ling, Characterizing Solar Energetic Particle Event Profiles with Two-Parameter Fits. Sol. Phys. **292**(4), 59 (2017). doi:10.1007/s11207-017-1085-4. http://dx.doi.org/10.1007/s11207-017-1085-4 http://link.springer.com/10.1007/s11207-017-1085-4

M. Karlický, E. Dzifčáková, J. Dudík, *On the physical meaning of n-distributions in solar flares*, 2012. doi:10.1051/0004-6361/201117860

J. Kašparová, M. Karlický, Kappa distribution and hard X-ray emission of solar flares. Astron. Astrophys. **497**(3), 13–16 (2009). doi:10.1051/0004-6361/200911898. http://www.aanda.org/10.1051/0004-6361/200911898

C.F. Kennel, F.L. Scarf, F.V. Coroniti, C.T. Russell, K. Wenzel, T.R. Sanderson, W.C. Feldman, G.K. Parks, E.J. Smith, B.T. Tsurutani, F.S. Mozer, R.R. Anderson, J.D. Scudder, M. Scholer, Plasma and Energetic Particle Structure Upstream of a Quasi-Parallel Interplanetary Shock. J. Geophys. Res. Sp. Phys. **89**(A7), 5419–5435 (1984). doi:10.1029/JA089iA07p05419

Y.V. Khotyaintsev, C.M. Cully, A. Vaivads, M. André, C.J. Owen, Plasma Jet Braking: Energy Dissipation and Nonadiabatic Electrons. Phys. Rev. Lett. **106**(16), 165001 (2011). doi:10.1103/PhysRevLett.106.165001. https://link.aps.org/doi/10.1103/PhysRevLett.106.165001

A. Klassen, N. Dresing, R. Gómez-Herrero, B. Heber, R. MüllerMellin, Unexpected spatial intensity distributions and onset timing of solar electron events observed by closely spaced STEREO spacecraft. Astron. Astrophys. **593**, 31 (2016). doi:10.1051/00046361/201628734. http://www.aanda.org/10.1051/0004-6361/201628734%5Cnhttp://www.aanda.org/articles/aa/abs/2016/09/aa28734-16/aa28734-16.html

K.-L. Klein, S. Dalla, Acceleration and Propagation of Solar Energetic Particles. Space Sci. Rev. (2017). doi:10.1007/s11214-017-0382-4. http://dx.doi.org/10.1007/s11214-017-0382-4 http://link.springer.com/10.1007/s11214-017-0382-4

C.A. Kletzing, Auroral source region: Plasma properties of the high-latitude plasma sheet. J. Geophys. Res. Sp. Phys. **108**(A10), 1360 (2003). doi:10.1029/2002JA009678. http://doi.wiley.com/10.1029/2002JA009678

B. Kliem, Particle orbits, trapping, and acceleration in a filamentary current sheet model. Astrophys. J. Suppl. Ser. **90**, 719 (1994). doi:10.1086/191896. http://adsabs.harvard.edu/doi/10.1086/191896

S. Knight, Parallel electric fields. Planet. Space Sci. **21**(5), 741–750 (1973). ISBN 0032-0633. doi:10.1016/0032-0633(73)90093-7. http://linkinghub.elsevier.com/retrieve/pii/0032063373900937

E.P. Kontar, I.G. Hannah, A.L. MacKinnon, Chromospheric magnetic field and density structure measurements using hard X-rays in a flaring coronal loop. Astron. Astrophys. **489**(3), 57–60 (2008). doi:10.1051/0004-6361:200810719. http://www.aanda.org/10.1051/0004-6361:200810719

E.P. Kontar, J.C. Brown, a.G. Emslie, W. Hajdas, G.D. Holman, G.J. Hurford, J. Kašparová, P.C.V. Mallik, a.M. Massone, M.L. McConnell, M. Piana, M. Prato, E.J. Schmahl, E. Suarez-Garcia, *Deducing electron properties from hard X-ray observations*, 2011. 1121401198. doi:10.1007/s11214-011-9804-x

E.P. Kontar, N.H. Bian, a.G. Emslie, N. Vilmer, TURBULENT PITCH-ANGLE SCATTERING AND DIFFUSIVE TRANSPORT OF HARD X-RAY-PRODUCING ELECTRONS IN FLARING CORONAL LOOPS. Astrophys. J. **780**(2), 176 (2014). doi:10.1088/0004-637X/780/2/176. http://stacks.iop.org/0004-637X/780/i=2/a=176?key=crossref.e09c5a8bcff6ccd5cad20376beb0b743

S. Krucker, M. Battaglia, PARTICLE DENSITIES WITHIN THE ACCELERATION REGION OF A SOLAR FLARE. Astrophys. J. **780**(1), 107 (2014). doi:10.1088/0004-637X/780/1/107. http://stacks.iop.org/0004-637X/780/i=1/a=107?key=crossref.d057ea6556b8f92736350d57f649d9b7

S. Krucker, R.P. Lin, Hard XRay Emissions from Partially Occulted Solar Flares. Astrophys. J. **673**(2), 1181–1187 (2008). doi:10.1086/524010. http://stacks.iop.org/0004-637X/673/i=2/a=1181

S. Krucker, R.P. Lin, RELATIVE TIMING AND SPECTRA OF SOLAR FLARE HARD X-RAY SOURCES. Sol. Phys. **210**(1/2), 229–243 (2002). doi:10.1023/A:1022469902940. http://link.springer.com/10.1023/A:1022469902940

S. Krucker, P.H. Oakley, R.P. Lin, Spectra of Solar Impulsive Electron Events Observed Near Earth. Astrophys. J. **691**(1), 806–810 (2009). doi:10.1088/0004-637X/691/1/806. http://stacks.iop.org/0004-637X/691/i=1/a=806?key=crossref.3218edf10192dd45ec1b5d9825615a7c

S. Krucker, E.P. Kontar, S. Christe, R.P. Lin, Solar Flare Electron Spectra at the Sun and near the Earth. Astrophys. J. **663**(2), 109–112 (2007). doi:10.1086/519373. http://adsabs.harvard.edu/cgi-bin/nph-data_query?bibcode=2007ApJ...663L.109K&link_type=ABSTRACT http://stacks.iop.org/1538-4357/663/i=2/a=L109

S. Krucker, G.J. Hurford, A.L. MacKinnon, A.Y. Shih, R.P. Lin, Coronal γ-Ray Bremsstrahlung from Solar Flare-accelerated Electrons. Astrophys. J. **678**(1), 63–66 (2008a). doi:10.1086/588381. http://stacks.iop.org/1538-4357/678/i=1/a=L63

S. Krucker, P. SaintHilaire, S. Christe, S.M. White, A.D. Chavier, S.D. Bale, R.P. Lin, Coronal Hard XRay Emission Associated with Radio Type III Bursts. Astrophys. J. **681**(1), 644–649 (2008b). doi:10.1086/588549. http://adsabs.harvard.edu/abs/2008ApJ...681..644K http://stacks.iop.org/0004-637X/681/i=1/a=644

S. Krucker, M. Battaglia, P.J. Cargill, L. Fletcher, H.S. Hudson, a.L. MacKinnon, S. Masuda, L. Sui, M. Tomczak, A.M. Veronig, L. Vlahos, S.M. White, Hard X-ray emission from the solar corona. Astron. Astrophys. Rev. **16**(3-4), 155–208 (2008c). ISBN 0015900800. doi:10.1007/s00159-008-0014-9. http://www.springerlink.com/index/10.1007/s00159-008-0014-9

S. Krucker, H.S. Hudson, L. Glesener, S.M. White, S. Masuda, J.-P. Wuelser, R.P. Lin, Measurements of the Coronal Acceleration Region of a Solar Flare. Astrophys. J. **714**, 1108–1119 (2010). doi:10.1088/0004-637X/714/2/1108. http://stacks.iop.org/0004-637X/714/i=2/a=1108?key=crossref.a73431f792680e1210d232a7f386304c

R. Kulsrud, *Plasma Physics for Astrophysics Plasma Physics for Astrophysics , Russell M. Kulsrud , Princeton U. Press, Princeton, NJ, 2005. $99.50, $45.00 paper (468 pp.). ISBN 0-691-10267-8, ISBN 0-691-12073-0 paper*, 1st edn. (Princeton University Press, Princeton, 2005), p. 468. ISBN 0691120730. doi:10.1063/1.2180179. http://physicstoday.scitation.org/doi/10.1063/1.2180179

D. Lario, ACE Observations of Energetic Particles Associated with Transient Interplanetary Shocks, in *AIP Conf. Proc.*, vol. 679 (AIP, ???, 2003), pp. 640–643. ISBN 0735401489. doi:10.1063/1.1618676. http://adsabs.harvard.edu/abs/2003AIPC..679..640L http://scitation.aip.org/content/aip/proceeding/aipcp/10.1063/1.1618676

D. Lario, Advances in modeling gradual solar energetic particle events. Adv. Sp. Res. **36**(12), 2279–2288 (2005). doi:10.1016/j.asr.2005.07.081. http://linkinghub.elsevier.com/retrieve/pii/S0273117705009865

D. Lario, Q. Hu, G. Ho, Statistical Properties of Fast Forward Transient Interplanetary Shocks and Associated Energetic Particle Events: ACE Observations, in *Proc. Sol. Wind 11 / SOHO 16*, ed. by H.L. B. Fleck, T.H. Zurbuchen, Whistler, Canada, 2005. http://adsabs.harvard.edu/full/2005ESASP.592...81L

M. Lazar, H. Fichtner, P.H. Yoon, On the interpretation and applicability of κ -distributions. Astron. Astrophys. **589**, 39 (2016). doi:10.1051/0004-6361/201527593. http://arxiv.org/abs/1602.04132 http://www.aanda.org/10.1051/0004-6361/201527593

J. Lee, D. Lim, G.S. Choe, K.-S. Kim, M. Jang, CORONAL THICK TARGET HARD X-RAY EMISSIONS AND RADIO EMISSIONS. Astrophys. J. **769**(1), 11 (2013). doi:10.1088/2041-8205/769/1/L11. http://stacks.iop.org/2041-8205/769/i=1/a=L11?key=crossref.1f468fa186366a13859ef639ce82f17d

J. Lemaire, M. Scherer, Ionosphere-plasmasheet field-aligned currents and parallel electric fields. Planet. Space Sci. **22**(11), 1485–1490 (1974). ISBN 0032-0633. doi:10.1016/0032-0633(74)90013-0. http://linkinghub.elsevier.com/retrieve/pii/0032063374900130

M.P. Leubner, Fundamental issues on kappa-distributions in space plasmas and interplanetary proton distributions. Phys. Plasmas **11**(4), 1308 (2004). doi:10.1063/1.1667501. http://scitation.aip.org/content/aip/journal/pop/11/4/10.1063/1.1667501

M.P. Leubner, A nonextensive entropy approach to kappa-distributions. Astrophys. Space Sci. **282**(3), 573–579 (2002). doi:10.1023/A:1020990413487. http://link.springer.com/10.1023/A:1020990413487

T.W. Lezniak, J.R. Winckler, Experimental study of magnetospheric motions and the acceleration of energetic electrons during substorms. J. Geophys. Res. **75**(34), 7075–7098 (1970). doi:10.1029/JA075i034p07075. http://doi.wiley.com/10.1029/JA075i034p07075

T.C. Li, J.F. Drake, M. Swisdak, SUPPRESSION OF ENERGETIC ELECTRON TRANSPORT IN FLARES BY DOUBLE LAYERS. Astrophys. J. **757**(1), 20 (2012). doi:10.1088/0004-637X/757/1/20. http://stacks.iop.org/0004-637X/757/i=1/a=20?key=crossref.bd7b725dd8097887a42865497bc45fae

X. Li, D.N. Baker, M. Teremin, T.E. Cayton, G.D. Reeves, R.S. Selesnick, J.B. Blake, G. Lu, S.G. Kanekal, H.J. Singer, Rapid enchancements of relativistic electrons deep in the magnetosphere during the May 15, 1997, magnetic storm. J. Geophys. Res. Sp. Phys. **104**(A3), 4467–4476 (1999). doi:10.1029/1998JA900092. http://doi.wiley.com/10.1029/1998JA900092

J. Lin, S.R. Cranmer, C.J. Farrugia, Plasmoids in reconnecting current sheets: Solar and terrestrial contexts compared. J. Geophys. Res. Sp. Phys. **113**(A11), 1–21 (2008). ISBN 0148-0227. doi:10.1029/2008JA013409. http://www.agu.org/pubs/crossref/2008/2008JA013409.shtml

R.P. Lin, WIND OBSERVATIONS OF SUPRATHERMAL ELECTRONS IN THE INTERPLANETARY MEDIUM. Space Sci. Rev. **86**(1-4), 61–78 (1998). doi:10.1023/A:1005048428480

R.P. Lin, Energy release and particle acceleration in flares: Summary and future prospects. Space Sci. Rev. **159**(1-4), 421–445 (2011). ISBN 1121401198. doi:10.1007/s11214-011-9801-0

R.P. Lin, H.S. Hudson, 10-100 keV electron acceleration and emission from solar flares. Sol. Phys. **17**(2), 412–435 (1971). doi:10.1007/BF00150045. http://link.springer.com/10.1007/BF00150045

R.P. Lin, R.A. Schwartz, R.M. Pelling, K.C. Hurley, A new component of hard X-rays in solar flares. Astrophys. J. **251**, 109 (1981). doi:10.1086/183704. http://adsabs.harvard.edu/doi/10.1086/183704

R.P. Lin, B.R. Dennis, G.J. Hurford, D.M. Smith, A. Zehnder, P.R. Harvey, D.W. Curtis, D. Pankow, P. Turin, M. Bester, A. Csillaghy, M. Lewis, N. Madden, H.F.V.A.N. Beek, M. Appleby, T. Raudorf, J. Mctiernan, R. Ramaty, E. Schmahl, R. Schwartz, S. Krucker, R. Abiad, T. Quinn, P. Berg, M. Hashii, R. Sterling, R. Jackson, R. Pratt, R.D. Campbell, D. Malone, D. Landis, C. Cork, A.K. Tolbert, D. Zarro, F. Snow, K. Thomsen, R. Henneck, The Reuven Ramaty high-energy solar spectroscopic imager (RHESSI). Sol. Phys. **210**(1-2), 3–32 (2002). doi:10.1023/A:1022428818870. http://link.springer.com/chapter/10.1007/978-94-017-3452-3_1

R.P. Lin, S. Krucker, G.J. Hurford, D.M. Smith, H.S. Hudson, G.D. Holman, R.A. Schwartz, B.R. Dennis, G.H. Share, R.J. Murphy, a.G. Emslie, C. Johns-Krull, N. Vilmer, RHESSI Observations of Particle Acceleration and Energy Release in an Intense Solar Gamma-Ray Line Flare. Astrophys. J. **595**(2), 69–76 (2003). doi:10.1086/378932. http://stacks.iop.org/1538-4357/595/i=2/a=L69

J. Liu, V. Angelopoulos, A. Runov, X.-Z. Zhou, On the current sheets surrounding dipolarizing flux bundles in the magnetotail: The case for wedgelets. J. Geophys. Res. Sp. Phys. **118**(5), 2000–2020 (2013). doi:10.1002/jgra.50092. http://doi.wiley.com/10.1002/jgra.50092

J. Liu, V. Angelopoulos, X.-J. Zhang, D.L. Turner, C. Gabrielse, A. Runov, J. Li, H.O. Funsten, H.E. Spence, Dipolarizing flux bundles in the cis-geosynchronous magnetosphere: Relationship between electric fields and energetic particle injections. J. Geophys. Res. Sp. Phys. **121**(2), 1362–1376 (2016). doi:10.1002/2015JA021691. http://doi.wiley.com/10.1002/2015JA021691

R. Liu, Dynamical processes at the vertical current sheet behind an erupting flux rope. Mon. Not. R. Astron. Soc. **434**(2), 1309–1320 (2013). doi:10.1093/mnras/stt1090.

http://mnras.oxfordjournals.org/cgi/doi/10.1093/mnras/stt1090
W. Liu, Q. Chen, V. Petrosian, Plasmoid Ejections and Loop Contractions in an Eruptive M7.7 Solar Flare: Evidence of Particle Acceleration and Heating in Magnetic Reconnection Outflows. Astrophys. J. **767**(2), 168 (2013). doi:10.1088/0004-637X/767/2/168. http://stacks.iop.org/0004-637X/767/i=2/a=168?key=crossref.bf0b890bb4eae4ef92d3bf7458f4633d
W. Liu, V. Petrosian, B.R. Dennis, Y.W. Jiang, Double Coronal Hard and Soft X-ray Source Observed by RHESSI: Evidence for Magnetic Reconnection and Particle Acceleration in Solar Flares. Astrophys. J. Lett. **676**, 704–716 (2008). ISBN 0000000000000. doi:10.1086/527538. http://arxiv.org/abs/0709.1963
W. Liu, V. Petrosian, B.R. Dennis, G.D. Holman, CONJUGATE HARD X-RAY FOOTPOINTS IN THE 2003 OCTOBER 29 X10 FLARE: UNSHEARING MOTIONS, CORRELATIONS, AND ASYMMETRIES. Astrophys. J. **693**(1), 847–867 (2009). doi:10.1088/0004-637X/693/1/847. http://stacks.iop.org/0004-637X/693/i=1/a=847?key=crossref.e7d9ccbac79b0a127fe2afc75ac6de50
G. Livadiotis, Application of the theory of Large-Scale Quantization to the inner heliosheath. J. Phys. Conf. Ser. **577**(1), 012018 (2015). doi:10.1088/1742-6596/577/1/012018. http://stacks.iop.org/1742-6596/577/i=1/a=012018?key=crossref.b2028acaa2cc4e402897e116b932a859
G. Livadiotis, D.J. McComas, Electrostatic shielding in plasmas and the physical meaning of the Debye length. J. Plasma Phys. **80**(03), 341–378 (2014). doi:10.1017/S0022377813001335. http://www.journals.cambridge.org/abstract_S0022377813001335
G. Livadiotis, Introduction to special section on Origins and Properties of Kappa Distributions: Statistical Background and Properties of Kappa Distributions in Space Plasmas. J. Geophys. Res. Sp. Phys. **120**(3), 1607–1619 (2015a). doi:10.1002/2014JA020825. http://doi.wiley.com/10.1002/2014JA020825
G. Livadiotis, Kappa distribution in the presence of a potential energy. J. Geophys. Res. Sp. Phys. **120**(2), 880–903 (2015b). doi:10.1002/2014JA020671. http://doi.wiley.com/10.1002/2014JA020671
G. Livadiotis, Non-Euclidean-normed Statistical Mechanics. Phys. A Stat. Mech. its Appl. **445**, 240–255 (2016). doi:10.1016/j.physa.2015.11.002. http://linkinghub.elsevier.com/retrieve/pii/S0378437115009802
G. Livadiotis, *Kappa distributions: Theory and applications in plasmas*, 1st edn. (Elsevier, Netherlands, 2017)
G. Livadiotis, D.J. McComas, INVARIANT KAPPA DISTRIBUTION IN SPACE PLASMAS OUT OF EQUILIBRIUM. Astrophys. J. **741**(2), 88 (2011). doi:10.1088/0004-637X/741/2/88. http://stacks.iop.org/0004-637X/741/i=2/a=88?key=crossref.fd32347654dfe2630436ddeb674f3309
G. Livadiotis, D.J. McComas, Beyond kappa distributions: Exploiting Tsallis statistical mechanics in space plasmas. J. Geophys. Res. Sp. Phys. **114**(A11), 11105 (2009). doi:10.1029/2009JA014352. http://doi.wiley.com/10.1029/2009JA014352
M. Longair, *High Energy Astrophysics: Volume 2, Stars, the Galaxy and the Interstellar Medium*, 2nd edn. (Cambridge University Press, Cambridge, 1994), p. 412
D.W. Longcope, a.C. Jardins, T. Carranza-Fulmer, J. Qiu, A Quantitative Model of Energy Release and Heating by Time-dependent, Localized Reconnection in a Flare with Thermal Loop-top X-ray Source. Sol. Phys. **267**(1), 107–139 (2010). doi:10.1007/s11207-010-9635-z. http://link.springer.com/10.1007/s11207-010-9635-z
Q. Lu, L. Zhou, S. Wang, Particle-in-cell simulations of whistler waves excited by an electron κ distribution in space plasma. J. Geophys. Res. Sp. Phys. **115**(A2), (2010). doi:10.1029/2009JA014580. http://doi.wiley.com/10.1029/2009JA014580
Q. Lu, L. Shan, C. Shen, T. Zhang, Y. Li, S. Wang, Velocity distributions of superthermal electrons fitted with a power law function in the magnetosheath: Cluster observations. J. Geophys. Res. Sp. Phys. **116**(A3), 1–5 (2011). doi:10.1029/2010JA016118. http://doi.wiley.com/10.1029/2010JA016118
A.T.Y. Lui, Electron source at the outer boundary of the radiation belts: Storm time case. J. Geophys. Res. Sp. Phys. **118**(4), 1545–1551 (2013). doi:10.1002/jgra.50220. http://doi.wiley.com/10.1002/jgra.50220
a.T.Y. Lui, Q.-G. Zong, C. Wang, M.W. Dunlop, Electron source associated with dipolarization at the outer boundary of the radiation belts: Non-storm cases. J. Geophys. Res. Sp. Phys. **117**(A10), 10224 (2012). doi:10.1029/2012JA018084. http://www.agu.org/pubs/crossref/2012/2012JA018084.shtml http://doi.wiley.com/10.1029/2012JA018084
R. Lundin, I. Sandahl, Some characteristics of the parallel electric field acceleration of electrons over discrete auroral arcs as observed from two rocket flights. ESA Eur. Sound. Rocket. Balloon Relat. Res., with Emphas. Expt. High Latitudes, 125–136 (1978)
B. Luo, X. Li, W. Tu, J. Gong, S. Liu, Comparison of energetic electron flux and phase space density in the magnetosheath and in the magnetosphere. J. Geophys. Res. Sp. Phys. **117**(A5), (2012). doi:10.1029/2012JA017520. http://doi.wiley.com/10.1029/2012JA017520
L.R. Lyons, D.S. Evans, R. Lundin, An observed relation between magnetic field aligned electric fields and downward electron energy fluxes in the vicinity of auroral forms. J. Geophys. Res. **84**(A2), 457 (1979). doi:10.1029/JA084iA02p00457. http://doi.wiley.com/10.1029/JA084iA02p00457
R.L. Lysak, Electrodynamic coupling of the magnetosphere and ionosphere. Space Sci. Rev. **52**(1-2), 33–87

(1990). doi:10.1007/BF00704239. http://link.springer.com/10.1007/BF00704239

C.-y. Ma, D. Summers, Formation of power-law energy spectra in space plasmas by stochastic acceleration due to whistler-mode waves. Geophys. Res. Lett. **25**(21), 4099–4102 (1998). doi:10.1029/1998GL900108. http://doi.wiley.com/10.1029/1998GL900108

M. Maksimovic, Radial evolution of the electron distribution functions in the fast solar wind between 0.3 and 1.5 AU. J. Geophys. Res. Sp. Phys. **110**(A9), 09104 (2005). doi:10.1029/2005JA011119. http://doi.wiley.com/10.1029/2005JA011119

M. Manapat, M. Øieroset, T.D. Phan, R.P. Lin, M. Fujimoto, Field-aligned electrons at the lobe/plasma sheet boundary in the mid-to-distant magnetotail and their association with reconnection. Geophys. Res. Lett. **33**(5), 05101 (2006). doi:10.1029/2005GL024971. http://doi.wiley.com/10.1029/2005GL024971

G. Mann, A. Warmuth, H. Aurass, Generation of highly energetic electrons at reconnection outflow shocks during solar flares. Astron. Astrophys. **494**(2), 669–675 (2009). doi:10.1051/0004-6361:200810099. http://www.aanda.org/10.1051/0004-6361:200810099

E. Marsch, Kinetic Physics of the Solar Corona and Solar Wind. Living Rev. Sol. Phys. **3**, 1 (2006). doi:10.12942/lrsp-2006-1

S. Masuda, T. Kosugi, H. Hara, S. Tsuneta, Y. Ogawara, A loop-top hard X-ray source in a compact solar flare as evidence for magnetic reconnection. Nature **371**(6497), 495–497 (1994). doi:10.1038/371495a0. http://www.nature.com/doifinder/10.1038/371495a0

R.C. McIntosh, P.C. Anderson, Maps of precipitating electron spectra characterized by Maxwellian and kappa distributions. J. Geophys. Res. Sp. Phys. **119**(12), 10116–10132 (2014). doi:10.1002/2014JA020080. http://doi.wiley.com/10.1002/2014JA020080

J.A. Miller, T.N. Larosa, R.L. Moore, Stochastic Electron Acceleration by Cascading Fast Mode Waves in Impulsive Solar Flares. Astrophys. J. **461**, 445 (1996). doi:10.1086/177072. http://adsabs.harvard.edu/doi/10.1086/177072

J.A. Miller, P.J. Cargill, A.G. Emslie, G.D. Holman, B.R. Dennis, T.N. LaRosa, R.M. Winglee, S.G. Benka, S. Tsuneta, Critical issues for understanding particle acceleration in impulsive solar flares. J. Geophys. Res. Sp. Phys. **102**(A7), 14631 (1997). doi:10.1029/97JA00976. http://doi.wiley.com/10.1029/97JA00976

A.V. Milovanov, L.M. Zelenyi, Functional background of the Tsallis entropy: "coarse-grained" systems and "kappa" distribution functions. Nonlinear Process. Geophys. **7**(3/4), 211–221 (2000). doi:10.5194/npg-7-211-2000. http://www.nonlin-processes-geophys.net/7/211/2000/

T. Minoshima, S. Masuda, Y. Miyoshi, K. Kusano, CORONAL ELECTRON DISTRIBUTION IN SOLAR FLARES: DRIFT-KINETIC MODEL. Astrophys. J. **732**(2), 111 (2011). doi:10.1088/0004-637X/732/2/111. http://stacks.iop.org/0004-637X/732/i=2/a=111?key=crossref.24d5a14cf3e1f945afbd80e2257012b0

Y. Miyashita, S. Machida, Y. Kamide, D. Nagata, K. Liou, M. Fujimoto, A. Ieda, M.H. Saito, C.T. Russell, S.P. Christon, M. Nosé, H.U. Frey, I. Shinohara, T. Mukai, Y. Saito, H. Hayakawa, A state-of-the-art picture of substorm-associated evolution of the near-Earth magnetotail obtained from superposed epoch analysis. J. Geophys. Res. Sp. Phys. **114**(A1), 01211 (2009). doi:10.1029/2008JA013225. http://www.agu.org/pubs/crossref/2009/2008JA013225.shtml

Y. Miyoshi, R. Kataoka, Ring current ions and radiation belt electrons during geomagnetic storms driven by coronal mass ejections and corotating interaction regions. Geophys. Res. Lett. **32**(21), 21105 (2005). doi:10.1029/2005GL024590. http://doi.wiley.com/10.1029/2005GL024590

Y. Miyoshi, A. Morioka, T. Obara, H. Misawa, T. Nagai, Y. Kasahara, Rebuilding process of the outer radiation belt during the 3 November 1993 magnetic storm: NOAA and Exos-D observations. J. Geophys. Res. Sp. Phys. **108**(November 1993), 1–15 (2003). doi:10.1029/2001JA007542

E. Möbius, M. Scholer, D. Hovestadt, G. Paschmann, G. Gloeckler, Energetic particles in the vicinity of a possible neutral line in the plasma sheet. J. Geophys. Res. **88**(A10), 7742 (1983). doi:10.1029/JA088iA10p07742. http://doi.wiley.com/10.1029/JA088iA10p07742

M.D. Montgomery, S. Singer, J.P. Conner, E.E. Stogsdill, Spatial Distribution, Energy Spectra, and Time Variations of Energetic Electrons (<math display="inline"> <mi>E</mi> <mo>></mo> <mn/> <mn>50</mn> <mn/> </math> keV) at 17.7 Earth Radii. Phys. Rev. Lett. **14**(7), 209–213 (1965). doi:10.1103/PhysRevLett.14.209. https://link.aps.org/doi/10.1103/PhysRevLett.14.209

T. Nagai, Observed magnetic substorm signatures at synchronous altitude. J. Geophys. Res. Sp. Phys. **87**(A6), 4405 (1982). doi:10.1029/JA087iA06p04405. http://doi.wiley.com/10.1029/JA087iA06p04405

T. Nagai, I. Shinohara, M. Fujimoto, A. Matsuoka, Y. Saito, T. Mukai, Construction of magnetic reconnection in the near-Earth magnetotail with Geotail. J. Geophys. Res. Sp. Phys. **116**, 04222 (2011). doi:10.1029/2010JA016283. http://www.agu.org/pubs/crossref/2011/2010JA016283.shtml

T. Nagai, S. Zenitani, I. Shinohara, R. Nakamura, M. Fujimoto, Y. Saito, T. Mukai, Ion and electron dynamics in the ion-electron decoupling region of magnetic reconnection with Geotail observations. J. Geophys. Res. Sp. Phys. **118**(12), 7703–7713 (2013). doi:10.1002/2013JA019135

R. Nakamura, W. Baumjohann, B. Klecker, Y. Bogdanova, A. Balogh, H. Reme, J.M. Bosqued, I. Dandouras, J.A. Sauvaud, K.H. Glassmeier, L. Kistler, C. Mouikis, T.L. Zhang, H. Eichelberger, A. Runov, Motion of the dipolarization front during a flow burst event observed by Cluster. Geophys. Res. Lett. **29**(20), 1942 (2002). doi:10.1029/2002GL015763. http://www.agu.org/pubs/crossref/2002/2002GL015763.shtml

R. Nakamura, A. Retinò, W. Baumjohann, M. Volwerk, N.V. Erkaev, B. Klecker, E.a. Lucek, I. Dandouras, M. Andr?, Y. Khotyaintsev, Evolution of dipolarization in the near-Earth current sheet induced by Earthward rapid flux transport. Ann. Geophys. **27**(4), 1743–1754 (2009). doi:10.5194/angeo-27-1743-2009. http://www.ann-geophys.net/27/1743/2009/

R. Nakamura, W. Baumjohann, E. Panov, M. Volwerk, J. Birn, A. Artemyev, A.A. Petrukovich, O. Amm, L. Juusola, M.V. Kubyshkina, S. Apatenkov, E.A. Kronberg, P.W. Daly, M. Fillingim, J.M. Weygand, A. Fazakerley, Y. Khotyaintsev, Flow bouncing and electron injection observed by Cluster. J. Geophys. Res. Sp. Phys. **118**(5), 2055–2072 (2013). ISBN 2169-9402. doi:10.1002/jgra.50134

N. Narukage, M. Shimojo, T. Sakao, EVIDENCE OF ELECTRON ACCELERATION AROUND THE RECONNECTION X-POINT IN A SOLAR FLARE. Astrophys. J. **787**(2), 125 (2014). doi:10.1088/0004-637X/787/2/125. http://stacks.iop.org/0004-637X/787/i=2/a=125?key=crossref.bb1adc4fedfca3d293544b0fcd84b913

N.F. Ness, C.S. Scearce, S.C. Cantarano, Probable observations of the geomagnetic tail at 10 Earth radii by Pioneer 7. J. Geophys. Res. **72**(15), 3769–3776 (1967). doi:10.1029/JZ072i015p03769. http://doi.wiley.com/10.1029/JZ072i015p03769

A. Nishida, The Geotail Mission. Geophys. Res. Lett. **21**(25), 2871–2873 (1994). doi:10.1029/94GL01223. http://doi.wiley.com/10.1029/94GL01223

A. Nishida, D.N. Baker, S.W.H. Cowley (eds.), *New Perspectives on the Earth's Magnetotail*. Geophysical Monograph Series, vol. 105 (American Geophysical Union, Washington, D. C., 1998). ISBN 0-87590-088-7. doi:10.1029/GM105. http://doi.wiley.com/10.1029/GM105

N. Nishizuka, K. Shibata, Fermi Acceleration in Plasmoids Interacting with Fast Shocks of Reconnection via Fractal Reconnection. Phys. Rev. Lett. **110**(5), 051101 (2013). doi:10.1103/PhysRevLett.110.051101. http://link.aps.org/doi/10.1103/PhysRevLett.110.051101

G.M. Nita, G.D. Fleishman, A.A. Kuznetsov, E.P. Kontar, D.E. Gary, Three-dimensional Radio and X-ray Modeling and Data Analysis Software: Revealing Flare Complexity. Astrophys. J. **799**(2), 236 (2015). doi:10.1088/0004-637X/799/2/236. http://stacks.iop.org/0004-637X/799/i=2/a=236?key=crossref.1e570e7b182f3c270df0aa8b2c916e0e

T.G. Northrop, *The Adiabatic Motion of Charged Particles* (Interscience, New York, 1963)

T. Obayashi, Energy Build-up and Release Mechanisms in Solar and Auroral Flares. Sol. Phys. **40**, 217–226 (1975). doi:10.1007/BF00183163

K. Ogasawara, K. Asamura, T. Takashima, Y. Saito, T. Mukai, Rocket observation of energetic electrons in the low-altitude auroral ionosphere during the DELTA campaign. Earth, Planets Sp. **58**(9), 1155–1163 (2006). doi:10.1186/BF03352005. http://dx.doi.org/10.1186/BF03352005 http://earth-planets-space.springeropen.com/articles/10.1186/BF03352005

K. Ogasawara, G. Livadiotis, G.A. Grubbs, J.-M. Jahn, R. Michell, M. Samara, J.R. Sharber, J.D. Winningham, Properties of suprathermal electrons associated with discrete auroral arcs. Geophys. Res. Lett. **44**(8), 3475–3484 (2017). doi:10.1002/2017GL072715. http://doi.wiley.com/10.1002/2017GL072715

M. Øieroset, R.P. Lin, T.D. Phan, D.E. Larson, S.D. Bale, Evidence for Electron Acceleration up to 300 keV in the Magnetic Reconnection Diffusion Region of Earth's Magnetotail. Phys. Rev. Lett. **89**(19), 1–4 (2002). doi:10.1103/PhysRevLett.89.195001. http://link.aps.org/doi/10.1103/PhysRevLett.89.195001

M. Øieroset, T.D. Phan, J.P. Eastwood, M. Fujimoto, W. Daughton, M.A. Shay, V. Angelopoulos, F.S. Mozer, J. McFadden, D.E. Larson, K.-H. Glassmeier, Direct Evidence for a Three-Dimensional Magnetic Flux Rope Flanked by Two Active Magnetic Reconnection X Lines at Earth's Magnetopause. Phys. Rev. Lett. **107**(16), 165007 (2011). doi:10.1103/PhysRevLett.107.165007. http://link.aps.org/doi/10.1103/PhysRevLett.107.165007

M. Oka, T. Terasawa, Y. Seki, M. Fujimoto, Y. Kasaba, H. Kojima, I. Shinohara, H. Matsui, H. Matsumoto, Y. Saito, T. Mukai, Whistler critical Mach number and electron acceleration at the bow shock: Geotail observation. Geophys. Res. Lett. **33**(24), 24104 (2006). doi:10.1029/2006GL028156. http://www.agu.org/pubs/crossref/2006/2006GL028156.shtml http://doi.wiley.com/10.1029/2006GL028156

M. Oka, T. Terasawa, M. Fujimoto, H. Matsui, Y. Kasaba, Y. Saito, H. Kojima, H. Matsumoto, T. Mukai, Non-thermal electrons at the Earth's bow shock: A gradual' event. Earth, Planets Sp. **61**(5), 603–606 (2009). doi:10.1186/BF03352932. http://arxiv.org/abs/0810.4552 http://earth-planets-space.springeropen.com/articles/10.1186/BF03352932

M. Oka, M. Fujimoto, I. Shinohara, T.D. Phan, Island surfing mechanism of electron acceleration during magnetic reconnection. J. Geophys. Res. Sp. Phys. **115**(A8), 08223 (2010).

doi:10.1029/2010JA015392. http://www.agu.org/pubs/crossref/2010/2010JA015392.shtml http://doi.wiley.com/10.1029/2010JA015392

M. Oka, S. Ishikawa, P. Saint-Hilaire, S. Krucker, R.P. Lin, Kappa Distribution Model for Hard X-Ray Coronal Sources of Solar Flares. Astrophys. J. **764**(1), 6 (2013). doi:10.1088/0004-637X/764/1/6. http://stacks.iop.org/0004-637X/764/i=1/a=6?key=crossref.d4a1517146404b20c5488c5d0b92080f

M. Oka, S. Krucker, H.S. Hudson, P. Saint-Hilaire, Electron energy partition in the above-the-looptop solar hard X-ray sources. Astrophys. J. **799**(2), 129 (2015). doi:10.1088/0004-637X/799/2/129. http://stacks.iop.org/0004-637X/799/i=2/a=129?key=crossref.e0acb53dd9b0d4e6d977903c6f48287e

M. Oka, T.D. Phan, M. Øieroset, V. Angelopoulos, In situ evidence of electron energization in the electron diffusion region of magnetotail reconnection. J. Geophys. Res. Sp. Phys. **121**(3), 1955–1968 (2016). doi:10.1002/2015JA022040. http://doi.wiley.com/10.1002/2015JA022040

A. Olsson, P. Janhunen, Field-aligned conductance values estimated from Maxwellian and kappa distributions in quiet and disturbed events using Freja electron data. Ann. Geophys. **16**(3), 298–302 (1998). ISBN 0992-7689. doi:10.1007/s00585-998-0298-0. http://www.ann-geophys.net/16/298/1998/%5Cnhttp://dx.doi.org/10.1007/s00585-998-0298-0 http://www.ann-geophys.net/16/298/1998/

E.V. Panov, R. Nakamura, W. Baumjohann, V. Angelopoulos, a.a. Petrukovich, A. Retinò, M. Volwerk, T. Takada, K.-H. Glassmeier, J.P. McFadden, D. Larson, Multiple overshoot and rebound of a bursty bulk flow. Geophys. Res. Lett. **37**(8), 08103 (2010). doi:10.1029/2009GL041971. http://www.agu.org/pubs/crossref/2010/2009GL041971.shtml http://doi.wiley.com/10.1029/2009GL041971

G. Paschmann, S. Haaland, R.a. Treumann, In situ measurements in the auroral plasma, in *Auror. Plasma Phys.*, ed. by G. Paschmann, S. Haaland, R. Treumann 2003, pp. 93–208. Chap. 4. doi:10.1023/A:1023082700768. http://link.springer.com/chapter/10.1007/978-94-007-1086-3_4

M. Pesce-Rollins, N. Omodei, V. Petrosian, W. Liu, F.R. da Costa, A. Allafort, Q. Chen, FIRST DETECTION OF >100 MeV GAMMA-RAYS ASSOCIATED WITH A BEHIND-THE-LIMB SOLAR FLARE. Astrophys. J. **805**(2), 15 (2015). doi:10.1088/2041-8205/805/2/L15. http://stacks.iop.org/2041-8205/805/i=2/a=L15?key=crossref.b9a14c8e973e0cc8c11b411701d063ac

V. Petrosian, Stochastic Acceleration by Turbulence. Space Sci. Rev. **173**(1-4), 535–556 (2012). doi:10.1007/s11214-012-9900-6. http://link.springer.com/10.1007/s11214-012-9900-6

V. Pierrard, New model of magnetospheric current-voltage relationship. J. Geophys. Res. Sp. Phys. **101**(A2), 2669–2675 (1996). doi:10.1029/95JA00476. http://dx.doi.org/10.1029/95JA00476

V. Pierrard, M. Lazar, S. Poedts, Š. Štverák, M. Maksimovic, P.M. Trávníček, The Electron Temperature and Anisotropy in the Solar Wind. Comparison of the Core and Halo Populations. Sol. Phys. **291**(7), 2165–2179 (2016). doi:10.1007/s11207-016-0961-7. http://link.springer.com/10.1007/s11207-016-0961-7

D.H. Pontius, R.a. Wolf, Transient flux tubes in the terrestrial magnetosphere. Geophys. Res. Lett. **17**(1), 49–52 (1990). doi:10.1029/GL017i001p00049. http://doi.wiley.com/10.1029/GL017i001p00049

B.M. Randol, E.R. Christian, Coupling of charged particles via Coulombic interactions: Numerical simulations and resultant kappa-like velocity space distribution functions. J. Geophys. Res. Sp. Phys. **121**(3), 1907–1919 (2016). doi:10.1002/2015JA021859. http://doi.wiley.com/10.1002/2015JA021859

D.V. Reames, PARTICLE ACCELERATION AT THE SUN AND IN THE HELIOSPHERE. Space Sci. Rev. **90**, 413–491 (1999). doi:10.1023/A1005105831781

A. Retinò, R. Nakamura, A. Vaivads, Y. Khotyaintsev, T. Hayakawa, K. Tanaka, S. Kasahara, M. Fujimoto, I. Shinohara, J.P. Eastwood, M. André, W. Baumjohann, P.W. Daly, E.a. Kronberg, N. Cornilleau-Wehrlin, Cluster observations of energetic electrons and electromagnetic fields within a reconnecting thin current sheet in the Earth's magnetotail. J. Geophys. Res. Sp. Phys. **113**(A12), (2008). doi:10.1029/2008JA013511. http://doi.wiley.com/10.1029/2008JA013511

A. Runov, V. Angelopoulos, M.I. Sitnov, V.a. Sergeev, J. Bonnell, J.P. McFadden, D.E. Larson, K.-H. Glassmeier, U. Auster, THEMIS observations of an earthward-propagating dipolarization front. Geophys. Res. Lett. **36**, 14106 (2009). doi:10.1029/2009GL038980. http://www.agu.org/pubs/crossref/2009/2009GL038980.shtml

A. Runov, V. Angelopoulos, X.-Z. Zhou, X.-J. Zhang, S. Li, F. Plaschke, J. Bonnell, A THEMIS multicase study of dipolarization fronts in the magnetotail plasma sheet. J. Geophys. Res. Sp. Phys. **116**, 05216 (2011a). doi:10.1029/2010JA016316. http://www.agu.org/pubs/crossref/2011/2010JA016316.shtml

A. Runov, V. Angelopoulos, M.I. Sitnov, V.a. Sergeev, R. Nakamura, Y. Nishimura, H.U. Frey, J.P. McFadden, D.E. Larson, J. Bonnell, K.-H. Glassmeier, U. Auster, M. Connors, C.T. Russell, H.J. Singer, Dipolarization fronts in the magnetotail plasma sheet. Planet. Space Sci. **59**(7), 517–525 (2011b). doi:10.1016/j.pss.2010.06.006. http://linkinghub.elsevier.com/retrieve/pii/S0032063310001790

A. Runov, V. Angelopoulos, C. Gabrielse, J. Liu, D.L. Turner, X.-Z. Zhou, Average thermodynamic and spectral properties of plasma in and around dipolarizing flux bundles. J. Geophys. Res. Sp. Phys. **120**(6),

4369–4383 (2015). doi:10.1002/2015JA021166. http://doi.wiley.com/10.1002/2015JA021166

D.F. Ryan, R.O. Milligan, P.T. Gallagher, B.R. Dennis, A. Kim Tolbert, R.a. Schwartz, C. Alex Young, THE THERMAL PROPERTIES OF SOLAR FLARES OVER THREE SOLAR CYCLES USING GOES X-RAY OBSERVATIONS. Astrophys. J. Suppl. Ser. **202**(2), 11 (2012). doi:10.1088/0067-0049/202/2/11. http://stacks.iop.org/0067-0049/202/i=2/a=11?key=crossref.e69f754ed3d84a87d13a9d39560c505c

P. Saint-Hilaire, S. Krucker, R.P. Lin, A Statistical Survey of Hard X-ray Spectral Characteristics of Solar Flares with Two Footpoints. Sol. Phys. **250**(1), 53–73 (2008). doi:10.1007/s11207-008-9193-9. http://www.springerlink.com/index/10.1007/s11207-008-9193-9 http://link.springer.com/10.1007/s11207-008-9193-9

T. Sakanoi, H. Fukunishi, T. Mukai, Relationship between field-aligned currents and inverted-V parallel potential drops observed at midaltitudes. J. Geophys. Res. **100**(A10), 19343 (1995). doi:10.1029/95JA01285. http://doi.wiley.com/10.1029/95JA01285

T. Sakao, T. Kosugi, S. Masuda, K. Yaji, M. Inda-Koide, K. Makishima, Characteristics of hard X-ray double sources in impulsive solar flares. Adv. Sp. Res. **17**(4-5), 67–70 (1996). doi:10.1016/0273-1177(95)00544-O. http://www.sciencedirect.com/science/article/pii/027311779500544O http://linkinghub.elsevier.com/retrieve/pii/027311779500544O

T. Sakao, Characteristics of solar flare hard X-ray sources as revealed with the Hard X-ray Telescope aboard the Yohkoh satellite, PhD thesis, The University of Tokyo, 1994

E.T. Sarris, S.M. Krimigis, T.P. Armstrong, Observations of magnetospheric bursts of high-energy protons and electrons at 35 R E with Imp 7. J. Geophys. Res. **81**(13), 2341–2355 (1976a). doi:10.1029/JA081i013p02341. http://doi.wiley.com/10.1029/JA081i013p02341

E.T. Sarris, S.M. Krimigis, T. Iijima, C.O. Bostrom, T.P. Armstrong, Location of the source of magnetospheric energetic particle bursts by multispacecraft observations. Geophys. Res. Lett. **3**(8), 437–440 (1976b). doi:10.1029/GL003i008p00437. http://doi.wiley.com/10.1029/GL003i008p00437

F.L. Scarf, Pioneer 8 traversal of the geomagnetic tail at 1600 R E. J. Geophys. Res. **92**(A10), 11201 (1987). doi:10.1029/JA092iA10p11201. http://doi.wiley.com/10.1029/JA092iA10p11201

M. Scholer, F.M. Ipavich, G. Gloeckler, D. Hovestadt, Acceleration of low-energy protons and alpha particles at interplanetary shock waves. J. Geophys. Res. **88**(A3), 1977 (1983). doi:10.1029/JA088iA03p01977. http://doi.wiley.com/10.1029/JA088iA03p01977

J.D. Scudder, S. Olbert, A theory of local and global processes which affect solar wind electrons, 1. The origin of typical 1 AU velocity distribution functionsSteady state theory. J. Geophys. Res. **84**(A6), 2755 (1979). doi:10.1029/JA084iA06p02755. http://doi.wiley.com/10.1029/JA084iA11p06603 http://doi.wiley.com/10.1029/JA084iA06p02755

J.D. Scudder, R.D. Holdaway, W. Daughton, H. Karimabadi, V. Roytershteyn, C.T. Russell, J.Y. Lopez, First resolved observations of the demagnetized electron-diffusion region of an astrophysical magnetic-reconnection site. Phys. Rev. Lett. **108**(22), 1–5 (2012). doi:10.1103/PhysRevLett.108.225005

V. Sergeev, V. Angelopoulos, S. Apatenkov, J. Bonnell, R. Ergun, R. Nakamura, J. McFadden, D. Larson, A. Runov, Kinetic structure of the sharp injection/dipolarization front in the flow-braking region. Geophys. Res. Lett. **36**(21), 21105 (2009). doi:10.1029/2009GL040658. http://doi.wiley.com/10.1029/2009GL040658

K. Shibata, S. Masuda, M. Shimojo, H. Hara, T. Yokoyama, S. Tsuneta, T. Kosugi, Y. Ogawara, Hot-Plasma Ejections Associated with Compact-Loop Solar Flares. Astrophys. J. Lett. **451**, 83 (1995)

K. Shibata, T. Nakamura, T. Matsumoto, K. Otsuji, T.J. Okamoto, N. Nishizuka, T. Kawate, H. Watanabe, S. Nagata, S. UeNo, R. Kitai, S. Nozawa, S. Tsuneta, Y. Suematsu, K. Ichimoto, T. Shimizu, Y. Katsukawa, T.D. Tarbell, T.E. Berger, B.W. Lites, R.A. Shine, A.M. Title, Chromospheric Anemone Jets as Evidence of Ubiquitous Reconnection. Science (80-.). **318**(5856), 1591–1594 (2007). doi:10.1126/science.1146708. http://www.sciencemag.org/cgi/doi/10.1126/science.1146708

N. Shimada, T. Terasawa, M. Hoshino, T. Naito, H. Matsui, T. Koi, K. Maezawa, Diffusive SHock Acceleration of Electrons at an Interplanetary Shock Observed on 21 Feb 1994. Astrophys. Space Sci. **264**(1/4), 481–488 (1998). doi:10.1023/A:1002499513777. http://link.springer.com/chapter/10.1007/978-94-011-4203-8_37 http://link.springer.com/10.1023/A:1002499513777

K. Shiokawa, W. Baumjohann, G. Haerendel, Braking of high-speed flows in the near-Earth tail. Geophys. Res. Lett. **24**(10), 1179–1182 (1997). ISBN 0094-8276. doi:10.1029/97GL01062. http://dx.doi.org/10.1029/97GL01062 http://doi.wiley.com/10.1029/97GL01062

P.J.A. Simões, E.P. Kontar, Implications for electron acceleration and transport from non-thermal electron rates at looptop and footpoint sources in solar flares. Astron. Astrophys. **551**, 135 (2013). doi:10.1051/0004-6361/201220304. http://www.aanda.org/10.1051/0004-6361/201220304

M. Stepanova, E.E. Antonova, Role of turbulent transport in the evolution of the κ distribution functions in the plasma sheet. J. Geophys. Res. Sp. Phys. **120**(5), 3702–3714 (2015). doi:10.1002/2014JA020684. http://doi.wiley.com/10.1002/2014JA020684

Š. Štverák, M. Maksimovic, P.M. Trávníček, E. Marsch, A.N. Fazakerley, E.E. Scime, Radial evolution of nonthermal electron populations in the low-latitude solar wind: Helios, Cluster, and Ulysses Observations. J. Geophys. Res. Sp. Phys. **114**(A5), (2009). doi:10.1029/2008JA013883. http://doi.wiley.com/10.1029/2008JA013883

L. Sui, G.˜. Holman, B. Dennis, Evidence for Magnetic Reconnection in Three Homologous Solar Flares Observed by RHESSI. Astrophys. J. **612**(1987), 546–556 (2004). doi:10.1086/422515

L. Sui, G.D. Holman, Evidence for the Formation of a Large-Scale Current Sheet in a Solar Flare. Astrophys. J. **596**(2), 251–254 (2003). doi:10.1086/379343. http://stacks.iop.org/1538-4357/596/i=2/a=L251

D. Summers, R.M. Thorne, F. Xiao, Relativistic theory of wave-particle resonant diffusion with application to electron acceleration in the magnetosphere. J. Geophys. Res. Sp. Phys. **103**(A9), 20487–20500 (1998). ISBN 0148-0227. doi:10.1029/98JA01740. http://doi.wiley.com/10.1029/98JA01740

R.L. Swanson, Electron intensity and magnetic field changes at synchronous orbit for the auroral electrojet. MS thesis, Univ. Minn., 55455 (1978)

E. Tandberg-Hanssen, a.G. Emslie, *The Physics of Solar Flares* (Cambridge University Press, New York, 1988), p. 273. ISBN 978-0521115520

X. Tang, C. Cattell, J. Dombeck, L. Dai, L.B. Wilson, A. Breneman, A. Hupach, THEMIS observations of the magnetopause electron diffusion region: Large amplitude waves and heated electrons. Geophys. Res. Lett. **40**(12), 2884–2890 (2013). doi:10.1002/grl.50565. http://doi.wiley.com/10.1002/grl.50565

J. Tao, L. Wang, Q. Zong, G. Li, C.S. Salem, R.F. Wimmer-Schweingruber, J. He, C. Tu, S.D. Bale, QUIET-TIME SUPRATHERMAL (0.11.5 keV) ELECTRONS IN THE SOLAR WIND. Astrophys. J. **820**(1), 22 (2016). doi:10.3847/0004-637X/820/1/22. http://stacks.iop.org/0004-637X/820/i=1/a=22?key=crossref.e388f5022beb25798778342aba211603

W.-L. Teh, R. Nakamura, M. Fujimoto, E.a. Kronberg, a.N. Fazakerley, P.W. Daly, W. Baumjohann, Electron dynamics in the reconnection ion diffusion region. J. Geophys. Res. Sp. Phys. **117**(A12), (2012). doi:10.1029/2012JA017896. http://doi.wiley.com/10.1029/2012JA017896

T. Terasawa, M. Fujimoto, T. Mukai, I. Shinohara, Y. Saito, T. Yamamoto, S. Machida, S. Kokubun, a.J. Lazarus, J.T. Steinberg, R.P. Lepping, Solar wind control of density and temperature in the near-Earth plasma sheet: WIND/GEOTAIL collaboration. Geophys. Res. Lett. **24**(8), 935–938 (1997). ISBN 0148-0227. doi:10.1029/96GL04018. http://doi.wiley.com/10.1029/96GL04018

T. Terasawa, A. Nishida, Simultaneous observations of relativistic electron bursts and neutral-line signatures in the magnetotail. Planet. Space Sci. **24**(9), 855–866 (1976). doi:10.1016/0032-0633(76)90076-3. http://linkinghub.elsevier.com/retrieve/pii/0032063376900763

T. Terasawa, K. Shibata, M. Scholer, Comparative study of flares and substorms. Adv. Sp. Res. **26**(3), 573–583 (2000). doi:10.1016/S0273-1177(99)01087-X. http://linkinghub.elsevier.com/retrieve/pii/S027311779901087X

M.F. Thomsen, H.C. Barr, S.P. Gary, W.C. Feldman, T.E. Cole, Stability of electron distributions within the Earth's bow shock. J. Geophys. Res. Sp. Phys. **88**(A4), 3035 (1983). doi:10.1029/JA088iA04p03035. http://doi.wiley.com/10.1029/JA088iA04p03035

M. Tomczak, The analysis of hard X-ray radiation of flares with occulted footpoints. Astron. Astrophys. **366**, 294–305 (2001). doi:10.1051/0004-6361. http://www.issibern.ch/teams/CornSource/library/tomczak_01.pdf

M. Tomczak, The YOHKOH survey of partially occulted flares in hard X-rays. Astron. Astrophys. **502**(2), 665–678 (2009). doi:10.1051/0004-6361/200911732. http://www.aanda.org/10.1051/0004-6361/200911732

R.A. Treumann, Theory of super-diffusion for the magnetopause. Geophys. Res. Lett. **24**(14), 1727–1730 (1997). doi:10.1029/97GL01760. http://doi.wiley.com/10.1029/97GL01760

C. Tsallis, Possible generalization of Boltzmann-Gibbs statistics. J. Stat. Phys. **52**(1-2), 479–487 (1988). ISBN 0022-4715. doi:10.1007/BF01016429. http://link.springer.com/10.1007/BF01016429

C. Tsallis, R. Mendes, A.R. Plastino, The role of constraints within generalized nonextensive statistics. Phys. A Stat. Mech. its Appl. **261**(3-4), 534–554 (1998). ISBN 0378-4371. doi:10.1016/S0378-4371(98)00437-3. http://linkinghub.elsevier.com/retrieve/pii/S0378437198004373

S. Tsuneta, Particle Acceleration and Magnetic Reconnection in Solar Flares. Publ. Astron. Soc. Japan **47**, 691–697 (1995)

S. Tsuneta, Solar Flare and Particle Acceleration (in Japanese), in *Rev. Sp. Weather*, 1st edn. ed. by K. Shibata, Y. Kamide (Kyoto University Press, Kyoto, 2011), pp. 203–242. Chap. 6. ISBN 978-4-87698-554-8

B.T. Tsurutani, R.P. Lin, Acceleration of >47 keV ions and >2 keV electrons by interplanetary shocks at 1AU. J. Geophys. Res. Sp. Phys. **90**(A1), 1 (1985). doi:10.1029/JA090iA01p00001. http://doi.wiley.com/10.1029/JA090iA01p00001

B.T. Tsurutani, K. Shibata, S.-i. Akasofu, M. Oka, A two-step scenario for both solar flares and magnetospheric substorms : Short duration energy storage. Earth Planets Sp. **61**, 555–559 (2009)

N.a. Tsyganenko, Modeling the Earth's magnetospheric magnetic field confined within a realistic magnetopause.

J. Geophys. Res. Sp. Phys. **100**(A4), 5599–5612 (1995). doi:10.1029/94JA03193

D.L. Turner, J.F. Fennell, J.B. Blake, J.H. Clemmons, B.H. Mauk, I.J. Cohen, A.N. Jaynes, J.V. Craft, F.D. Wilder, D.N. Baker, G.D. Reeves, D.J. Gershman, L.A. Avanov, J.C. Dorelli, B.L. Giles, C.J. Pollock, D. Schmid, R. Nakamura, R.J. Strangeway, C.T. Russell, A.V. Artemyev, A. Runov, V. Angelopoulos, H.E. Spence, R.B. Torbert, J.L. Burch, Energy limits of electron acceleration in the plasma sheet during substorms: A case study with the Magnetospheric Multiscale (MMS) mission. Geophys. Res. Lett. **43**(15), 7785–7794 (2016). doi:10.1002/2016GL069691. http://doi.wiley.com/10.1002/2016GL069691

H.F. Van Beek, P. Hoyng, B. Lafleur, G.M. Simnett, The Hard X-ray Imaging Spectrometer (HXIS). Sol. Phys. **65**(1), 39–52 (1980). doi:10.1007/BF00151383. http://link.springer.com/10.1007/BF00151383

P. van Nes, R. Reinhard, T.R. Sanderson, K.-P. Wenzel, R.D. Zwickl, The energy spectrum of 35- to 1600-keV protons associated with interplanetary shocks. J. Geophys. Res. Sp. Phys. **89**(A4), 2122 (1984). doi:10.1029/JA089iA04p02122. http://doi.wiley.com/10.1029/JA089iA04p02122

V.M. Vasyliunas, A survey of low-energy electrons in the evening sector of the magnetosphere with OGO 1 and OGO 3. J. Geophys. Res. Sp. Phys. **73**(9), 2839–2884 (1968). doi:10.1029/JA073i009p02839. http://doi.wiley.com/10.1029/JA073i009p02839

O.P. Verkhoglyadova, G.P. Zank, G. Li, A theoretical perspective on particle acceleration by interplanetary shocks and the Solar Energetic Particle problem. Phys. Rep. **557**, 1–23 (2015). ISBN 0370-1573. doi:10.1016/j.physrep.2014.10.004. http://dx.doi.org/10.1016/j.physrep.2014.10.004

A.M. Veronig, J.C. Brown, A Coronal Thick-Target Interpretation of Two Hard X-Ray Loop Events. Astrophys. J. **603**(2), 117–120 (2004). doi:10.1086/383199. http://stacks.iop.org/1538-4357/603/i=2/a=L117

C.-P. Wang, M. Gkioulidou, L.R. Lyons, V. Angelopoulos, Spatial distributions of the ion to electron temperature ratio in the magnetosheath and plasma sheet. J. Geophys. Res. Sp. Phys. **117**(A8), (2012). doi:10.1029/2012JA017658. http://doi.wiley.com/10.1029/2012JA017658

H. Wang, Q. Lu, C. Huang, S. Wang, Electron acceleration in a secondary magnetic island formed during magnetic reconnection with a guide field. Phys. Plasmas **24**(5), 052113 (2017). doi:10.1063/1.4982813. http://aip.scitation.org/doi/10.1063/1.4982813

L. Wang, R.P. Lin, C. Salem, M. Pulupa, D.E. Larson, P.H. Yoon, J.G. Luhmann, QUIET-TIME INTERPLANETARY 2-20 keV SUPERHALO ELECTRONS AT SOLAR MINIMUM. Astrophys. J. **753**(1), 23 (2012). doi:10.1088/2041-8205/753/1/L23. http://stacks.iop.org/2041-8205/753/i=1/a=L23?key=crossref.8022ef530fe1e5708a64482316d5bb36

R. Wang, Q. Lu, X. Li, C. Huang, S. Wang, Observations of energetic electrons up to 200 keV associated with a secondary island near the center of an ion diffusion region: A Cluster case study. J. Geophys. Res. Sp. Phys. **115**(A11), 11201 (2010). doi:10.1029/2010JA015473. http://doi.wiley.com/10.1029/2010JA015473

A. Warmuth, G. Mann, Constraints on energy release in solar flares from RHESSI and GOES X-ray observations. Astron. Astrophys. **588**, 115 (2016). doi:10.1051/0004-6361/201527474. http://www.aanda.org/10.1051/0004-6361/201527475 http://www.aanda.org/10.1051/0004-6361/201527474

A. Warmuth, G.D. Holman, B.R. Dennis, G. Mann, H. Aurass, R.O. Milligan, RAPID CHANGES OF ELECTRON ACCELERATION CHARACTERISTICS AT THE END OF THE IMPULSIVE PHASE OF AN X-CLASS SOLAR FLARE. Astrophys. J. **699**(1), 917–922 (2009). doi:10.1088/0004-637X/699/1/917. http://stacks.iop.org/0004-637X/699/i=1/a=917?key=crossref.7afedb414d0c8721948df241a1b33c42

M.S. Wheatland, D.B. Melrose, Interpreting Yohkoh hard and soft X-ray flare observations. Sol. Phys. **158**(2), 283–299 (1995). doi:10.1007/BF00795664

S.M. White, A.O. Benz, S. Christe, F. Fárník, M.R. Kundu, G. Mann, Z. Ning, J.-P. Raulin, a.V.R. Silva-Válio, P. Saint-Hilaire, N. Vilmer, A. Warmuth, The Relationship Between Solar Radio and Hard X-ray Emission. Space Sci. Rev. **159**(1-4), 225–261 (2011). doi:10.1007/s11214-010-9708-1. http://www.springerlink.com/index/10.1007/s11214-010-9708-1

M. Wu, C. Huang, Q. Lu, M. Volwerk, R. Nakamura, Z. V?r?s, T. Zhang, S. Wang, In situ observations of multistage electron acceleration driven by magnetic reconnection. J. Geophys. Res. Sp. Phys. **120**(8), 6320–6331 (2015). ISBN 2169-9402. doi:10.1002/2015JA021165. http://doi.wiley.com/10.1002/2015JA021227 http://doi.wiley.com/10.1002/2015JA021165

Y. Xu, A.G. Emslie, G.J. Hurford, RHESSI Hard XRay Imaging Spectroscopy of Extended Sources and the Physical Properties of Electron Acceleration Regions in Solar Flares. Astrophys. J. **673**(1), 576–585 (2008). doi:10.1086/524184. http://adsabs.harvard.edu/abs/2008ApJ...673..576X http://stacks.iop.org/0004-637X/673/i=1/a=576

Y.-H. Yang, C.Z. Cheng, S. Krucker, M.-S. Hsieh, N.-H. Chen, Asymmetry of Hard X-Ray Emissions At Conjugate Footpoints in Solar Flares. Astrophys. J. **756**(1), 42 (2012). doi:10.1088/0004-637X/756/1/42. http://stacks.iop.org/0004-637X/756/i=1/a=42?key=crossref.3c871fb89043454d9543a7de0cc91520

P.H. Yoon, Electron kappa distribution and quasi-thermal noise. J. Geophys. Res. Sp. Phys. **119**(9), 7074–7087 (2014). doi:10.1002/2014JA020353. http://doi.wiley.com/10.1002/2014JA020353

P.H. Yoon, T. Rhee, C.-M. Ryu, Self-consistent formation of electron κ distribution: 1. Theory. J. Geophys. Res. Sp. Phys. **111**(A9), 09106 (2006). doi:10.1029/2006JA011681. http://www.agu.org/pubs/crossref/2006/2006JA011681.shtml http://doi.wiley.com/10.1029/2006JA011681

P.H. Yoon, L.F. Ziebell, R. Gaelzer, R.P. Lin, L. Wang, Langmuir Turbulence and Suprathermal Electrons. Space Sci. Rev. **173**(1-4), 459–489 (2012). doi:10.1007/s11214-012-9867-3. http://link.springer.com/10.1007/s11214-012-9867-3

P.H. Yoon, S. Kim, G.S. Choe, Y.-J. Moon, REVISED MODEL OF THE STEADY-STATE SOLAR WIND HALO ELECTRON VELOCITY DISTRIBUTION FUNCTION. Astrophys. J. **826**(2), 204 (2016). doi:10.3847/0004-637X/826/2/204

S. Zenitani, I. Shinohara, T. Nagai, Evidence for the dissipation region in magnetotail reconnection. Geophys. Res. Lett. **39**(11), (2012). doi:10.1029/2012GL051938. http://doi.wiley.com/10.1029/2012GL051938

V.V. Zharkova, K. Arzner, A.O. Benz, P. Browning, C. Dauphin, a.G. Emslie, L. Fletcher, E.P. Kontar, G. Mann, M. Onofri, V. Petrosian, R. Turkmani, N. Vilmer, L. Vlahos, Recent Advances in understanding particle acceleration processes in solar flares. Space Sci. Rev. **159**(1-4), 357–420 (2011). ISBN 1121401198. doi:10.1007/s11214-011-9803-y

V. Zhdankin, G.R. Werner, D.A. Uzdensky, M.C. Begelman, Kinetic Turbulence in Relativistic Plasma: From Thermal Bath to Nonthermal Continuum. Phys. Rev. Lett. **118**(5), 055103 (2017). doi:10.1103/PhysRevLett.118.055103

M. Zhou, T. Li, X. Deng, Y. Pang, X. Xu, R. Tang, S. Huang, H. Li, Statistics of energetic electrons in the magnetotail reconnection. J. Geophys. Res. Sp. Phys. **121**(4), 3108–3119 (2016). ISBN 2169-9402. doi:10.1002/2015JA022085. http://doi.wiley.com/10.1002/2015JA022085